REPORT DOCUMENTATION PAGE

Form Approved
OMB NO. 0704-0188

1. AGENCY USE ONLY (Leave Blank)	2. REPORT DATE 19 mar 01	3. REPORT TYPE AND DATES COVERED final report 17 aug 00 – 17 feb 01

4. TITLE AND SUBTITLE
Impact and High Strain Rate Response of 3-D Woven Systems

5. FUNDING NUMBERS
DAAD19-00-C-0108

6. AUTHOR(S)
J. N. Singletary, R. A. Coffelt, J. W. Gillespie Jr., B. A. Gama

7. PERFORMING ORGANIZATION NAME(S) AND ADDRESS(ES)
3TEX, Inc.
109 MacKenan Drive
Cary, NC 27511

8. PERFORMING ORGANIZATION REPORT NUMBER 8

9. SPONSORING / MONITORING AGENCY NAME(S) AND ADDRESS(ES)
U. S. Army Research Office
P.O. Box 12211
Research Triangle Park, NC 27709-2211

10. SPONSORING / MONITORING AGENCY REPORT NUMBER
ARO 41472.1-EG-ST1

11. SUPPLEMENTARY NOTES
The views, opinions and/or findings contained in this report are those of the author(s) and should not be construed as an official Department of the Army position, policy or decision, unless so designated by other documentation.

12 a. DISTRIBUTION / AVAILABILITY STATEMENT
Approved for public release; distribution unlimited.

12 b. DISTRIBUTION CODE

13. ABSTRACT (Maximum 200 words)

3-D and 2-D woven systems were characterized both statically and dynamically to assess the relative advantages of 3-D weaves in armor and impact resistant systems. Five different 3Weave™ 3-D orthogonal fabrics were woven from S-2 glass rovings, including both flat goods and near-net-shape preforms. 3Weave™ and a baseline, 2-D woven fabric were consolidated via vacuum assisted resin transfer molding using rubber toughened epoxy vinyl ester and rubber-toughened epoxy. Static mechanical properties, including mode 1 critical strain energy release rate, were determined. Composites were tested in drop tower impact, for visible damage area and compression strength after impact. Composites were tested in through-thickness compression in Hopkinson bar tests at strain rates ranging from 500-1200/s. Composites were used to back aluminum plates, and tested against fragment simulating projectiles in non-perforating ballistic impact, to determine visible damage area. Finally, prototype body armor inserts were developed, using alumina ceramics, which 3-D woven backings enabled the design to meet NIJ 0101.04 level 3 standalone requirements at an article weight of 8.1 lbs, while similar weight backings made from the 2-D fabric could not meet the NIJ requirements.

14. SUBJECT TERMS	15. NUMBER OF PAGES
3-D weave; 3-D woven; fiber reinforced plastic; armor; ballistic; vartm; S-2 glass composite; impact	71
	16. PRICE CODE

17. SECURITY CLASSIFICATION OR REPORT	18. SECURITY CLASSIFICATION ON THIS PAGE	19. SECURITY CLASSIFICATION OF ABSTRACT	20. LIMITATION OF ABSTRACT
UNCLASSIFIED	UNCLASSIFIED	UNCLASSIFIED	UL

NSN 7540-01-280-5500

Standard Form 298 (Rev.2-89)
Prescribed by ANSI Std. 239-18
298-102

20010413 020

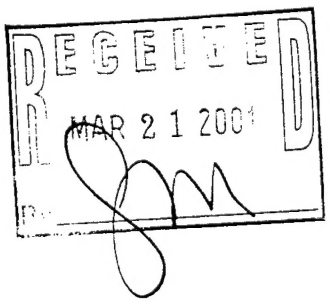

Foreword

This report was prepared by James Singletary and Robert Coffelt of 3TEX, Inc. Sections 4.3 and 5 came from subcontract reports submitted to 3TEX by Bazle Gama and John W. Gillespie Jr. of the University of Delaware Center for Composite Materials.

Table of Contents

List of Figures

List of Tables

Summary

The objective of this research was to demonstrate improvements possible in impact-resistant, fiber-reinforced plastics by using a 3-D weave reinforcements instead of currently used, 2-D weaves. Five 3-D orthogonal S-2 glass roving fabrics were designed and woven by the 3Weave™ process. Composite panels were made from single plies and laminates of the 3-D weaves, as well as 2-D, plain woven S-2 glass rovings, via vacuum assisted resin transfer molding (VARTM). Dow Derakane 8084 rubber-toughened epoxy vinyl ester, and Applied Poleramics SC-15 rubber-toughened epoxy, were used, as both of these systems are of interest in commercial applications of FRP for structural armor materials.

Composites were characterized both statically and dynamically. Static strengths and stiffnesses of composites in both resins were determined for single ply panels of three combinations of fabric and resin, yielding up to seven of the nine elastic constants, as well as strengths. Static data was compared to predictions from an internally developed models of 3-D woven composite elasticity. Mode 1 critical strain energy release rate was determined by a novel double cantilever beam test, for interlaminar crack propagation in 2-D and 3-D laminates, and intralaminar crack propagation inside 3-D plies.

Dynamic tests were performed across several orders of strain rate, from drop tower to ballistic testing. Drop tower impact and compression after impact (CAI) tests were performed on two 3-D woven laminates and the baseline material. Strain rate dependent inelastic transverse compressive response was determined via Split Hopkinson bar for strain rates of 500-1200/s. Non-perforating ballistic tests were performed using 12.7 mm fragment simulating projectiles against roughly 0.28-in thick composite panels (bonded to thin aluminum strike faces) of the baseline 2-D laminate, and a single 3-D woven ply. Perforating ballistic tests were performed per NIJ-101.04 Level III standalone on prototype body armor inserts containing monolithic alumina and laminates of 3-D and the baseline 2-D weave as backing.

3-D woven composites showed the following advantages over the plain woven baseline:

1. Faster and more complete wet out during VARTM processing, probably due to resin channels inherent in their more heterogeneous fabric structure. This was observed during composite fabrication and in unrelated, product development work performed by 3TEX, but has not yet been quantified.
2. Reduction in preforming labor, corresponding to the reduction in ply count by using thicker, 3-D woven plies.
3. 6-20% improvements in static strengths over the baseline and several S-2 glass systems taken from the literature, even though the single ply 3-D woven composites tested have lower fiber volume fractions than the multiple ply baseline composites compared to them.
4. About 20% improvement in interlaminar G_{Ic}, using a rubber-toughened resin.
5. About 500% improvement in intralaminar G_{Ic}, using a rubber-toughened resin.
6. Up to about 20% smaller visible impact damage area under high energy drop tower impact testing.
7. Up to about 20% higher CAI strengths.
8. About 50% smaller visible impact damage area in non-perforating ballistic impact tests, at 6% lower areal weight.
9. The ability to pass NIJ 0101.04 level 3 standalone certification, backing an alumina core, at a weight of 8.1 lbs, while comparable weight inserts with the 2-D baseline as backing could not contain more than half of the six-shot protocol.

1. Introduction

This report details work performed in STTR ARMY00-T002. The objective of this investigation was to demonstrate improvements in composites for impact resistant and armor materials by using 3-D[1] woven (figure 1) instead of conventional, 2-D woven fabrics in fiber-reinforced plastic materials. To meet this objective, 3TEX, Inc. (3TEX) and the Center for Composite Materials at the University of Delaware (CCM) undertook the design, weaving, consolidation, static, laboratory dynamic, and ballistic testing of composites using 3-D weaves and comparable, currently used, mil-spec 2-D weaves. We restricted our investigation to fiber and resin systems of commercial interest for personnel and vehicle armor, choosing S-2 glass rovings in epoxy vinyl ester and epoxy (both rubber-toughened). The project culminated with the successful demonstration of a remarkably lightweight personnel body armor insert (BAI), using a 3-D woven fabric backing, under National Institute of Justice (NIJ) 0.101-04 Level III standalone.

Each set of tests is discussed individually. Final discussion includes practical considerations for FRP armor and impact-resistant systems made from 3-D weaves, and lays out 3-D woven FRP armor applications based on test results and practical considerations. We have submitted almost two hundred pages of photographic documentation as appendices in interim reports during this project. We omit these additional images here, wherever they do not contribute materially to the report. 3TEX will furnish any of these images upon request.

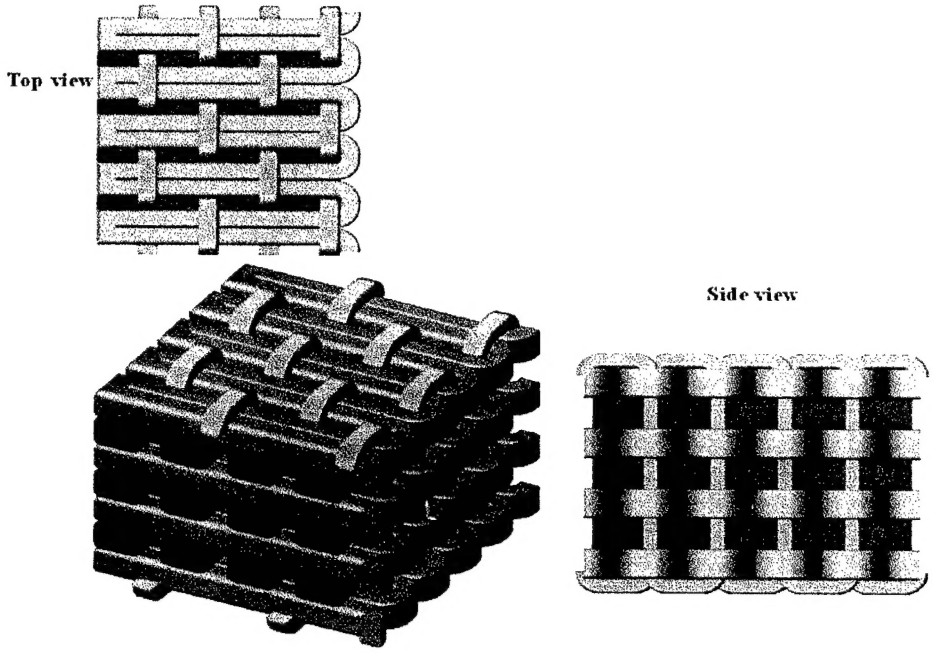

Figure 1: 3-D orthogonal woven structure. *N* planes of essentially straight, machine- or warp-direction yarns (shown in red) are separated by *N+1* planes of essentially straight, cross- or fill-direction yarns (shown in blue). The two systems are interlaced by a third set of yarns, called z-yarns (shown in green), which provide through-thickness reinforcement.

[1] '2-D' woven fabrics are defined as weaves which are two yarns thick, while '3-D' weaves are defined as thicker weaves. In this study, fabrics with areal weights of approximately 4-12 times the thickness and areal weight of the baseline, 2-D fabric were examined.

2. 3-D Woven Composite Design

2.1 Baseline Material

The baseline material considered was SBA240F-50", a 50-in wide, 24-oz/yd^2 plain weave (which we will generically categorize as '2-D') woven by Knytex. This fabric is woven from Advanced Glass Fibers (AGY) 250-yd/lb S-2 glass *rovings*[2], and is used for several current and planned military vehicles and personnel armor, including the Crusader and Composite Armored Vehicle programs. The fabric was finished with AGY style 463 sizing, which is epoxy compatible.

2.2 Design Constraints and 3Weave™ Fabric Design

The following constraints guided the design of the 3-D woven fabrics:

1. Use the same size and finish rovings – 250-yd/lb, size 463.
2. Fabric should be balanced in the weaver's sense, that is, there should be very similar amounts of reinforcement in the warp and fill directions.
3. Resulting composite should be balanced in the laminate sense, that is, there should be very similar elastic and strength properties in the warp and fill directions.
4. Resulting fabrics should have roughly square unit cells, of sizes close to the 24-oz baseline (0.4-in x 0.4-in).
5. Use 1-2% by fiber volume fraction of fiber in through-thickness direction.
6. Inventory cost of fiber needed for weaving set up should be minimized to stay within STTR budget.

Constraint 2 is not trivial to ensure, due to the 3-D orthogonal weave structure used (figure 1). 3-D orthogonal weaves have N+1 layers of fill for every N layers of warp. Thus, to satisfy constraint 2, the fabric must have either fewer yarns per inch in fill planes than in warp planes (compromising constraint 5), or use at least some yarns in the fill that are smaller than 250-yd/lb (compromising constraint 1). In 3-D orthogonal weaves, there is little crimp in either the warp or fill directions, therefore, there is approximately equal efficiency at translating fiber stiffness and strength into fabric stiffness and strength in either direction. This means that satisfying constraint 2 nearly assures satisfaction of constraint 3. Constraint 4 is to facilitate a rational comparison between the 3-D woven structure and the baseline fabric. The ratio of impact area to unit cell area may play a significant and unknown role in experimental impact response of FRP. The influence of this relation on comparisons between 2-D and 3-D architectures is mitigated by making 3-D weaves with unit cell sizes equal to the baseline.

Constraint 5 results from the competition for volume between in-plane and out-of-plane reinforcement inherent in 3-D reinforced fiber architectures. As seen by figure 1, the addition of through-thickness reinforcement 3-D orthogonal structure causes void pockets in the warp and fill yarn planes, reducing total fiber volume fraction. The influence of z yarn content (by percent weight in the unconsolidated fabric – assuming warp, fill and z yarns are made from the same type of fiber) on total fiber volume fraction is shown for a balanced fabric (*i.e.*, meeting constraint 2 above) in figure 2. Total fiber volume fraction would be a maximum at the (unrealizable) limiting cases of either no z-yarn (which would leave a cross-plied, nonwoven [0/90] laminate) or all z-yarn (which would leave a unidirectional material in z). Total fiber

[2] A *roving* is an untwisted assembly of bundles of fibers. AGY 250-yd/lb rovings consist of 30 bundles of 400 fibers each, with each bundle spun from a separate spinneret. Using multiple, small spinnerets assures uniform, fine fiber diameter and cooling-related microstructure at reduced cost. The disadvantage of rovings is that, because uniform tension cannot be maintained during the spinning of rovings, some of the fiber bundles are invariably slack, leaving rovings more difficult to weave than other forms of tows.

volume fraction is a minimum when warp, fill and z fiber weight fractions in the fabric are all equal at 1/3, which would result in a cubically orthotropic composite with $E_1=E_2=E_3$. Since total fiber volume fraction drops quickly from the limiting case of unidirectional cross ply as z-yarn content increases, a design compromise between in-plane and through-thickness reinforcement for impact-resistant 3-D woven composites is to use the minimum z-yarn content necessary to adequately suppress delamination. Many studies on low-velocity impact and static fracture mechanics (*e.g.*, [Dickinson *et al.* 1999]) of stitched and 3-D woven composites have shown that 2% through thickness reinforcement by preform weight is a good rule of thumb to compromise between high in-plane mechanical properties and delamination suppression. Prior development work at 3TEX on S-2 glass fabrics for ballistic applications corroborated this rule of thumb.

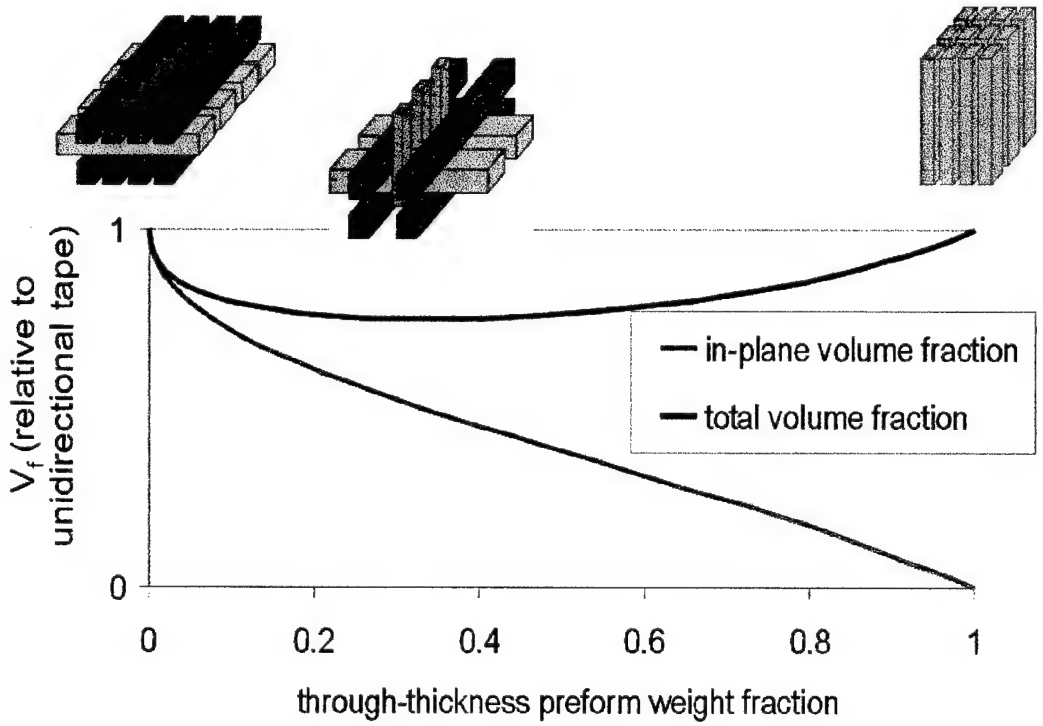

Figure 2: Total fiber volume fraction (relative to unidirectional tape) as a function of through-thickness fiber content for 3-D orthogonal composite. Note that the extreme cases (no through-thickness reinforcement, and no in-plane reinforcement) are not practically realizable.

The last constraint is a consideration for the economics of 3-D weaving of glass rovings. Since glass rovings are easily damaged by unwinding and rewinding, they are woven directly from the packages supplied by the yarn manufacturer. Therefore, one package is needed for every yarn in the warp direction of the fabric. Figure 3 gives an idea of the fiber inventory required to weave a thick 3-D fabric directly from packages. The lightest commercially available packages of S-2 glass are 10-lb. Current prices for 250-yd/lb S-2 glass rovings are ~$7.50/lb, or ~$75/package. For a balanced fabric (2 above), this translates into roughly $8/in width/(oz/yd^2) of fabric, excluding additional fiber for the fill- and z-directions. Since the final deliverable was ballistic data, requiring panels roughly 16-in x 16-in or more, 16-in fabric was considered the minimum useful width for this fabric. Thus, for reference, a 16-in wide fabric of around 100 oz/yd^2 would require about $3500 in fiber inventory for the warp direction only. Labor to feed so many yarns into the weaving machine would add to cost. Note that this does not make 3-D weaving uneconomical for full length weaving runs. Once prepared for weaving, this amount of fiber would convert all the fiber feed into fabric at about the same efficiency as conventional weaving, and could weave more than 2000 yards of fabric (if an equal amount of fiber was added in the fill

direction), more than needed for the STTR. When amortized over the entire weight of a long run, 3-D weaving set up costs are comparable to 2-D weaving set up costs.

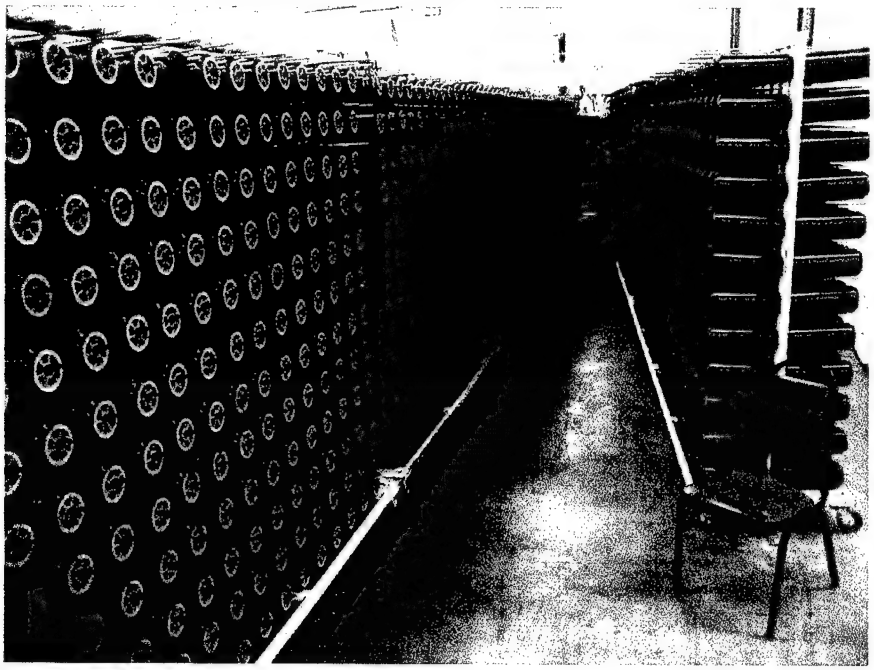

Figure 3: Fiber packages needed to weave thick 3-D weaves, for glass rovings and carbon fiber tows, which cannot be beamed. These rows of packages (or *creels*) is about a quarter of the fiber needed to weave a 1.5-in thick, 18-in wide fabric from 12K carbon tows. The number of fiber packages needed to weave a thick, wide fabric from S-2 glass rovings would be comparable.

The STTR budgeted $2000 for S-2 glass rovings. This is about the cost of the fiber actually *used* in weaving fabrics for the STTR, but much less than the cost of the fiber required to set up the weaving machine. Thus, a serious constraint on the STTR was timing fabric production for the STTR to follow commercial runs of S-2 glass roving fabrics, so that the cost of fiber inventory and machine set up labor could be defrayed from the STTR budget. This ultimately meant that most of the testing, which required several months after weaving, could only be performed on relatively thin 3-D weaves, which were woven early in the progam.

3TEX designed fabrics for the STTR using fabric geometry models developed in-house, to related weaving parameters to the resulting fabric structure. Composite elastic properties were predicted by in-house developed models based on stiffness averaging [Kregers & Melbardis 1978] and a generalization of the modified matrix method [Tarnopol'skii *et al.* 1973, Yushanov *et al.* 1999], as a check on composite balance (constraint 3 above) and for comparison to static mechanical testing. Table 1 describes the constructions of the baseline, and the fabrics designed and woven for STTR ARMY00-T002. Table 2 describes the unit cell sizes and weight fraction of fibers in warp, fill and z. Table 3 describes how each of the fabrics was used in phase 1.

Table 1:Weaving Construction of 3-D woven fabrics used in this STTR, and of baseline 2-D weave.

FABRIC	WARP			FILL				Z		HARNESS
	number of layers	ends per inch (1/in)	yield (yd/lb)	number of layers	picks per inch (1/in)	yield (yd/lb)		Z ends per inch (1/in)	yield (yd/lb)	
2	2	10	250	3	11	750 250	(top, bottom) (middle)	5	1250	2x2 basket
1	2	10	250	3	8	250 1250	(top, middle) (bottom)	5	1250	2x2 basket
3	4	10	250	5	11	750 250	(top, bottom) (middle)	5	1250	2x2 basket
4	5	10	250	6	11	750 250	(top, bottom) (middle)	5	1250	2x2 basket
5	2	20	250	3	22	750 250	(top, bottom) (middle)	5	1250	4x4 basket *(see text)*
SBA240F control	*1*	*10*	*250*	*1*	*10*	*250*	*n/a*	*not applicable*		*1x1 (plain weave)*

Fabrics 1 and 2 differed essentially in their surface roughness, with fabric 2 having a relatively smooth and a relatively coarse side, and fabric 1 having two identical sides, with profiles intermediate between those of fabric 1. Fabrics 3 and 4 had similar constructions to fabric 1, but added additional warp and fill layers to yield thicker fabrics (up to ~0.27-in per ply when consolidated under vacuum). Fabrics 3 and 4 are expected to have mechanical properties similar to fabric 2.

Fabric 5 was specially designed to weave a flap into the side of the fabric. This takes advantage of one of the unique features of 3-D weaves – profiles which can be woven to net shape. Fabric 5 was used to create double cantilever beam (DCB) coupons, with the flaps serving as the precracked regime. The fabric and DCB testing is described in section 4.3.

Table 2: Fabric areal weight, preform weight fractions, and unit cell sizes.

FABRIC	AREAL WEIGHT			PREFORM WEIGHT FRACTIONS			UNIT CELL SIZE	
	(oz/yd^2)	(psf)	(kg/m^2)	warp (%)	fill (%)	z (%)	warp (in)	fill (in)
1	93	0.65	3.12	50.9%	46.7%	2.4%	0.40	0.36
2	90	0.63	3.02	52.0%	45.7%	2.3%	0.40	0.50
3	190	1.32	6.37	49.0%	49.4%	1.6%	0.40	0.36
4	270	1.88	9.05	49.1%	49.5%	1.4%	0.40	0.36
5	180	1.25	6.03	49.0%	49.3%	1.7%	0.40	0.36
SBA240F control	*24*	*0.17*	*0.80*	*50.0%*	*50.0%*	*n/a*	*0.40*	*0.40*

Table 3: Testing Performed, broken down by fabric type. Additional testing performed in parallel to but outside of the STTR contract, as part of 3TEX's product development, are shaded in gray. Tests marked in bold used Derakane 8084 epoxy vinyl ester; others used SC-15 epoxy.

FABRIC	TEST						
	static stiffness &strength	double cantilever beam (DCB)	dynatup low velocity impact	compression after impact (CAI)	Hopkinson bar compression through thickness	non-perforating ballistic impact	NIJ ballistic impact (body armor inserts)
1	XX	X	X	X	X		
2			X	X	X		X
3	X						
4						X	
5		X					
baseline		X	X	X	X	X	X

2.4 3Weave™ Manufacture

All 3-D woven fabrics were manufactured by the 3Weave™ process, patented by 3TEX's founder [Mohamed & Zhang 1992]. In the 3Weave™ process (figure 3), multiple planes of straight warp yarns feed into the weaving zone, and are interplied with multiple planes of straight fill yarns. A third set of yarns, called z-yarns, weaves the fabric together. As shown in figure 1, the 3Weave™ structure contains N warp planes and $N+1$ fill planes. When compacted, the z-yarns travel essentially parallel to the fabric mid-plane normal in the interior of the fabric, and essentially parallel to the warp direction on the fabric surfaces. This process differs from 2-D weaving primarily by the simultaneous insertion of multiple fill yarns. In 2-D weaving, fill yarns are inserted singly. Therefore, the weaving time of a 2-D weaving process is proportional to the *volume* of material produced. By inserting multiple fill yarns simultaneously, weaving time via the 3Weave™ process is proportional to the *area* of fabric produced, mitigating the high weaving times which are one of the greatest disadvantages in weaving thick fabrics on 2-D looms. A drawback to the 3Weave™ process is that it requires custom weaving machines. During this STTR, 3TEX built and put into service four new 3Weave™ machines, one of which wove fabrics 3 and 4.

At the start of the STTR, the special T-shaped fabric 5 was already in inventory. It was used to make special DCB coupons, as described later. Initial fabric production for the STTR was limited by the cost of fiber inventory to fabrics 1 and 2, thus, most of the work on low strain rate testing was performed on these materials. In about the fifth month of the STTR, 3TEX was able to combine needs for thicker fabrics for the STTR with other requirements for S-2 glass fabrics, and weave fabrics 3 and 4.

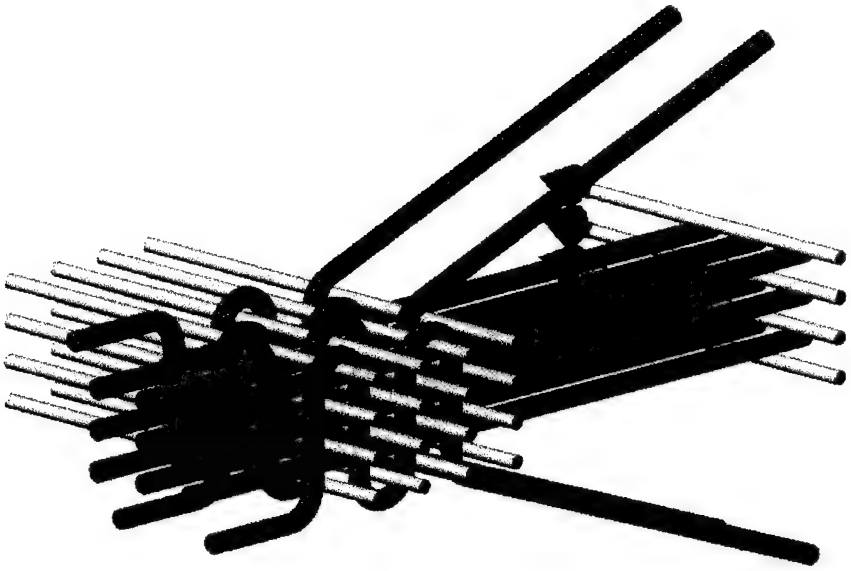

Figure 4: The 3Weave™ process: multiple, non-interlaced fill yarns (shown in pink) are inserted simultaneously between multiple non-interlaced planes of warp yarns (shown in blue). A third set of yarns, called z yarns (shown in red), travels through the thickness of the fabric and weaves it together.

2.5 Discussion

3-D woven fabric design and construction was limited by the cost of buying and drawing in a large number of S-2 glass rovings into a 3-D woven fabric. As seen in figure 4 above, a single 3Weave™ fabric uses the same number of yarns as multiple 2-D fabrics, weaving simultaneously. Therefore, while weaving set up costs *per weight* of fabric produced for a long weaving run are comparable to those of traditional weaving, set up costs *per area* of fabric produced, or for short production runs typical of development projects, can be high. A consequence for this project was that most fabrics woven early in the project were fairly thin (with each ply the equivalent of ~4 plies of the baseline), while thicker fabrics had to wait until unrelated development work on S-2 glass rovings fabrics at 3TEX could defray set up costs.

We did not have a rigorous design criterion for determining through-thickness reinforcement content. We used an amount (~2% by preform weight) which has been seen to be the minimum necessary to significantly improve G_{1c}, compression after impact strength, and decrease impact delamination area in studies conducted primarily at NASA on carbon fiber / epoxy systems subjected to static or low velocity impact loading [Dickinson *et al.* 1999]. Our simulations and experience show that more through-thickness reinforcement comes at the expense of in-plane strengths and stiffnesses. Previous development of 3Weave™ S-2 glass roving fabrics for FRP armor systems has shown this design guideline to be acceptable, however, we do not know if changing the amount of through-thickness reinforcement will improve performance in armor and impact-resistant systems.

3. Composite Manufacture

S-2 glass fabrics were consolidated into composites using vacuum assisted resin transfer molding (VARTM). In this process, a composite preform is laid up on a surface, which forms the tool for

one or more sides of the composite. A plumbing system is built around the preform, to allow at least one inlet for resin, and at least one exhaust to a vacuum source. A vacuum bag is built around the preform and plumbing, and forms the tool surface for at least one side of the part. The bag is then evacuated, resin introduced, the part filled, the resin supply and vacuum exhaust sealed, and the part allowed to cure. The process offers advantages in part-to-part consistency, controlling porosity, relatively high fiber volume fraction (50-55% is typical for many VARTM parts), the ability to scale to large, non-autoclavable parts such as boats and ground vehicles, and low mold cost. The difficulty of the VARTM process is developing a plumbing system, which accounts for the permeability tensor of the preform, the shape and thickness of the part, and the time-viscosity curve of the resin, to allow complete wet out shortly before gel. Approaches are described in the patent and the academic literature. Table 4 gives typical properties of the resins used, as reported by the manufacturers.

Table 4: Properties of resins used in this study. Specific gravity of SC-15 determined by CCM. All other data is from manufacturers' data sheets. All data is from clear casts.

trade name resin type Manufacturer	Derakane 8084 rubber-toughened epoxy vinyl ester Dow Chemicals	SC-15 rubber-toughened epoxy cycloaliphatic amine Applied Poleramics, Inc.
Number of components	3	2
specific gravity	1.13	1.19
room temp. viscosity (cPs)	350	350
tensile failure strain (eng)	8-11%	*not available*
K_{1c} (psi sqrt in / MPa sqrt m)	*not available*	1400 / 1.53
tensile strength (ksi / MPa)	10.5 / 72	*not available*
tensile modulus (Msi/GPa)	460 / 3.2	*not available*
flexural strength (ksi / MPa)	17 / 117	19.1 / 131
flexural modulus (ksi / GPa)	440 / 3.0	390 / 2.7
cost in drum quantity	$2.25/lb	$7.50/lb

Composite plates of fabrics 1,2, 4 and the baseline were made at 3TEX. Polyethylene and polypropylene sheeting was used as the tool. To minimize warpage, the tool sheeting was sealed by vacuum to a 0.5-in thick steel plate. Single ply panels of fabric 2 were made for static mechanical characterization. About 200 lbs of plates, with nominal thicknesses of 0.26-in to 0.,28-in were made for low velocity and ballistic impact testing. Laminates up to 1.2-in thick were made for Hopkinson bar testing. After cure, panels sent for static and low velocity impact testing were post-cured at CCM at 180°F for 3 hours. Panels for non-perforating ballistic impact could not fit into the oven used, and so were post-cured for one week in ambient and 54 hours at 140°F.

Single ply composites of fabrics 1 and 3, and DCB specimens of fabrics 1, 5 and the baseline, were manufactured using Applied Poleramic, Inc. (API) SC-15, a two-phase rubber-toughened epoxy resin. This resin requires either long evacuation times (~24 hours) or a heated tool to gel, making it more difficult to work with in laboratory quantities. Single ply flat panels were consolidated and tested at North Carolina Agricultural and Technical State University, in Greensboro, NC. Special DCB test coupons were manufactured at CCM. Both studies were part of work outside of the STTR program, whose results were promised in our proposal.

The fiber volume fraction attainable in 3Weave™ composites increases with the number of plies in a part. Figure 5 shows fiber volume fractions (determined by ASTM D3171, method 2) for

composites of fabric 1 made by VARTM with Derakane 8084. Single ply composites were made for static characterization, and had fiber volume fractions (later verified by ignition) of ~49%. This is an important concern, because a pitfall common in 3-D woven composite design and manufacture has been low total fiber volume fraction (*e.g.*, [Jarmon *et al.* 1998]). We believe that the influence of ply count on fiber volume fraction in the fabrics used is caused by the rough surface of the 3Weave™ fabrics produced. As seen in figure 1, the fabrics leave resin-rich channels, parallel to the fill yarns. Cuts across multiple ply 3Weave™ composites show that neighboring layers nest to fill these interstices, leaving resin-rich regions only on panel surfaces. Three-ply composites used in subsequent low-velocity impact tests had fiber volume fractions of ~56%, which is a typical range for VARTM multi-ply laminates of 2-D weaves (figure 5).

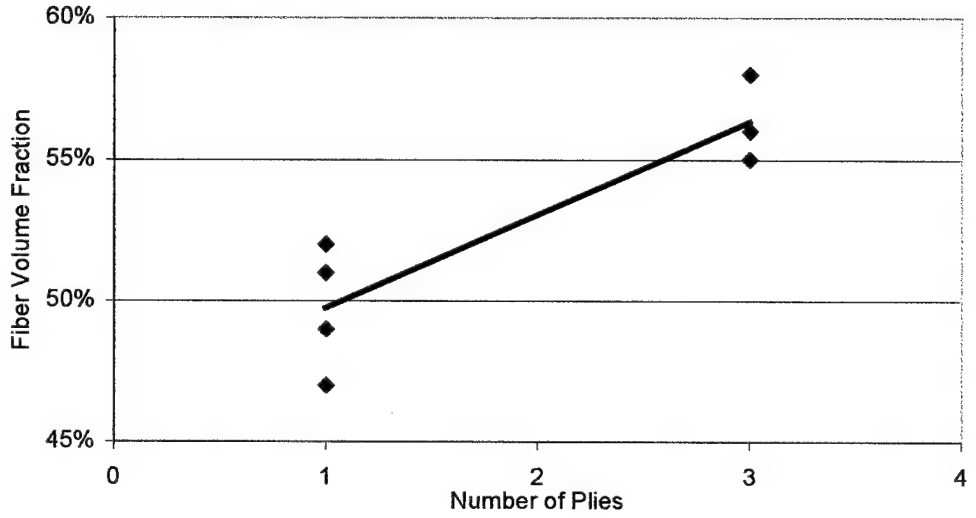

Figure 5: Fiber volume fraction (ASTM D3171, method 2) versus number of plies for VARTM composites of 3Weave™ fabric 1 in Derakane 8084.

4. Static Testing

4.1 Introduction

Table 5 lists the tests performed to determine static elasticity constants and strengths. Table 6 lists mode 1 crack propagation tests performed to determine in-plane G_{1c}. All static tests except the through-thickness compression tests were conducted as part of 3TEX product development, in parallel to the STTR program, and are reported here as promised in our proposal.

Table 5: Tests performed to determine static elasticity constants and strengths on 3-D woven S-2 glass composites during STTR.

3Weave™ fabric	2	2	3	2
Number of plies	1	1	1	12
Resin	Derakane 8084	SC-15	SC-15	Derakane 8084
consolidated at	3TEX	NCA&TSU	NCA&TSU	3TEX
tested at	IPM	NCA&TSU	NCA&TSU	CCM
ASTM test method for...				
Tension	D3039	D3039		
Compression	D3410	D3410		D695
Flexure	D790 (16:1)	D790 (16:1)		
Short beam shear	D2344	modified D2344		
In-plane shear	D5379	D5379		
Fiber volume fraction	D3171	D3171		D3171 (method 2)

Table 6: Tests performed at CCM to determine in-plane G_{1c} of 2-D and 3-D woven S-2 glass composites during STTR.

fabric	baseline	2	5
matrix	SC-15	SC-15	SC-15
test method	modified D5528		
to test...	interply G_{1c}	interply G_{1c}	Intraply G_{1c}

4.2 Static Strengths and Stiffnesses

This report will not discuss the testing methods employed. Interested readers are referred to [Tarnopol'skii & Kincis 1985] for a discussion of test methodology, and [Bogdanovich & Pastore 1996] for commonly understood difficulties of static testing textile-reinforced composites.

Table 7 gives the reported elasticity constants and strengths. Also included for comparison are unpublished tests performed at CCM on laminates from the baseline fabric in SC-15 resin. Note that the plain woven composite has a higher fiber volume fraction than the single-ply 3-D woven composites examined, for reasons discussed above. The Institute of Polymer Mechanics, Riga, Latvia (IPM), performed additional in-plane shear tests, using single rail shear (ASTM D4255) and plate twist [Tarnopol'skii & Kincis 1985] to verify the double-notched shear tests reported. Results of the additional in-plane shear tests are within about 10% the ASTM D5379 values. IPM performed ASTM D2344 short beam shear tests, to determine apparent interlaminar shear strengths, using 5:1 aspect ratio. They found that the specimens crushed at the central contact point before interlaminar shear failure, and therefore did not determine apparent interlaminar shear strengths.

The short beam shear tests performed by NCA&TSU were modified from the ASTM D2344 standard, by using a steel platen with a stiff, rubber face as the center support. This essentially created a four-point bend rather than a three-point bend loading, but with the bearing stress concentration mitigated by the rubber. The method is described in [Abali *et al.* 2000]. NCA&TSU performed flexure tests in four-point bend, using 25:1 aspect ratio tests (the minimum recommended aspect ratio to ensure flexural failure of balanced glass laminates in ASTM D790 is 16:1). They reported that failure in the flexural tests failure appeared induced by mixed in-plane load (from flexure) and interlaminar shear. Thus, their reported flexural strengths are lower bounds of the actual composite flexural strengths.

Table 7: Static elasticity constants and strengths of composites of 3Weave™ and baseline S-2 glass composites. 1 is warp direction, 2 is fill direction, 3 is z or through-thickness direction. All work except CCM tests of fabric 1 was conducted outside of the STTR program, but is reported here as promised in our proposal.

Fabric	1						3		baseline	
resin	Derakane 8084				API SC-15		API SC-15		API SC-15	
processed at:	3TEX				NCA&TSU		NCA&TSU		CCM U-Del	
tested at:	IPM, Riga, Latvia		CCM U-Del		NCA&TSU		NCA&TSU		CCM U-Del	
	value	std dev	value	std dev	value	std dev	value	std dev	value	std dev
tension	D3039				D3039		D3039		D3039	
E_{1t} (Msi)	3.58	2%			3.19	3%	3.17	2%	3.99	
E_{2t} (Msi)	3.01	2%			2.64	1%	3.24	3%		
ν_{12}	0.10	10%			0.11	0%	0.12	0%	0.11	
ν_{21}	0.11	12%			0.10	0%	0.11	0%		
σ_{1t} (ksi)	104.46	3%			103.9	6%	104.6	2%	87.6	
σ_{2t} (ksi)	93.26	1%			89.8	9%	105.2	2%		
compression	D3410		D695		D3410		D3410		D3410/D695	
E_{1c} (Msi)	4.47	2%								
E_{2c} (Msi)	4.15	2%								
E_{3c} (Msi)			1.50						1.67	
ν_{31}			0.19						0.18	
ν_{32}			0.19							
σ_{1c} (ksi)	47.9	6%			55.9	16%	74.7	8%	42.1	
σ_{2c} (ksi)	36.2	9%			36	10%	68.9	5%		
σ_{3c} (ksi)			86.3						94.5	
flexure	D790 (3-point, 16:1)				D790 (4-point, 25:1)		D790 (4-point, 25:1)			
E_{1f} (Msi)	3.23	5%			3.43	4%	3.43	4%		
E_{2f} (Msi)	3.03	4%			3.32	5%	3.32	5%		
σ_{1f} (ksi)	59.4	5%			*50.8*	*0%*	51.1	4%		
σ_{2f} (ksi)	52.2	4%			*56.9*	*0%*	47.0	3%		
in-plane shear	D5379				D5379		D5379		D5379	
G_{12} (Msi)	0.65	0.22			1.01	35%	1.41	13%	0.414	
G_{21} (Msi)	0.56	0.15			1.07	22%	1.29	5%		
τ_{12} (ksi)	7.93	0.06			4.6	7%	5.24	4%	10.9	
τ_{21} (ksi)	7.49	0.04			4.45	5%	5.39	1%		
Short beam shear	D2344 (5:1)				D2344 modified (5:1)		D2344 modified (5:1)			
τ_{13}* (ksi)	*crushing failure*				6.63	2%	6.83	2%		
τ_{23}* (ksi)	*crushing failure*				5.60	5%	6.84	4%		
Fiber Volume Fraction	D3171				D3171 (method 2)		D3171 (method 2)		D3171 (method 2)	
% V_f	49%				52%	6%	51%	1%	55%	

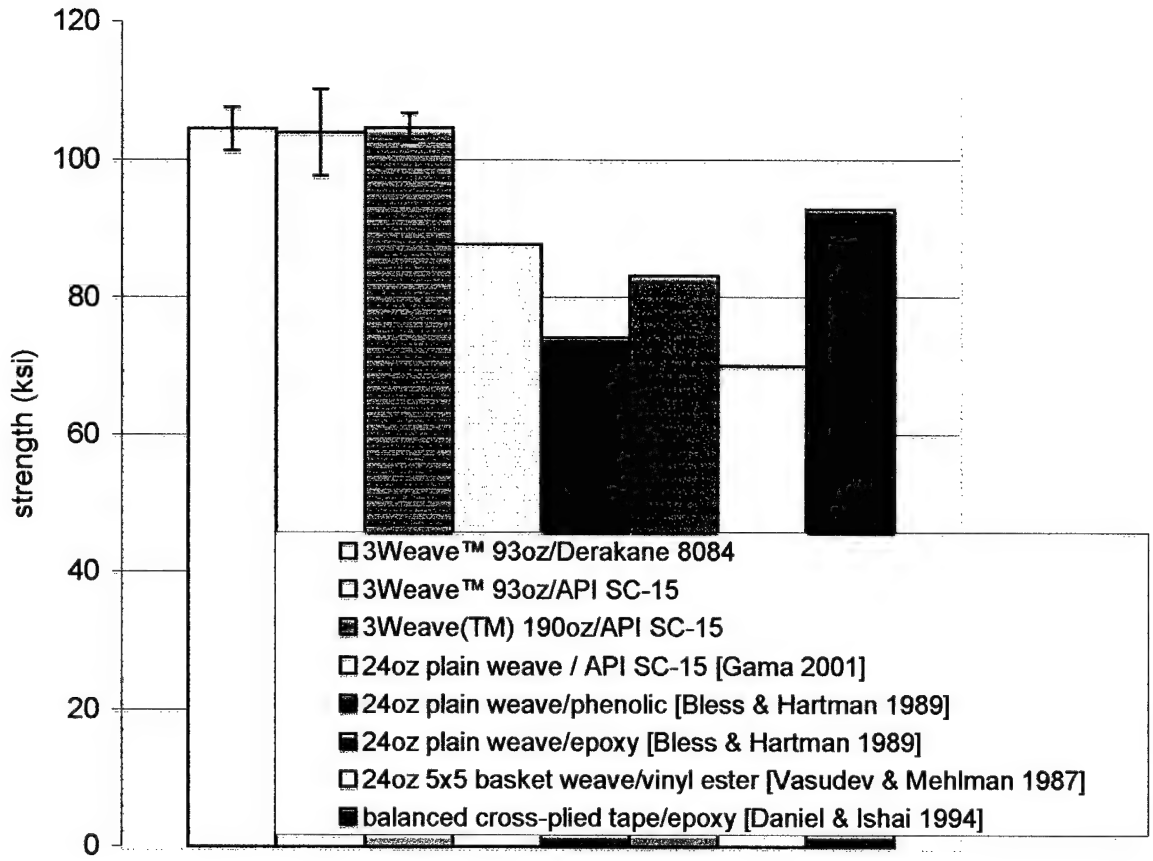

Figure 6: Warp tensile strengths of 3Weave™ S-2 Glass composites, compared to other S-2 glass composites considered for armor applications from the literature. Typical strengths of cross-plied laminates are also shown for comparison. Error bars on 3Weave™ values are standard deviations.

Tensile strengths of 3Weave™ S-2 glass composites are compared with S-2 glass laminates considered for ballistic applications, reported in the literature, in figure 6. The 3-D woven composite tensile strengths, in Derakane 8084 or SC-15, are higher than other textile systems found in the literature, including typical strengths of cross-plied unidirectional S-2 glass / epoxy laminates.

4.3 Mode 1 In-Plane Crack Propagation

4.3.1 Introduction

A parallel investigation, funded by 3TEX for internal research and conducted by CCM and conducted at the same time as the STTR, determined mode 1 in-plane critical strain energy release rates, G_{1c}, in 2-D and 3-D woven composites. The tests used a modification of ASTM D5528 double cantilever beam (DCB) tests, developed at CCM for 3-D woven composites [Guenon *et al.* 1989, Byun *et al.* 1990]. Information presented here is taken from the final report submitted by Gama and Gillespie of CCM to 3TEX. This report does not cover the background of mode 1 fracture toughness testing in laminates; interested readers are referred to elementary texts on fiber-reinforced composites, such as [Daniel & Ishai 1994], and to [Chou 1992] for a general discussion of fracture toughness testing on 3-D reinforced composites. The number of repetitions was not sufficient to determine G_{1c} values with precision. However, we believe the observed increase in G_{1c} given by through-thickness reinforcement proved sufficiently large (about a factor of five increase) to be insensitive to uncertainty in the test results due to small sample population.

4.3.2 DCB Coupon Weaving, Consolidation, and Fabrication

Using D5528 specimens on composites with significant through-thickness fiber reinforcement tends to fail the specimen not by interlaminar crack propagation, but by hinge failure in one of the specimen legs, starting from the crack tip. Forcing in-plane crack propagation in through-thickness reinforced composites requires a modifed test specimen. This section describes such modified tests, used to determine interlaminar G_{1c} of the 24-oz baseline, interlaminar G_{1c} of laminated 3Weave™ (fabric 2, 93-oz), and G_{1c} of in-plane cracks inside a 3Weave™ ply (fabric 5, 180-oz), for the S-2 glass roving fabrics studied. Figure 7 shows a schematic of fabric 5. The integrally woven flap allowed the in-plane starter crack, necessary for DCB tests, to be embedded into the preform by release film prior to infiltration.

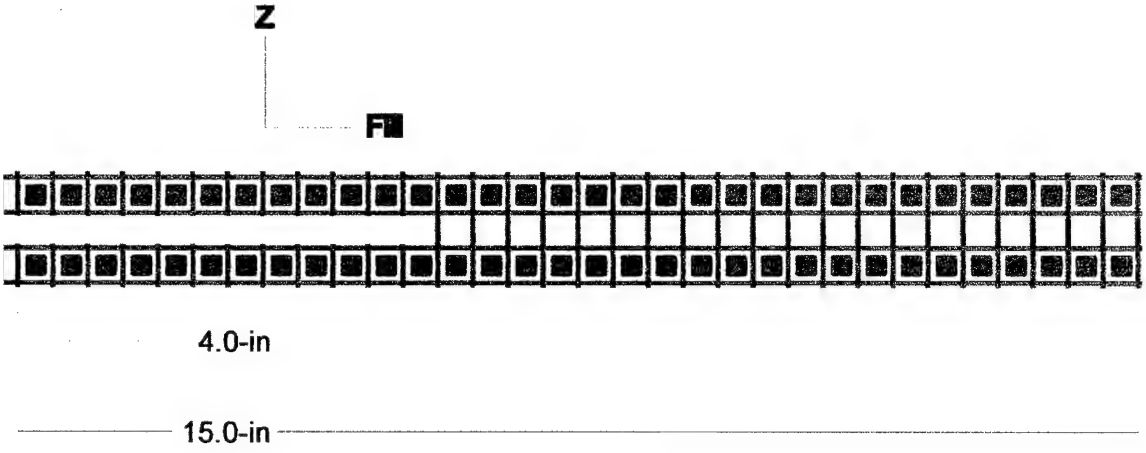

Figure 7: Structure of 3Weave™ fabric 5 in fill-z plane, used for DCB coupons. Warp yarns are red, fill yarns blue, and z yarns green. Unit cell size not to scale (there are many more warp yarns than pictured). Note that z yarns do not reinforce entire thickness on one side, allowing precrack to be formed by film insertion prior to infiltration.

A double bag vacuum assisted resin transfer molding (VARTM) process (previously found suitable in processing 3Weave™ fabric) was used to fabricate the composite laminate for DCB specimens. The lay-up in the VARTM process was as follows, starting from the tool side:

Tool
One layer breather cloth
One layer peel ply
Preform (see below)
One layer peel ply
One layer breather cloth
Distribution media
Vacuum Bag

The lay-up sequence of the preforms was:

Baseline Fabric: The DCB specimen lay-up sequence was $[24\text{-oz}]_{5s}$, with Kapton film placed in the plane of symmetry.

3Weave™ Fabric number 2: The DCB specimen lay-up sequence was $[24\text{-oz}/\ 93\text{-oz}]_{2s}$, with Kapton film placed in the plane of symmetry.

3Weave™ Fabric number 5: The DCB specimen lay-up sequence was [24 oz/ 180 oz/ 24 oz], with Kapton film placed between the leaves of the Y-beam.

The vacuum line was placed in the Kapton film delamination side of the bag. The 180-oz Y-beam fabric had two Z-yarns on the intersection line, to facilitate weaving of the transition between an open and a closed section. This was double the density of Z-yarns throughout the laminate. This inconsistency was eliminated by taking one of the Z-yarns out from the intersection line.

The preforms were infiltrated with SC-15 epoxy and cured at room temperature. This two-phase, rubber-toughened epoxy arguably represents a worst-case to demonstrate G_{Ic} improvements via through-thickness fiber reinforcement, because G_{Ic} of a 2-D laminate with such a tough resin will be high without through-thickness fiber reinforcement [Byun *et al.* 1990]. The post curing cycle was 30 min at 200 °F followed by 90 min at 260 °F. The post-cured laminates were slot ground to make DCB specimens (L = 10-in and b = 1-in, Figure 8). Aluminum loading blocks (1-in x 1-in x 1-in with a 0.5-in central hole) were adhesively bonded to the cracked end of two 24-oz and two 93-oz specimens such that the initial nominal crack length, a_0 = 2-in (Figure 8). Steel flat bars of cross section 1-in x 0.25-in and length 9-in were used as metal tabs. Aluminum loading blocks were bolted at one end of the steel bars (figure 9). Three specimens made from 180 oz (3-D composite) material were bonded with steel tabs. In order to examine the effect of steel tabs, one specimen from each 24-oz and 93-oz material was also bonded with steel tabs.

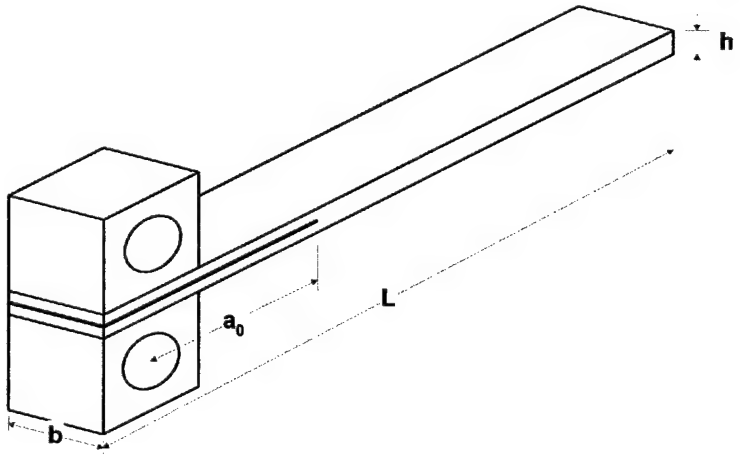

Figure 8: Double cantilever beam (DCB) specimen, showing nomenclature.

4.3.3 DCB Testing

A displacement control Instron 4484 universal testing machine with a 1000-lb load cell was used to conduct the experiments. Applied load, P, and load point deflection, δ, data were acquired through an interfaced computer. The propagation of crack front was monitored with a magnifying glass and the corresponding deflection was recorded from the Instron display. The correct applied load and load point deflection was determined from the load-deflection data acquired in the computer. All specimens were tested at room temperature and at a crosshead speed of 0.075 inch/min. Figures 10-12 show DCB specimens of the 24-oz baseline, the 93-oz 3Weave™ #1, and the 180-oz 3Weave™ #5 being tested. The tabbing used, and its effects on results, are described below. Note the irregular surface between the nested plies of the 93-oz fabric, and the pull-out of the z-yarns on the surface of the 180-oz fabric.

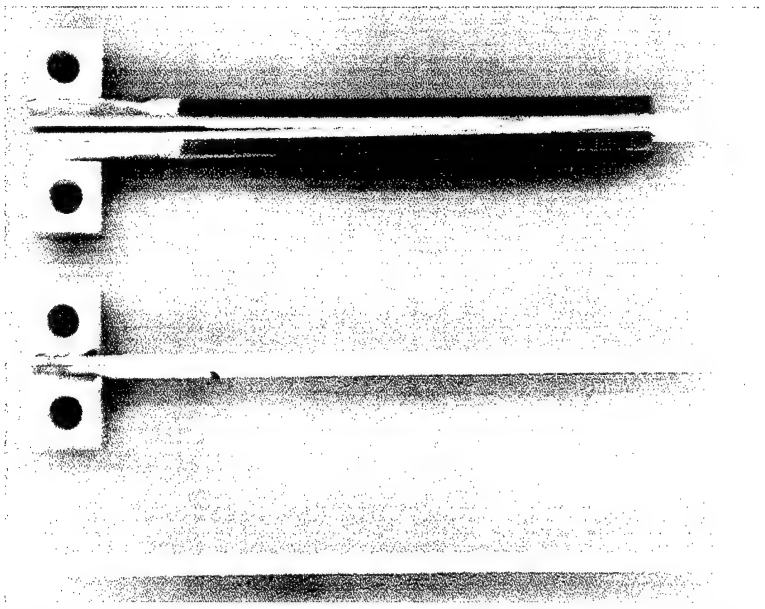

Figure 9: DCB coupon fabrication steps. Bottom: infused panel, with Kapton film crack initiator on left side. Center: aluminum loading blocks, bonded directly to coupon per ASTM D5528. Top: tabbed DCB coupon, developed at CCM to determineG_{1c} in 3-D woven composites.

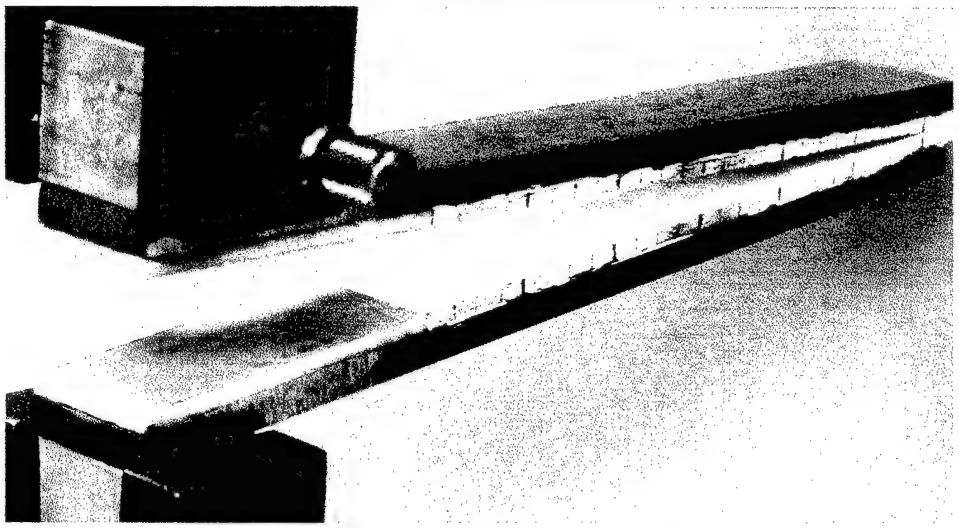

Figure 10: Tabbed DCB specimen (specimen 3) for 24-oz (baseline).

4.3.4 DCB Data Reduction

The deflection, δ, of a cantilever beam is given by:

$$\delta = \frac{PL^3}{3E_f I} + \frac{6PL}{5bhG} \qquad [1]$$

where P is the applied load, L is the beam length, E_f is the flexural modulus, E_fI is the flexural rigidity of the beam, b is the width, h is beam height and G is the interlaminar shear modulus. The first term of Equation 1 is the bending deflection and the second term is shear deflection. The compliance of the DCB specimen is expressed as:

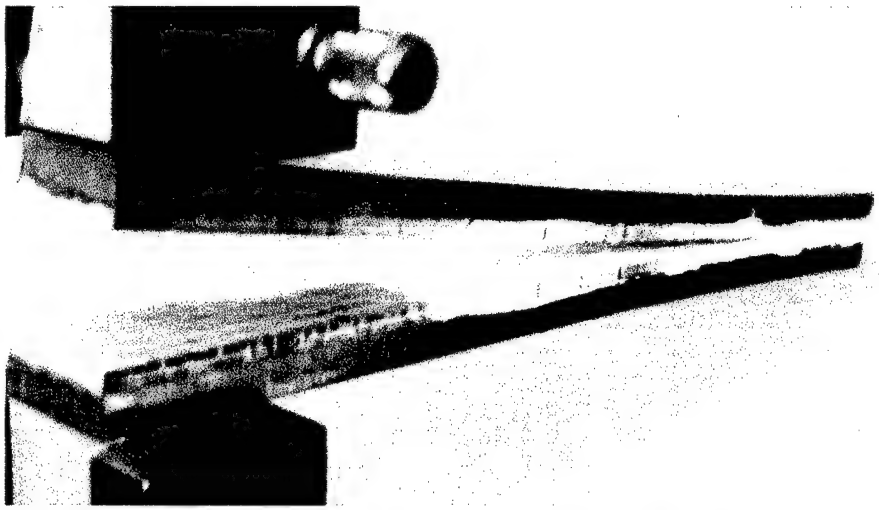

Figure 11: Tabbed DCB specimen (specimen 3) for 93-oz (3Weave™ #1).

Figure 12: Tabbed DCB specimen (specimen 3) for 180-oz (3Weave™ #5).

$$C = \frac{\delta}{P} = \frac{8a^3}{E_f bh^3} + \frac{12a}{5bhG} \qquad [2]$$

where a is the crack length. Equation 2 shows that the bending dominated compliance is a cubic function of crack length and the shear deflection is a linear function of crack length.

The mode I strain energy release rate is given by:

$$G_I = \frac{dU}{da} = \frac{P^2}{2b}\frac{dC}{da} \qquad [3]$$

where U is the strain energy stored in the specimen.

If the shear deformation is negligible, then the critical strain energy release rate of a built-in double cantilever beam is given by:

$$G_{IC} = \frac{3P_C\delta_C}{2ba} \qquad [4]$$

where a is the instantaneous delamination length, and the subscript c stands for critical. Equation [4] can be modified using compliance calibration (CC) method as:

$$G_{IC} = \frac{nP_C\delta_C}{2ba} \qquad [5]$$

where n is determined from the least square slope of log(C) vs. log(a) plot.

The strain energy stored in a specimen can be experimentally determined by measuring the area under the load-deflection curve. For an incremental crack growth, da, the incremental strain energy release, dU, can be calculated by unloading the specimen at regular crack intervals. This method is the area method of determining G_{IC}, and can be expressed as:

$$G_{IC} = \frac{\Delta A_i}{b\Delta a} \qquad [6]$$

where ΔA_i is the area bounded by the loading unloading curves. In this study, both compliance calibration and area methods were used to calculate the G_{Ic} values.

Figure 13 shows the load-deflection plot of a regular 24-oz DCB specimen at a constant displacement rate. The solid circles represent the load deflection point where a specific crack growth is recorded. The step drops of load represent crack propagation and arrest previously observed for plain weave S-2 glass/vinyl ester systems tested at CCM. The second, regular 24-oz DCB specimen was unloaded at different crack lengths (figure 14). Solid circles connected with a solid line represent the load-deflection points used in CC data reduction scheme. A linear load drop to the origin is assumed in the area method. Figure 15 shows the superposition of figure 16 and figure 17, which shows that these load-deflection data are consistent. The tabbed 24-oz specimen is loaded at constant displacement rate and the load-deflection plot is presented in figure 18. Incremental crack growth points are marked with solid circles. Compliance data have been calculated from the load-deflection curves as a function of crack length. Figure 19 shows the compliance of regular and tabbed 24-oz DCB specimens as a function of crack length. A linear growth pattern in log-log scale shows that the deflection is bending dominated and the shear is negligible. The exponent n is determined by least square curve fitting and subsequently used to compute G_{IC} using Equation 5. Figure 20 shows the critical strain energy release rate of 24-oz material as a function of crack extension. The CC method using regular DCB method is presented as hollow circles and squares, and an average propagation value, G_{IC} = 8.6 in-lbs/in^2 is calculated. The tabbed 24-oz DCB specimen (inverted open triangles) gave about 8% higher G_{IC} (9.3 in-lbs/in^2) values. The area method for regular DCB specimens (open circles with a "+") showed consistent results while the tabbed DCB specimen (double-cross) showed a R-curve behavior having the plateau region being consistent with the data obtained from CC method.

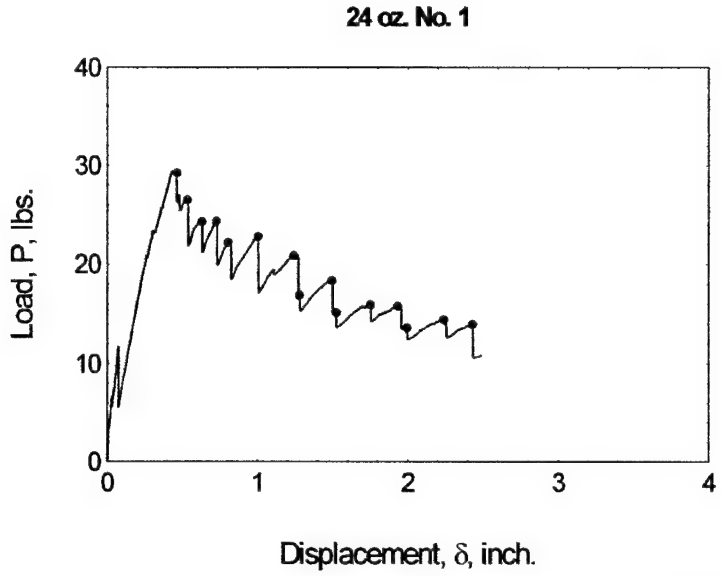

Figure 13: Load-displacement plot of regular DCB 24-oz baseline (Specimen No. 1) at constant displacement rate.

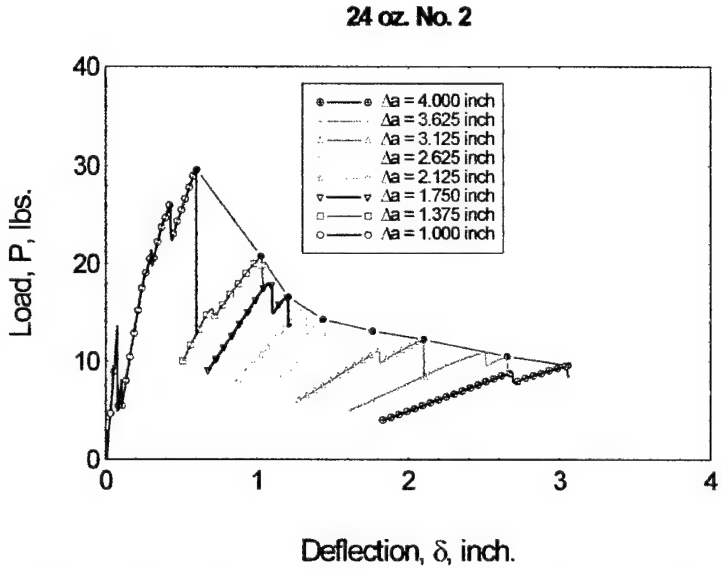

Figure 14: Load-displacement plot of regular DCB 24-oz baseline (Specimen No. 2) with unloading and reloading at different crack extension.

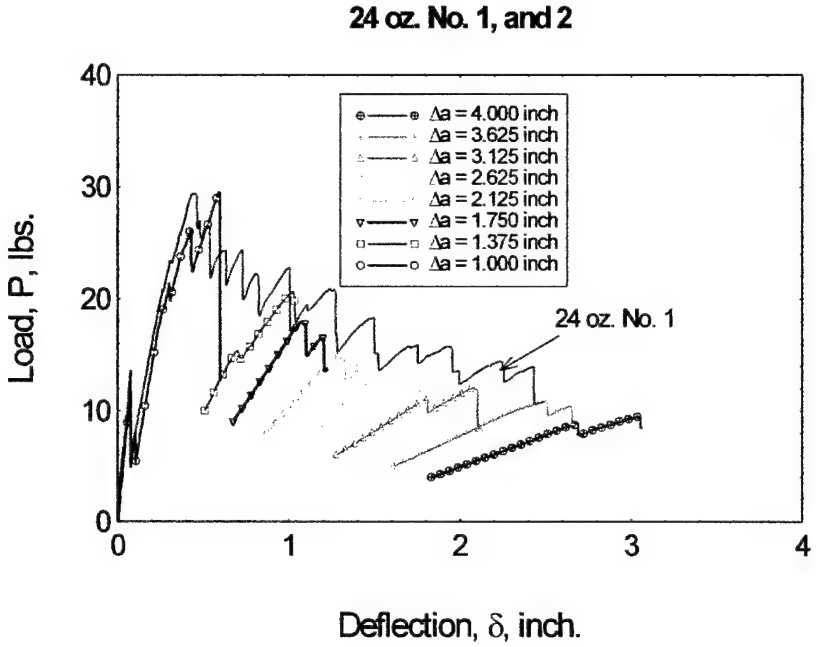

Figure 15: Load-displacement plot of 24-oz specimens 1 and 2 superposed.

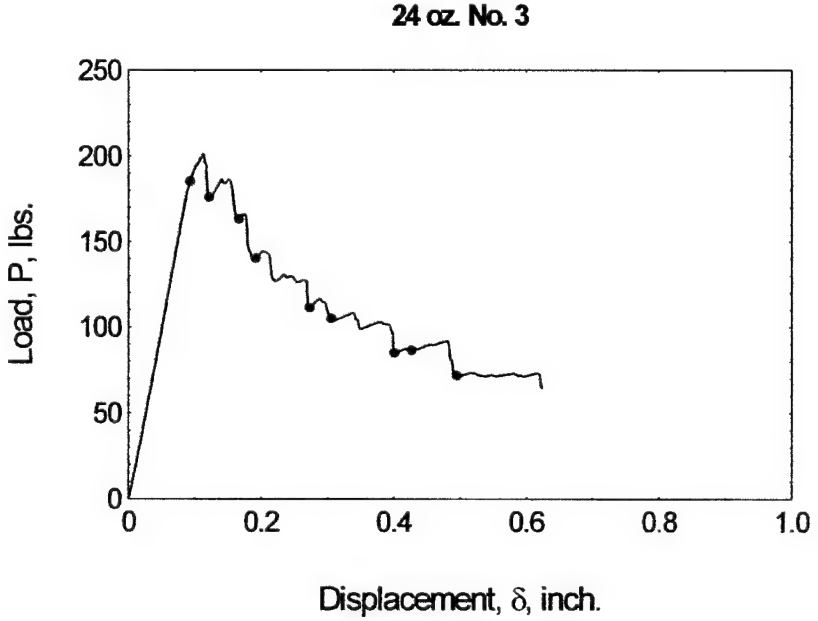

Figure 16 Load-displacement plot of tabbed DCB 24 oz baseline (Specimen No. 3) at constant displacement rate.

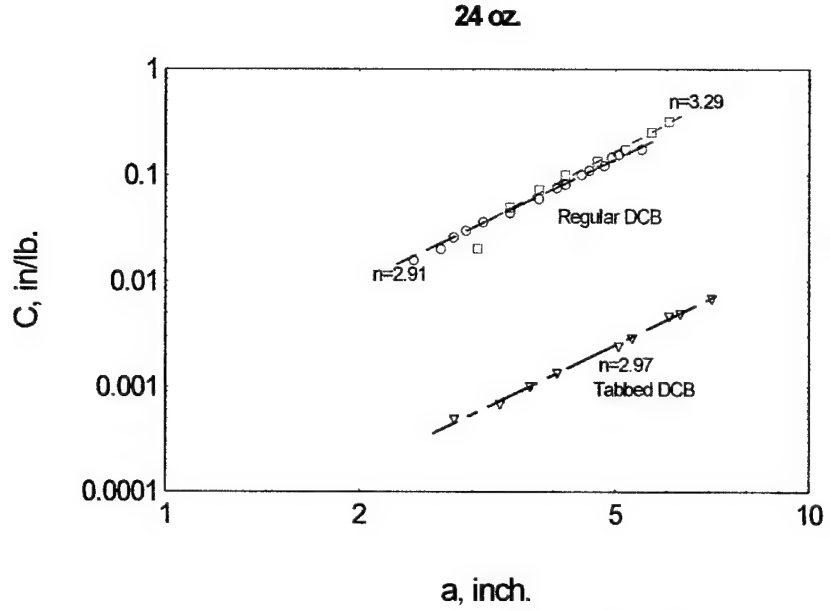

Figure 17: Compliance versus crack length for all 24-oz baseline specimens.

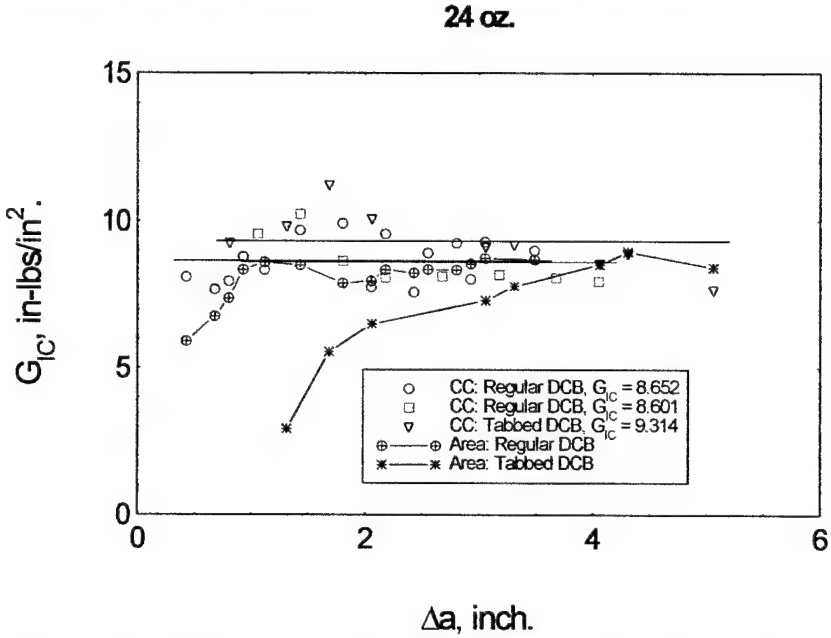

Figure 18: Critical energy release rate as a function of crack extension (24-oz baseline).

One regular 93-oz DCB specimen was tested under constant displacement rate (figure 19), and one regular 93-oz DCB specimen was unloaded at incremental crack growth (figure 20). Solid circles in figure 20 represent the load-deflection pair at incremental crack growth. Figure 21 shows the load-deflection plot of the tabbed DCB specimen. The compliances as a function of crack length are presented in Figure 22. All the three specimens showed linearity in log-log scale, indicating that shear deflection is negligible. CC and area methods were used to reduce the load-deflection and compliance data into G_{IC} values (figure 23). Open circles and squares represent the regular DCB data and open inverted triangles represent the tabbed DCB data processed using CC method. Circles with a "+" mark inside represent the area method of regular DCB data and double-cross points represent the area method of tabbed DCB data. The average critical energy release rate for regular DCB specimens was 9.2 in-lbs/in^2 and for tabbed DCB

specimens was 12.9 in-lbs/in^2 (CC method). The G_{IC} values for tabbed DCB specimen is about 40% higher than that calculated using CC method. The area method for regular DCB specimens are consistent with CC data, however, the tabbed DCB data obtained using area method showed an R-curve behavior, similar to the baseline, 24-oz specimens.

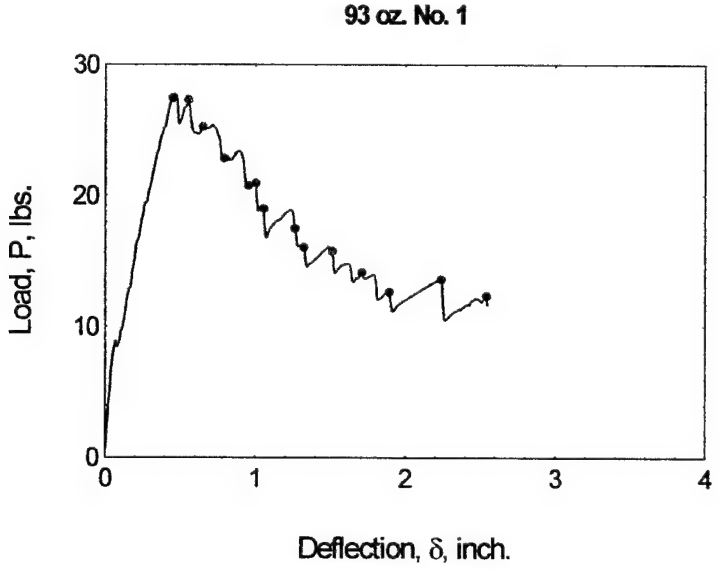

Figure 19: Load-displacement plot of regular DCB 93-oz specimen (No. 1) at constant displacement rate.

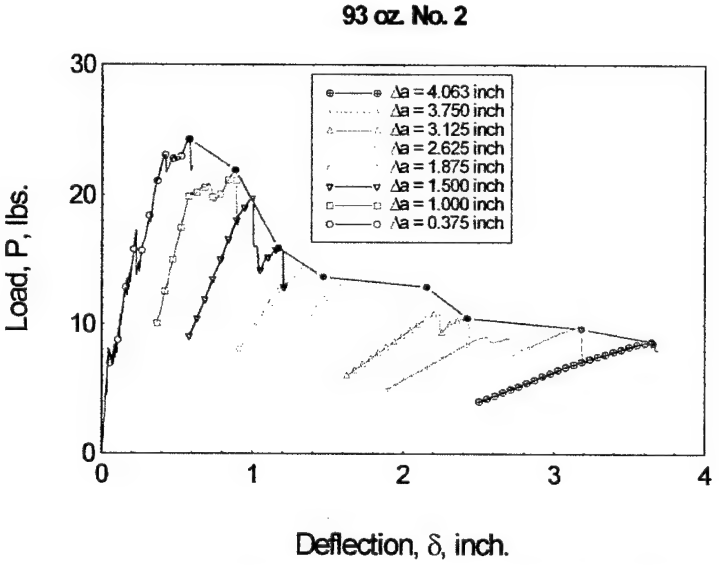

Figure 20: Load-displacement plot of regular DCB 93-oz specimen (No. 2) with unloading and reloading at different crack extension.

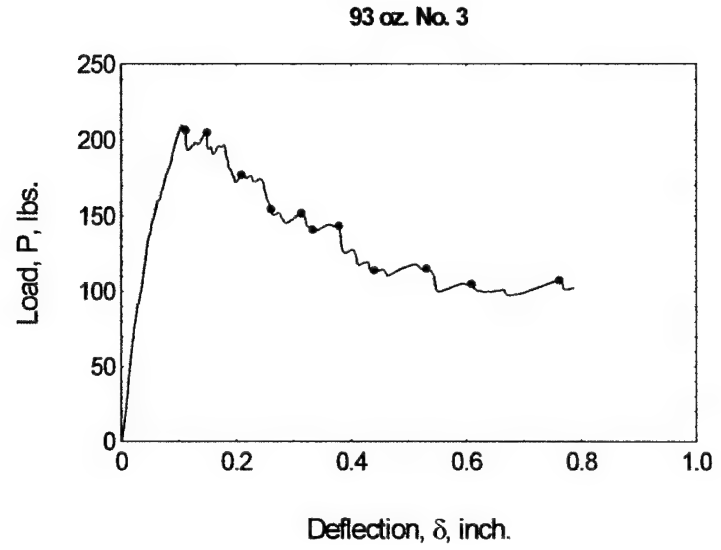

Figure 21:Load-displacement plot of tabbed DCB 93-oz specimen (No. 3) at constant displacement rate.

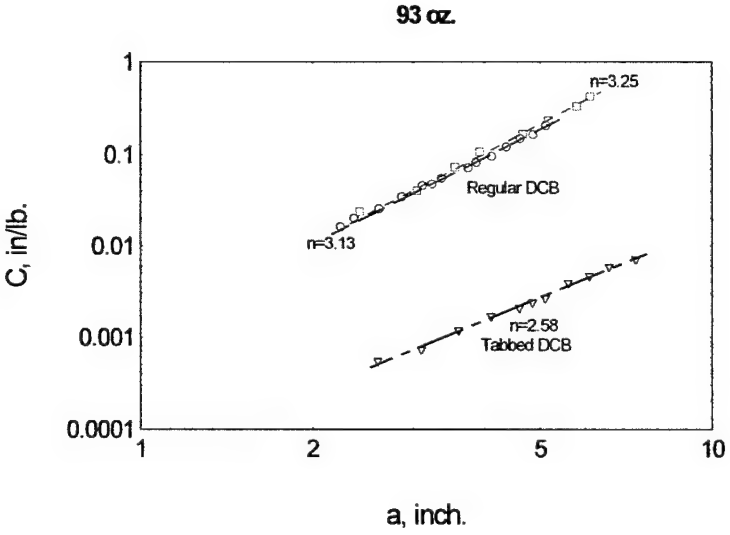

Figure 22:Compliance vs. crack length of all 93-oz specimens.

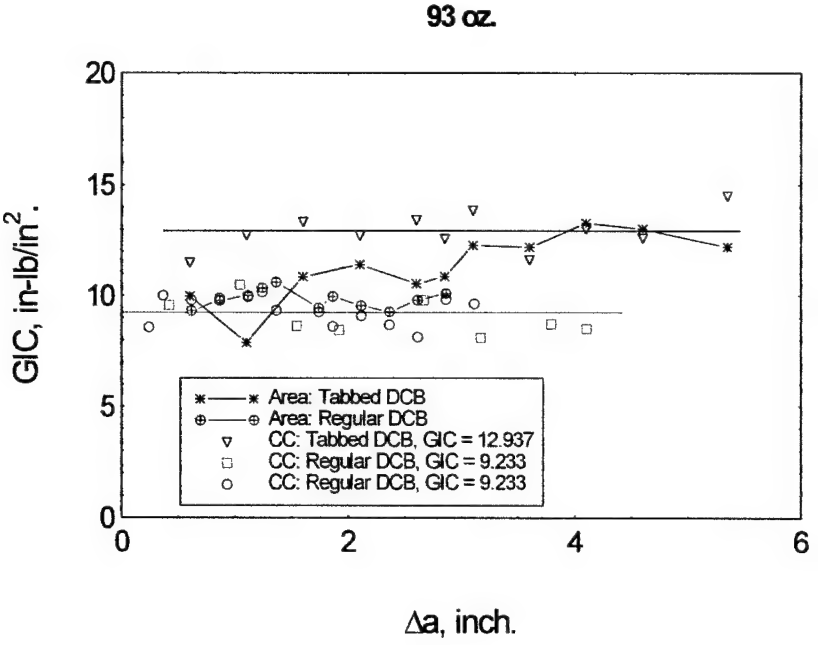

Figure 23:Critical energy release rate as a function of crack extension (3Weave #1).

All three 180 oz specimens had steel tabs bonded to the composites. Two specimens were tested using constant displacement rate (figures 24 and 25) and one specimen was unloaded at incremental crack growth (figure 26). Figure 27 shows the load-deflection data of all three specimens, which appear consistent with each other. The compliance data (figure 28) shows some non-linear behavior (in log-log scale) in the beginning of crack growth, indicating that shear deflection may not be negligible in the initiation part of the crack growth. However, shear deflection became negligible with the propagation of crack front.

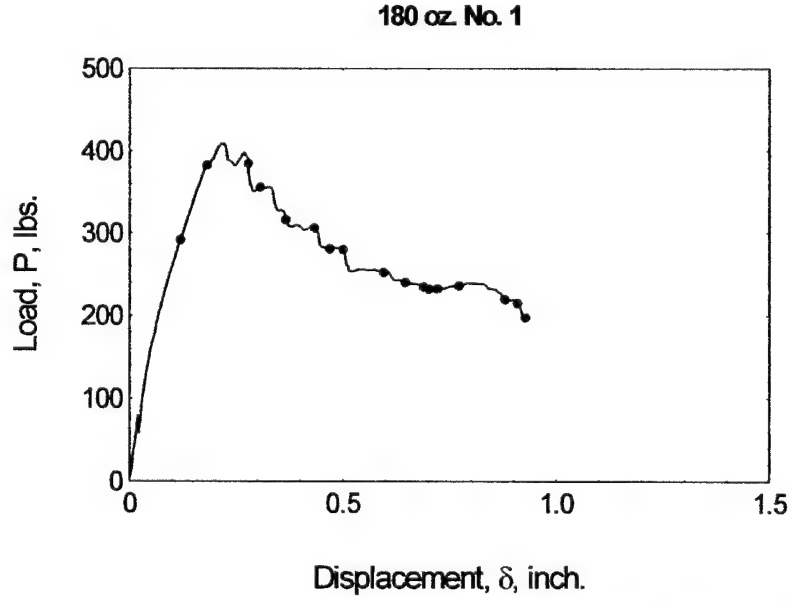

Figure 24: Load-displacement plot of tabbed DCB 180-oz specimen (3Weave™ #5 specimen 1) at constant displacement rate.

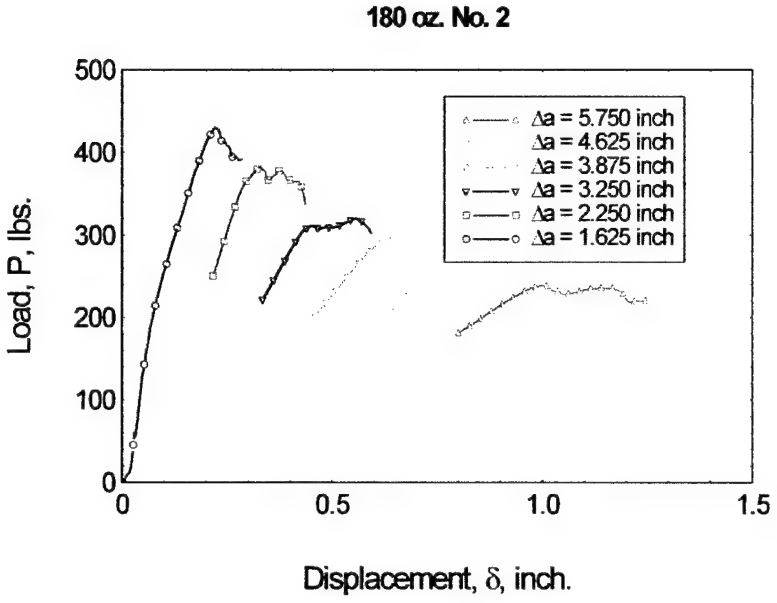

Figure 25: Load-displacement plot of tabbed DCB 180-oz specimen (3Weave™ #5 specimen 2) with unloading and reloading at different crack extension.

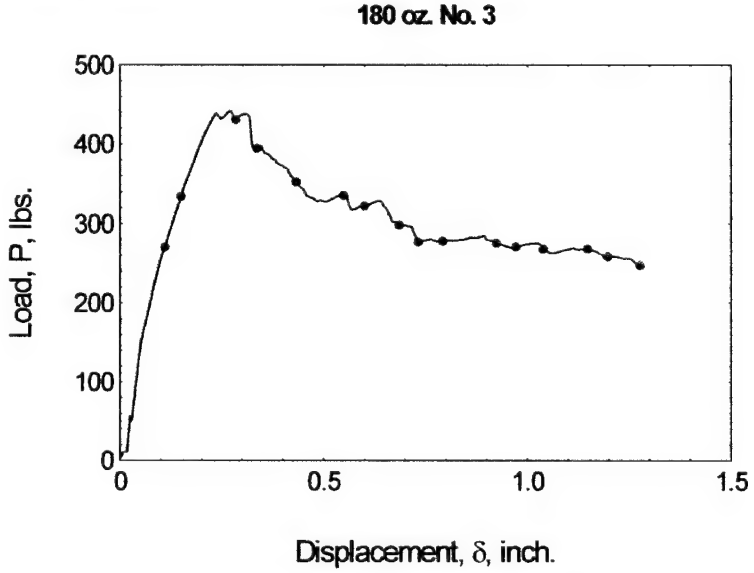

Figure 26: Load-displacement plot of tabbed DCB 180-oz specimen (3Weave™ #5 specimen 3) at constant displacement rate.

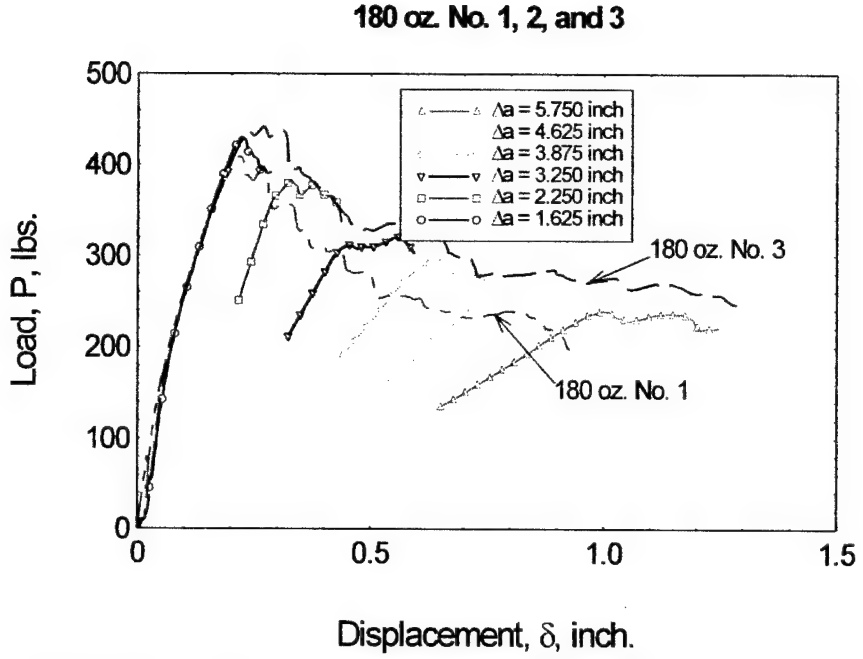

Figure 27: Load-displacement plot for all 93-oz (3Weave™ #1) DCB specimens.

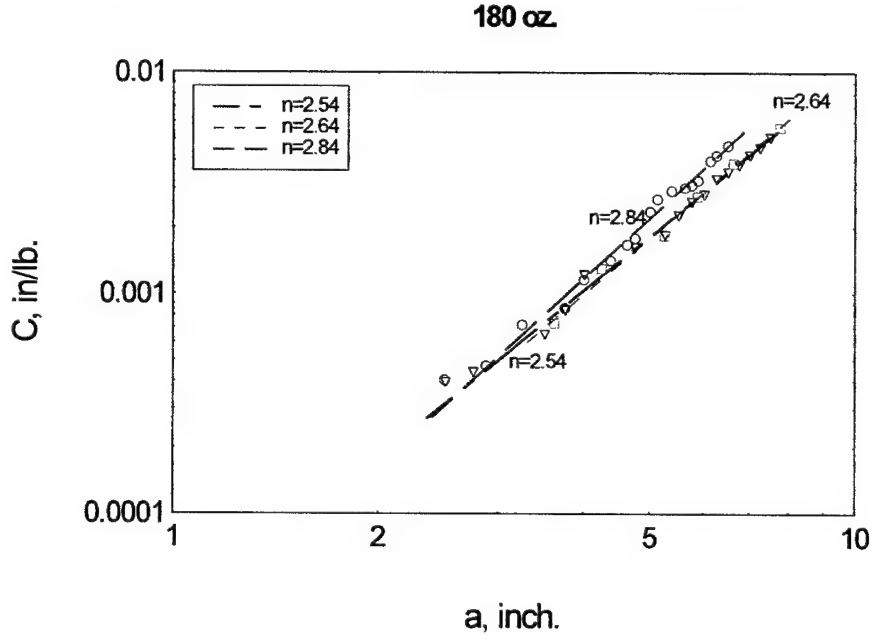

Figure 28: Compliance versus crack length for all 93-oz (3Weave™ #1) DCB specimens, plotted on log-log scale.

The CC method was used to reduce all data into energy release rate as a function of crack extension (figure 29). The energy release rate shows distinct crack initiation and propagation values (R-curve behavior). The average R-curve behavior can be expressed as:

$$G_{IC} = 46.897\left(1 - 1.700e^{-1.938\Delta a}\right) \qquad [8]$$

which gives $G_{Ic} = 46.9$ in-lbs/in^2 for fully developed cracks. The G_{IC} for 3-D composite is about five times the baseline 24-oz specimens.

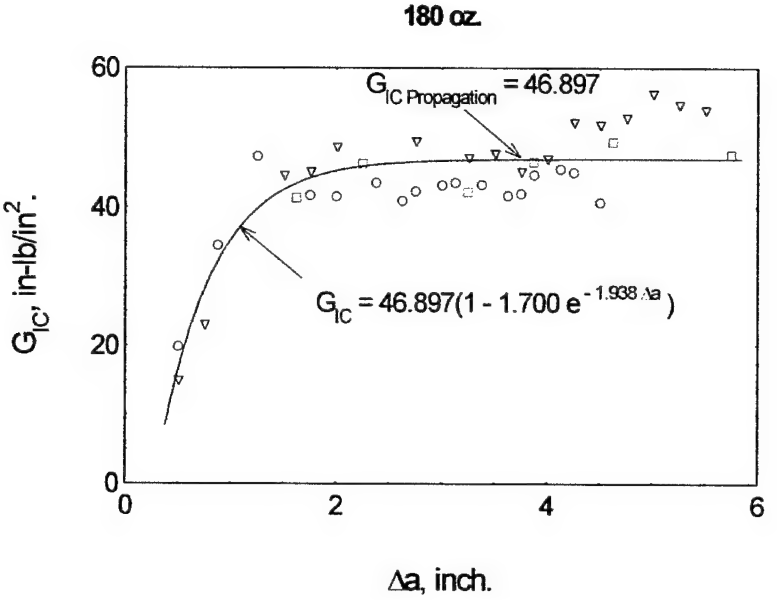

Figure 29: Critical strain energy release rate for 180-oz (3Weave™ #5) DCB specimens.

Table 8 shows the comparison of G_{IC} values for all three material types tested. For comparison, DCB test results on VARTM-consolidated baseline S-2 glass / Derakane 411-C50 epoxy vinyl ester are also presented [Gama 2001].

Table 8: Comparison of Critical Energy Release Rates of 3Weave™ and Baseline Composites

Identification	Regular DCB G_{IC}, in-lbs/in^2 CC method	Tabbed DCB G_{IC}, in-lbs/in^2 (% Difference)
Baseline (24-oz)	8.6	9.3 (+8%)
3Weave™ #1 (93-oz)	9.2	12.9 (+40%)
3Weave™ #5 (180-oz, 3-D)	-	46.9
*24 oz S-2 Glass/VE**	*7.1*	-

** Previous DCB test results of similar24-oz plain weave S-2 glass fabric and vinyl ester composites.*

4.4 Discussion

The unit cell sizes of the 3Weave™ and baseline fabrics examined in this study (table 2) are large relative to the dimensions of standardized test coupons. Further, the presence of through-thickness reinforcement makes in-plane failure in modes 1 and 2 more difficult than in traditional laminates, as seen by difficulties obtaining DCB (section 4.3) and short beam shear (section 4.2) data, respectively. These two effects of coarse, textile reinforcement architecture on static mechanical tests can be mitigated through a variety of means [Bogdanovich & Pastore 1996]. A rule of thumb developed by independently by several researchers is that coupon dimensions and strain integration distances should contain at least two unit cells. This was achieved in tension (by using extensometers), but not in in-plane shear or in compression, where the ASTM D5379 and ASTM D3410 gage areas are both about one unit cell dimension for all composites tested. Additional tests on in-plane shear, comparing the Iosipescu shear (ASTM D5379) data presented in table 7 to single rail shear (ASTM D4255) and plate twist [Tarnopol'skii & Kincis 1985, Bogdanovich & Pastore 1996], suggest that the ASTM D5379 results for 3Weave™ 1 in Derakane 8084 are reasonable, however, we have no independent verification of compression data.

Given the expected experimental difficulties, we believe the clearest comparison of test results between different materials is tension. The 3Weave™ composites were about 10-20% more compliant than the baseline, 2-D laminates, but had 6-20% higher strengths. [Vasudev & Mehlman 1987] examined the correlation of several static mechanical properties with ballistic limit (V_{50} – see section 6) versus 20 mm fragment simulating projectiles for heavy (~20 psf) laminates of 2-D woven S-2 glass in a variety of resins. They found that tensile strength had the best correlation with V_{50}. Figure 6 compares warp tensile strengths[3] of the 3Weave™ composites with other S-2 glass composites reported in the literature, which were considered for armor applications. Typical values for balanced, cross-plied S-2 glass / epoxy unidirectional tape is also given. The 3Weave™ composites appear strongest in warp tension of the materials referenced. It should be remembered that 3Weave™ mechanical data is for single ply composites. As shown in figure 5, the fiber volume fractions of 3Weave™ laminates are seen to increase to values around those typical of 2-D VARTM laminates (V_f ~55%). (Fiber volume fractions of ~55% were also obtained in laminates of fabric 1 made with SC-15 via VARTM in a previous SBIR contract, DAAD17-00-C-0054.) This suggests that the mechanical data reported here for 3-D weaves, on single ply composites, with V_f~49-52%, understate laminate strengths realizable in thicker VARTM parts.

Through-thickness compression data was generated in order to interpret split Hopkinson pressure bar tests, and will be detailed in section 5.4. They show that the 3Weave™ #1 (and by inference, the other 3Weave™ fabrics woven for this study, which have similar structure and z-reinforcement volume fractions) has ~7% lower transverse stiffnesses, E_3, and ~10% lower compressive strength, σ_{3c}, than the 2-D woven baseline. [Vaidya *et al.* 1999] examined VARTM laminates of the baseline fabric in Shell Epon RSL2704/RSC 2705 epoxy, both stitched with Kevlar® 29 cord and unstitched, and also found that light through-thickness reinforcement lowered E_3 and σ_{3c} moderately. They attributed this reduction to the introduction of compliant resin channels through the laminate thickness created around the through-thickness fiber reinforcement, as well as to a slight decrease in total fiber volume fraction.

Table 9 compares experimental and predicted elastic constants for single plies of 3Weave™ #1 in Derakane 8084. Predictions were made via the Modified Matrix Method (MMM) [Yushanov *et al.* 1999] and Stiffness Averaging (SA) [Kregers & Melbardis 1978]. Both used the micromechanics of Abolinsh (see [Bogdanovich & Pastore 1996]) to predict local mechanical properties. Input properties were nominal fiber and resin stiffnesses given by the manufacturers, and Poisson's ratios for fiber and resin assumed to be 0.25 and 0.4, respectively. The MMM formulation used does not predict Poison's ratios. The predictions do not account for the slight crimp imparted into the outermost fill yarns at the fill-z interlacings, thus overpredicting E_2. Note that, since ν_{12} and ν_{12} are related by reciprocity, seven of the nine expected independent elastic constants were determined experimentally. The range of errors is similar to those reported in predicted elastic constants for carbon fiber / epoxy composites in [Bogdanovich & Pastore 1996, Cox 1995], who used similar predictive methods. Neither MMM or SA appears clearly superior.

Table 9: Experimental and predicted elastic constants for single plies of 3Weave™ #1 in Derakane 8084.

[3] The warp and fill strengths of composites reinforced with 2-D weaves often differ, due to differences in the amount of warp and fill reinforcement, and in crimp levels. Thus, like 3-D weaves, 2-D weaves which appear to have the same warp and fill contents may have significantly different mechanical properties in the warp and fill directions. Data in papers cited only report warp strengths, reflecting a typical assumption in the literature, that 2-D fabrics balanced (in the weaving sense) yield balanced composites.

Constant	experimental	Modified Matrix Method		Stiffness Averaging	
	value	prediction	error	prediction	error
E_1 (Msi)	3.58	3.86	-8%	3.78	-6%
E_2 (Msi)	3.01	3.65	-21%	3.56	-18%
E_3 (Msi)	1.50	1.34	11%	1.38	8%
G_{12} (Msi)	0.61	0.46	24%	0.43	29%
ν_{12}	0.10			0.10	0%
ν_{21}	0.11			0.10	11%
ν_{31}	0.19			0.17	-12%
ν_{32}	0.19			0.17	-12%

Short beam shear test results underscore the difficulty of forcing 3-D woven composites to fail by in-plane cracking. IPM, following ASTM D2344, were unable to get interlaminar shear failure, with the composites instead failing under bearing stress at the center contact. NCA&TSU was able to force interlaminar shear failure in the 3-D woven composites by distributing the center load with a fixture very similar to four-point bend at low aspect ratio, as described in [Abali *et al.* 2000].

In-plane cracking was also difficult to force in DCB tests. CCM resorted to reinforcing specimens with steel tabs, to prevent hinge failure at the crack root. This change to ASTM D5528 required a different approach be used to reduce the data, as discussed in [Byun *et al.* 1990]. Only three specimens were tested for each material, therefore, the (unquantified) confidence interval for each result is probably high. Accepting the uncertainty in the data, the roughly 20% increase in G_{1c} between plies of 3Weave™ #1 and the baseline could be explained by the increased surface area of the coarser, nested 3-D woven plies. This would correspond to modest improvements seen in efforts to develop so-called 'bumpy' fabrics with improved delamination resistance in earlier work performed for NASA on carbon fiber / epoxy systems [Dow & Ramnath 1987].

The factor of five increase in G_{1c} between the baseline material and 3Weave™ 5 is due to the addition of through-thickness reinforcement. This large increase arguably represents a worst case to contrast 3-D woven performance, because of the very tough resin, two-phase epoxy resin used. Greater increases would be expected in G_{1c} if a more brittle resin was used. Impact damage resistance is generally seen to correlate more closely with G_{2c} than G_{1c}, however, the through-thickness fiber reinforcement in 3-D woven composites has also been shown to improve G_{2c} [Chou 1992].

Note that in all cases, critical strain energy release rate increased asymptotically with increasing crack length. In the interply delamination tests on the baseline and 3Weave™ #1, this was due to fiber bridging. In the intraply cracking tests on 3Weave™ #5, this was partly due to both fiber bridging, but mostly due to through-thickness fiber tension generated by the passing crack. As the crack passes the z-yarn, the opening delamination tenses the yarn, in turn applying a closing force to advancing crack. Therefore, it should be expected that through-thickness fiber reinforcement will not contribute substantially to resistance to in-plane crack initiation, but will contribute substantially to suppression of crack advancement once cracks are created. This leads to localization of in-plane cracks around impact sites, as observed in impact tests described in the next two sections.

5. Low Velocity Impact Testing

5.1 Introduction

This section covers drop tower impact testing, compression strength after impact testing, and split Hopkinson pressure bar (SHPB) testing, performed by CCM under the STTR contract. The materials examined were laminates of 3Weave™ #1 and #2, and of the baseline fabric, all in Derakane 8084. Information presented here is taken from the CCM subcontract final report. That report contained extensive photographic documentation of all coupons, which we have edited for brevity in this report. 3TEX will provide all images of low velocity impact testing upon request.

5.2 Drop Tower Impact Testing

5.2.1 Materials

Two different 3-D preforms and one 2-D plain weave were used throughout this research effort. They were termed as 3Weave1, 3Weave2 and Baseline, and had the following lay up:
3Weave1: 3 plies 93-oz/yd^2 of 3Weave™ S-2 Glass
3Weave2: 3 plies 90-oz/yd^2 of 3Weave™ S-2 Glass
Baseline: 12 plies 24-oz/yd^2 of plain weave S-2 Glass

All composites were laid up warps parallel. Composite laminates were fabricated with these preforms using Dow Derakane® 8084 toughened vinyl ester. The panels were post-cured at 250 °F for two hours.

5.2.2 Low Velocity Impact Experiments

The post-cured lamiantes were machined into 4-in x 6-in impact specimens using circular diamond cutter such that they fit in the compression after impact (CAI) setup. The direction of compression (6-in direction) in CAI test corresponded to the fill direction of the fabric.

The specimens were impacted using a low velocity impact machine (Dynatup-Impact Tower, Figure 30). This machine is based on the free fall of a mass on the specimen. Three nominal impact energies were used: 25, 50 and 75 joules. Changing the drop height and the weight of the impactor set the energy level. Table 10 gives the heights and weights used for each impact energy level.

Table 10: Dynatup impact test energies, drop heights, and masses.

Energy [J]	Height [cm]	Weight [kg]
25	40.6	5.84
50	81.3	5.84
75	81.3	9.07

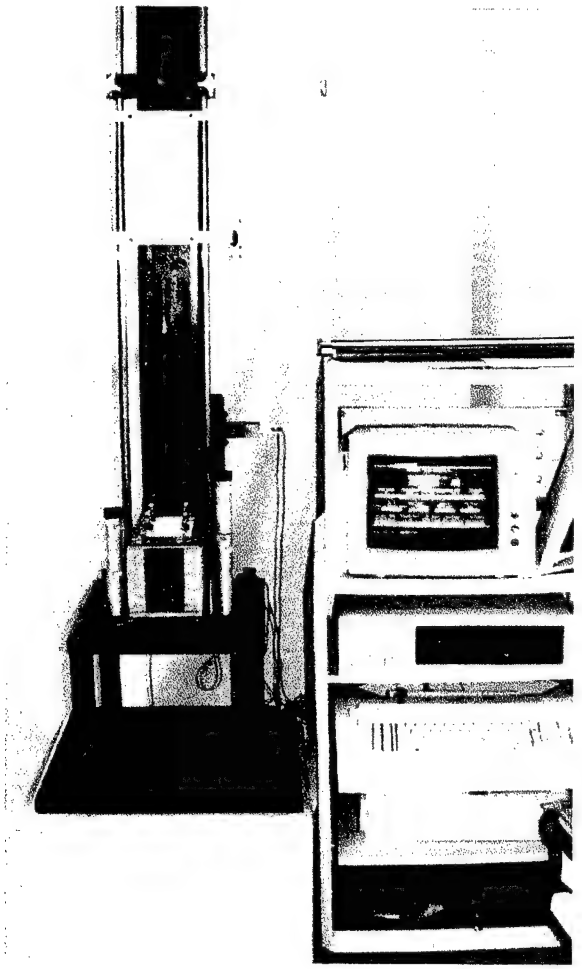

Figure 30: Dynatup Impact Tower.

A 5/8-in tup was used, following SACMA recommendations. For each impact energy levels, 12 3Weave1 specimens, seven 3Weave2 and eight Baseline specimens are tested. The instrumented tup of the impact machine and the velocity sensors allowed the determination of impactor energy, the load and the deflection as a function of time. The force-time curves were similar in all the cases. The level of damage induced in the impacted panels is described next.

5.2.3 Damage Evaluation Through Digital Photography

All specimens were visually examined and digital pictures of representative specimens were taken. 3TEX will provide any images requested. Figures 32-34 show the impact damage on the impact and rear face of three different test panels at 25-J impact energy. The orthogonal 3Weave panels show diamond shape impact damage, however, the plane weave baseline show circular-shaped damage (*cf.* Figure 51).

These pictures were used to estimate the damage area on the impact face and on the rear face of the specimens. These areas were measured using a grid printed on a transparent slide. This grid was superimposed on a print of the picture and the number of squares of the damage counted. Damage areas are summarized in table 11.

Table 11: Average visible impact damage areas.

Impact	3Weave1		3weave2		Baseline	
Energy	Front face	Rear face	Front face	Rear face	Front face	Rear face
25 J	5.6 cm^2	11.1 cm^2	7.9 cm^2	12.6 cm^2	5 cm^2	10.7 cm^2
50 J	11.5 cm^2	20.6 cm^2	13.8 cm^2	26.6 cm^2	10 cm^2	20.3 cm^2
75 J	17.6 cm^2	33.3 cm^2	21 cm^2	39.1 cm^2	21.9 cm^2	38.4 cm^2

Figure 35 shows the average visible impact damage area on the front (impact) face as a function of impact energy. The average front face damage area of 3Weave1 panels is less than that of 3Weave2 panels for all impact energy levels. The front face damage of Baseline is less than both 3Weave1 and 3Weave2 at impact levels of 25 J and 50 J. However, the impact damage of Baseline is more than both of 3Weave1 and 3Weave2 panels at impact level of 75 J. In non-penetrating strikes, drop tower impact damage on FRP strike faces is generally seen to be tow debonding in the upper plies. The lack of interlacing in the 3-D orthogonal structure may facilitate tow debonding [Cox 1995], as it facilitates yarn pull through in ballistic impacts on 3-D orthogonal fabric [Singletary & Bogdanovich 2000].

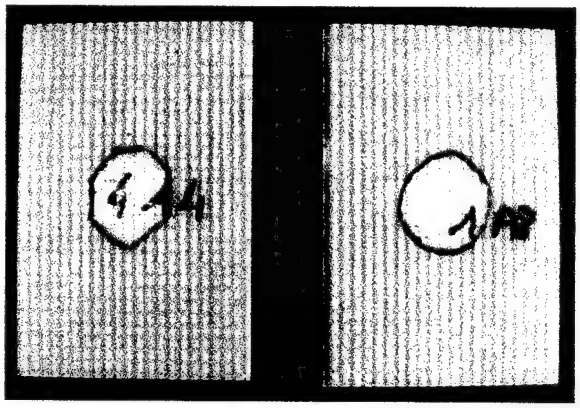

Figure 31: Typical visible impact damage in 3Weave™ #1 from drop tower testing at 25J.

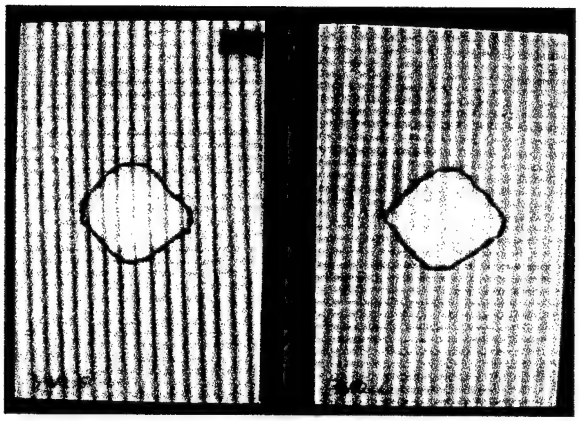

Figure 32: Typical visible impact damage in 3Weave™ #2 from drop tower impact at 25J.

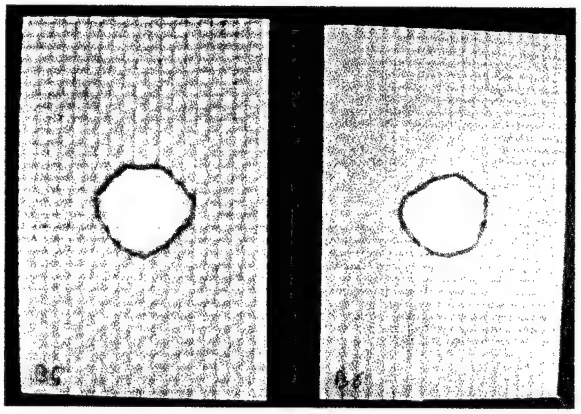

Figure 33: Typical visible impact damage in baseline composite from tower impact at 25J.

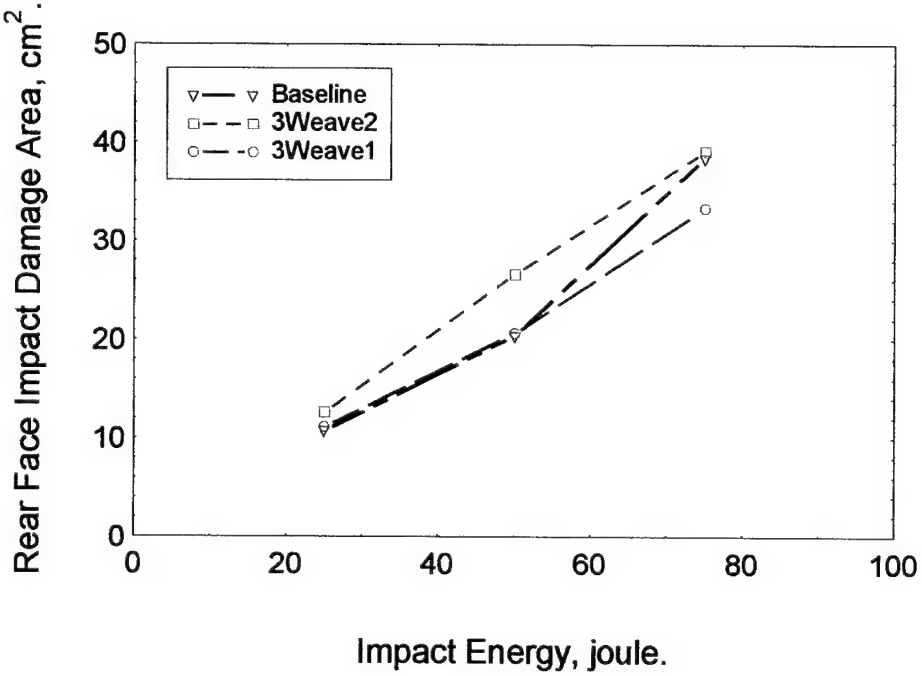

Figure 34: Average visible damage in the impact (front) face.

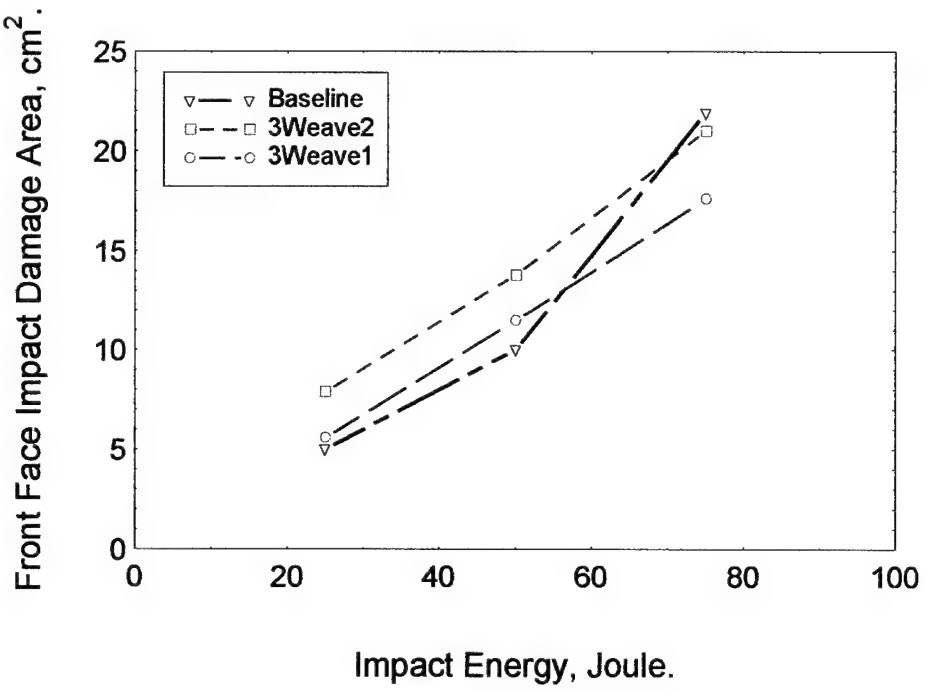

Figure 35: Average visible damage in the rear face.

The rear face damage area is about twice as much as that of the front face (figure 36). Like the front face damage area, the overall rear face damage area of 3Weave1 is less than that of 3Weave 2. The rear face damage area of the baseline is almost same as that of 3Weave1 at impact levels 25 J and 50 J. However, at 75 J, the damage in the baseline panel is more than 3Weave1, and almost same as the 3Weave2.

5.2.4 Damage Evaluation through Ultrasonic C-Scan

Ultrasonic C-Scan was used to evaluate the quality of the composite panels before and after impact. A 5 MHz piezo-electric transducer was used in pulse-echo mode to perform the C-Scan using water as the coupling media. A trial panel of 3Weave1 was scanned to verify the scanning process. Weaving pattern and resin rich areas were observed. The same scanning setting was used to C-Scan the 3Weave1 panels. Results showed some resin-starved region in the composite panels (Figure 37). CAI specimens were machined from these and individual specimens were C-Scanned before and after impact. C-Scans were taken at three equally spaced gate locations, such that each gate represented approximately one-third of through the thickness of the specimens. The through-thickness damage area could be qualitatively identified, but not confidently quantified from these C-Scans (Figure 38). This is why digital photography of visible damage was used to quantify impact damage area rather than ultrasound.

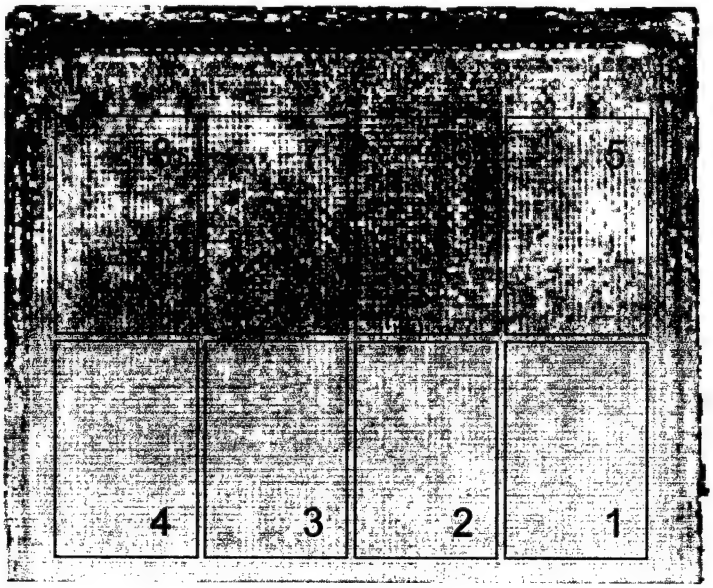

Figure 36: Overall part quality of 3Weave™ #1-1a and CAI specimen layout.

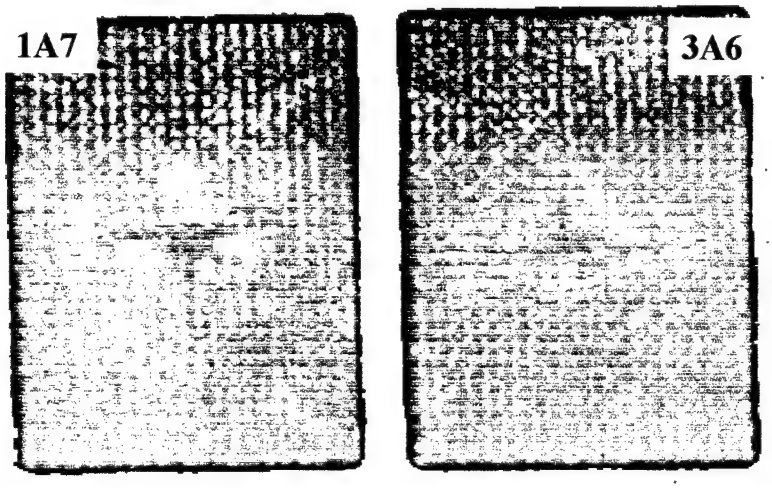

Figure 37: C-scan of 3Weave™ #1 specimens after impact at 50J.

5.3 Compression After Impact

Compression after impact tests were performed following SACMA method SRM-2. Figure 39 shows the impact and CAI fixtures. The impacted specimens were loaded under compression in an Instron Testing Machine with a load cell of 30,000 pounds. The maximum load from the load deflection curves was used to determine the CAI strength. The average CAI strength as a function of impacted energy is presented in Figure 40.

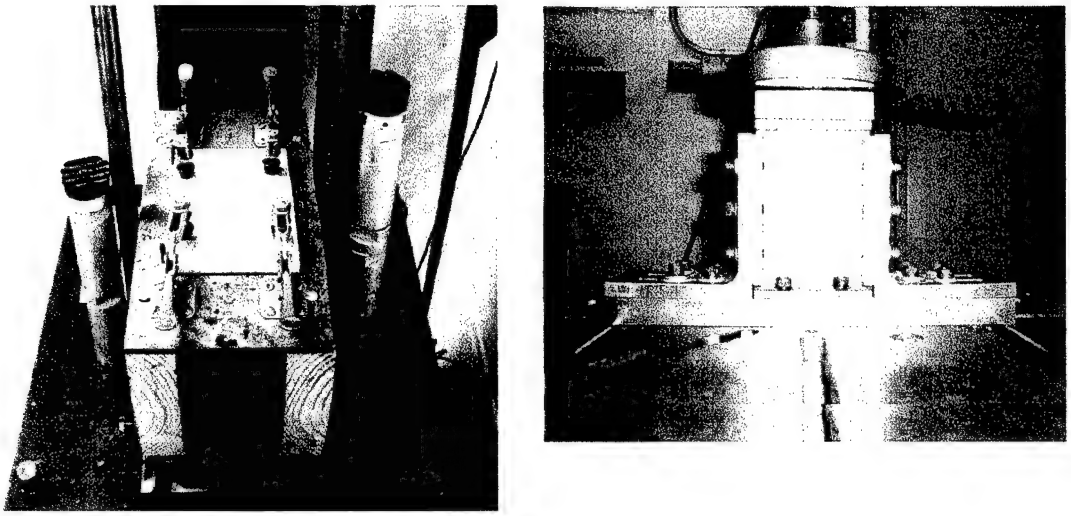

Figure 38: SACMA CAI testing. Left: Impact fixture. Right: compression fixture.

3Weave1 specimens have higher CAI strength than 3Weave2 and the baseline. The CAI strength of 3Weave2 and Baseline are almost the same for 50 J and 75 J impact levels. In order to compare the CAI strength with the strength of virgin specimens, undamaged samples were loaded in the same CAI fixture. The results are not presented here, because the specimens failed in modes other than that observed in CAI experiments. The CAI specimens failed in the vicinity of the centerline perpendicular to the loading direction through kink band formation at an angle approximately 45-degrees out-of-plane. The CAI specimens were sectioned through the center of impact and the failure behavior investigated through digital photography. Figure 41 shows the damage after CAI test along the centerline (in the loading direction) for 3Weave1, 3Weave2 and Baseline at impact energy 50 J. The top face of the specimens represents the impact side. The damage in the 3Weave1 panel is least among the three and that of baseline is the most. The compressive failure in the form of kink band formation appears as a single line at an angle about 45 degrees with the loading direction. However, the process zone of the baseline appears much larger in comparison to 3Weave1 with similar kink band formation under compression. The damage in 3Weave2 is somewhat in between. No visible delamination is observed in any of these specimens. The size of CAI specimen was 4-in x 6-in and the impact energies chosen was 25 ~ 50 J. It will be necessary to test larger specimens at higher impact energies to investigate severe damage.

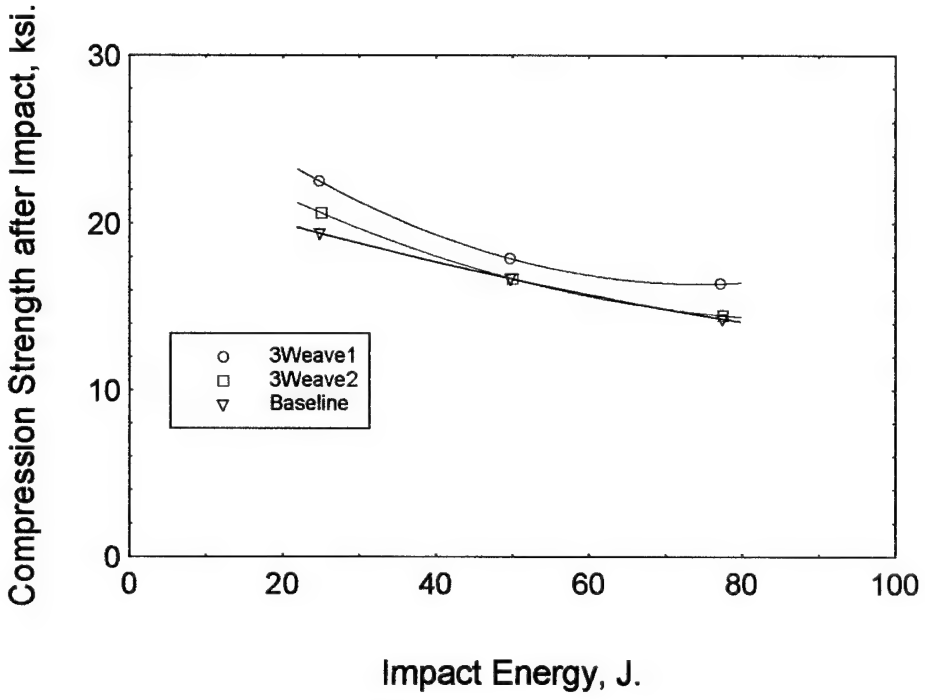

Figure 39: CAI strength as a function of impact energy.

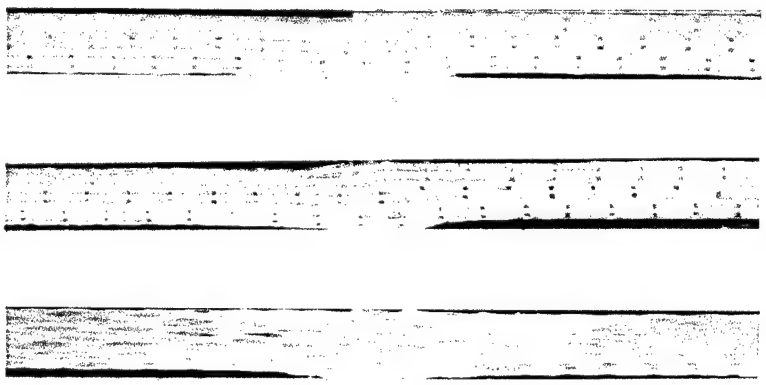

Figure 40: Damage after CAI Strengths Tests at 50J. Top: 3Weave™ #1; center: 3Weave™ #2; bottom: baseline.

5.4 Through-Thickness Compression Experiments

Through-thickness compression tests of 3Weave1 and Baseline were performed following ASTM D-695. Rectangular block specimens were made from thick composites plates following surface grinding and slot grinding. The nominal dimensions of 3Weave1 specimens are 0.6-in x 0.6-in x 0.925-in and those of Baseline specimens were 0.6-inch x 0.6-inch x 1.0-inch. These nominal

dimensions are close to ASTM specifications of 0.5-in x 0.5-in x 1.0-in. A slightly higher cross section was chosen to accommodate at least four in-plate unit cells in the specimen. The specimens were oven dried, and the dimensions measured. Specimens were left in a desiccator until the test. Three specimens from each type of material were mounted with back to back 0/90 strain gauge rosettes to measure the through-thickness elastic properties. Specimens were loaded between two parallel platens in an Instron testing machine with a 55,000 pounds load cell. Load-deflection data for all specimens without and with strain gages were recorded. Load-strain data was obtained only for strain gauged specimens.

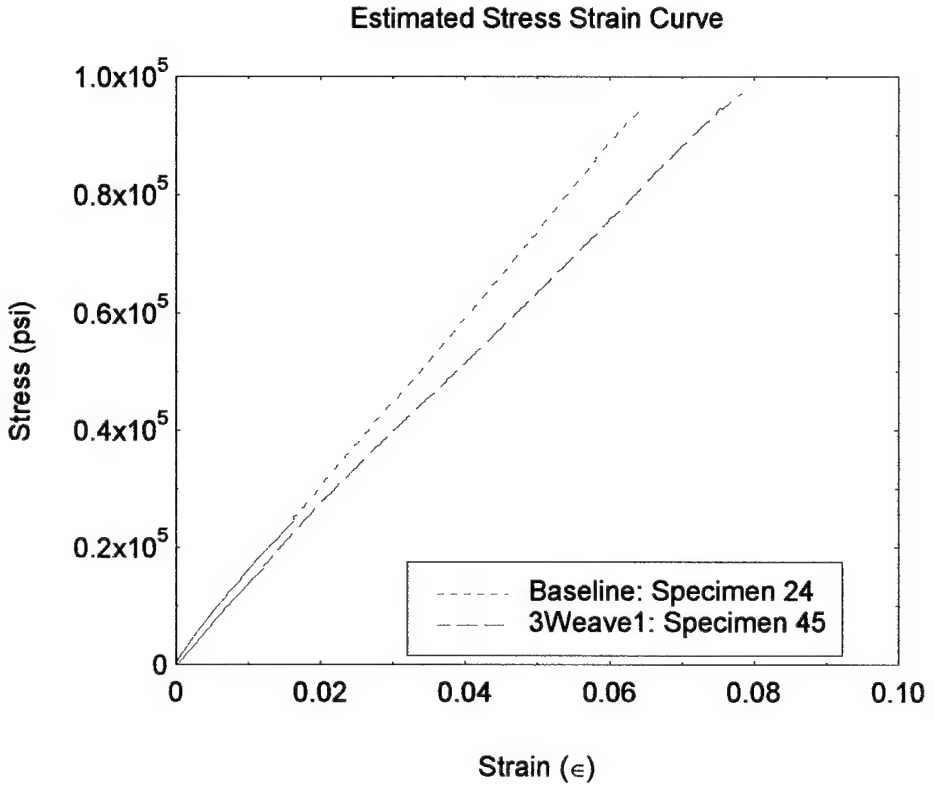

Figure 41: Through-thickness stress-strain behavior of 3Weave™ #1 and baseline.

Figure 42 shows representative stress-strain plots for through-thickness quasi-static compression. The initial, solid lines represent the response from the strain gages. The dotted extensions are corrected for initial contact nonlinearity, and correcting the modulus for machine compliance by matching it to the strain gauge data. The average modulus, Poisson's ratio and strength is presented in table 12.

Table 12: Quasi-static through-thickness compression results.

Material Type	Modulus, E_{33}, Msi	Poisson's Ratio $\nu_{31}=\nu_{32}$	Strength, X_3^C, ksi
3Weave1	1.496	0.193	86.3
Baseline	1.666	0.180	94.5

Both the through-thickness modulus and compressive strength of 3Weave1 are less than that of the Baseline, and Poisson's ration is higher. Both in-plane and out-of-plane failure was observed in 3Weave1 and Baseline specimens (figure 43).

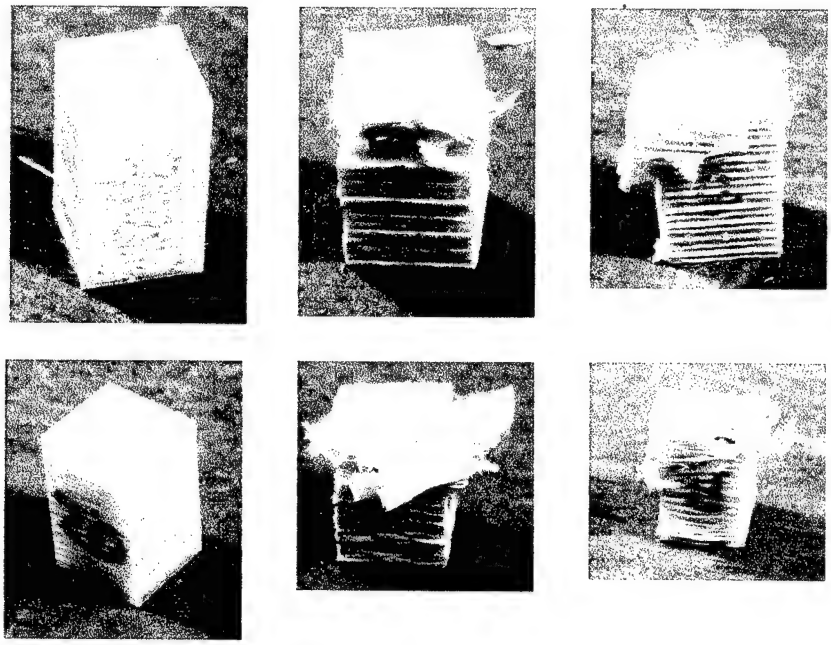

Figure 42: Quasi-static through-thickness damage. Top: 3Weave™ #1; bottom: baseline. Left: untested specimen; Middle: in-plane failure; right: out-of-plane failure.

5.5 Split Hopkinson Pressure Bar Testing

Through-thickness high strain rate testing of 3Weave1, 3Weave2 and Baseline specimens were performed using compression split Hopkinson pressure bar (SHPB) testing facility at Tuskegee University's Center for Advanced Materials (T-CAM). This section describes Hopkinson bar experimental procedure, the equipment used, data representation and results.

Specimens were machined using surface grinding and slot grinding. All specimens had a nominal cross-section of 0.5-in x 0.5-in, however, the thickness of 3Weave1, 3Weave2 and Baseline were 0.42-in, 0.46-in and 0.55-in, respectively.

In the SHPB technique (figure 43), a small specimen is sandwiched between two elastic bars of common cross-sectional area and modulus, called the *incident bar* and *transmitter bar*. An elastic stress pulse is imparted to the incident bar by impacting it with a striker bar of the same cross-sectional area and modulus. The impact of the striker bar generates an elastic stress wave equal to twice the length of the striker bar and propagates through the incident bar with the velocity of sound in the bar media and passes through the specimen while deforming it. The particle velocity imparted on the incident bar is half the impact velocity of the striker bar. The stress in the bar is given by $\sigma = \rho_b C_0 u_p$, where ρ_b is the density of bar material, C_0 is the bar velocity and u_p is the particle velocity. When the elastic wave reaches the specimen-incident bar interface, part of it is reflected back, and part of it is transmitted through the specimen and passes through the transmission bar. To acquire the direct incident pulse, the reflected pulse and the transmitted pulse, strain gages are mounted on both the incident and transmitter bars. One-dimensional wave propagation is assumed to analyze the strain signals from the strain gages. If the modulus, cross-section area and density of the bar are denoted by E_b, A_b and ρ_b and those of the specimen are E_s, A_s and ρ_s, the equations for the strain-rate ($\dot{\varepsilon}$), strain (ε), and stress (σ) of the specimen are given by:

$$\dot{\varepsilon}(t) = -\frac{2C_o}{L_s}\varepsilon_R(t) \quad (9)$$

$$\varepsilon(t) = -\frac{2C_o}{L_s}\int_0^t \varepsilon_R(t)dt \quad (10)$$

$$\sigma(t) = \frac{E_b A_b}{A_s}\varepsilon_T(t) \quad (11)$$

where, $C_o = \sqrt{E_b/\rho_b}$ is the bar velocity, L_s is the specimen length, and $\varepsilon_R(t)$ and $\varepsilon_T(t)$ are the strain-gage signal of the reflected and the transmitted pulses respectively. Equations (1) through (3) is based on the assumption that the dynamic forces on both side of the specimen are equal and can be expressed as:

$$\varepsilon_I + \varepsilon_R = \varepsilon_T \quad (12)$$

Equations (9) through (11) give the average stress and strain in the specimen as a function of time. The equations also show that the strain can be obtained by integrating the reflected pulse and the stress in the specimen from the transmitted pulse.

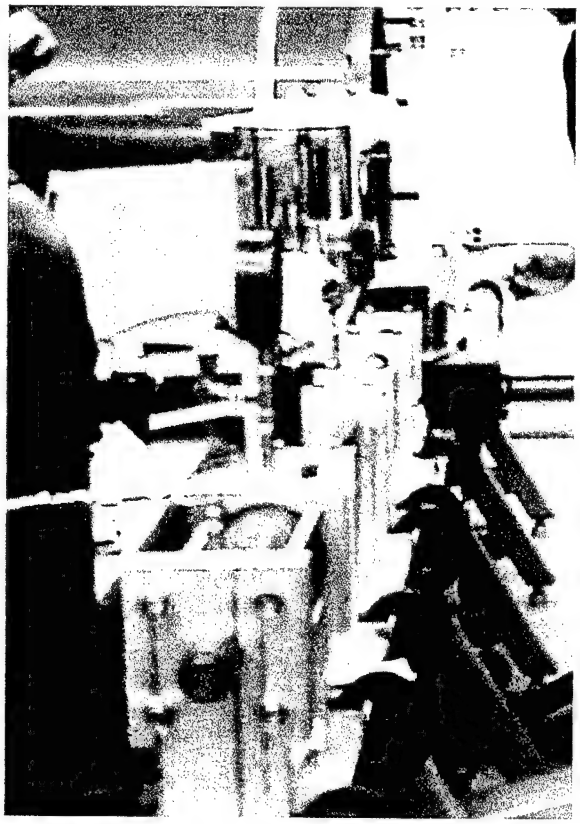

Figure 43: Split Hopkinson pressure bar apparatus.

The compression split Hopkinson pressure bars (SHPB) used in the present investigation consisted of a 1.5-in gas gun, two maraging steel bars of diameter 1.5-inch and of length 60-inch. The gas gun operates on compressed nitrogen gas and can fire striker bars of different lengths ranging from 6 inch to 12 inch. Throughout the present tests, a 6-inch striker bar is used. The impact velocity of the striker bar can be controlled by changing the breech pressure of the gas gun. The gas gun is pre-calibrated, and the calibration equation is incorporated into a program to

determine the relationship between the impact velocity and the breech pressure. Depending on the desired input values of stress (σ_s), strain (ε_s), equivalent diameter (d_s), length (L_s) of the specimen, and length of the striker bar (L_{sb}) the program can calculate the test strain-rate ($\dot{\varepsilon}$), the impact velocity of the striker bar (v_{sb}), the strain scale factor (SF_ε), and the stress scale factor (SF_σ) using the following equations:

$$\varepsilon_T = \frac{\sigma_s A_s}{E_b A_b}, \quad \varepsilon_R = \frac{\varepsilon_s L_s}{4L_{sb}}, \tag{13}$$

$$\dot{\varepsilon}_s = \frac{\varepsilon_s C_o}{2L_{sb}}, \quad v_{sb} = 2C_o\varepsilon_I \tag{14}$$

$$SF_\varepsilon = \frac{2C_o}{L_s V_{BS}}, \quad SF_\sigma = \frac{E_b A_b}{A_s V_{BSR}} \tag{15}$$

where, V_{BS} is the incident bar bridge voltage, and V_{BSR} is the transmitter bar bridge voltage. The relationship between the breech pressures to the striker bar velocity is expressed through a calibration equation.

The strain signals are obtained as a function of time from a pair of strain-gages mounted on the incident bar and on the transmitter bar. These signals are stored in a computer with the help of data acquisition software. Another program converts the signal files into ASCII text files. The data is processed and converted to determine the derived $\varepsilon(t)$ and $\sigma(t)$ values for each strain-rate of interest. A stress-strain curve is then plotted from these strain-time and stress-time curves by eliminating the time axes.

The responses from the strain-gages mounted on the incident and transmitter bars are presented in figure 44.

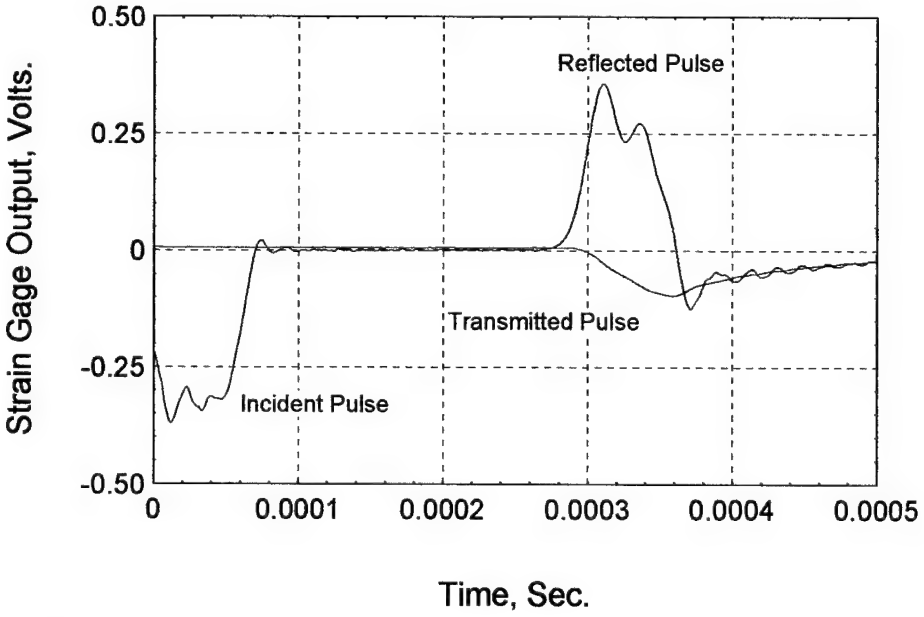

Figure 45: Hopkinson bar responses.

Figure 45 shows the incident and reflected pulses and also the shape of these pulses for a 6-in striker bar. The duration of the incident pulse is directly proportional to the striker bar length, while the amplitude is a function of impact velocity. The reflected pulses (in volts), when multiplied by the strain scale factor, SF_ε (Equation (15)), give the strain-rate vs. time curve. The reflected pulse is not constant over time; rather, it increases from zero to a maximum value in a short period of time, then fluctuates about a constant value and finally drops to zero. The duration of the transmitted pulses is similar to the incident pulses. The transmitted voltage signals are converted to the average stress of the specimen via multiplying by the stress scale factor, SF_σ (Equation (15)).

The strain-time curves shown in figure 46 are obtained by integrating the strain-rate vs. time curves. The slopes of the curves give the test strain-rates. In this study, the test strain-rate is found to vary with time. Therefore, a time average of the variable strain-rate for each test is defined as the average strain-rate (ASR) and is represented as:

$$ASR = \frac{1}{t_2 - t_1}\int_{t_1}^{t_2} \frac{d\varepsilon}{dt} dt \qquad (16)$$

where the time range t_1 - t_2 is selected by excluding the initial non-linear portion of the strain-rate vs. time curve. Similarly, the ASR can also be obtained by determining the average slope of the strain-time curve up to the maximum strain obtained, and the results are quite similar. However, Equation (15) is used for our calculation because it is easier to choose the time range than the strain range. The ASR can be controlled by changing the impact velocity of the striker bar. At constant striker bar length (SB), an increase in impact velocity gives an increase in the average stress level and strain-rate in the specimen.

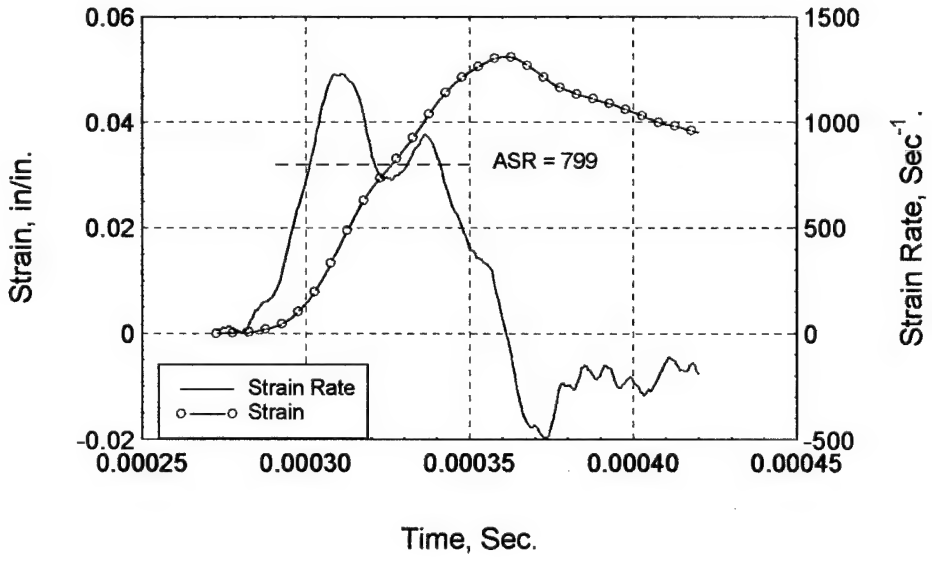

Figure 46: strain and strain rate versus time, and time-averaged strain rate (ASR).

It is well known from HSR testing of isotropic systems that strain measurement within the elastic strain response obtained from the Hopkinson bar experiment is not accurate because of wave dispersion in the bar and wave reverberation in the specimen before the stress equilibrium is achieved. Consequently, elastic modulus results are qualitative, but can provide trends in strain-rate-dependent behavior. Previous research on Hopkinson bar testing of isotropic materials has shown that the large/plastic strain response can be measured with higher confidence. In the

present study, the HSR engineering strain (ε) of is expressed as the sum of elastic strain (ε_{el}) and non-linear strain (ε_{nl}).

$$\varepsilon = \varepsilon_{el} + \varepsilon_{nl} \quad (17)$$

The initial linear region of the stress-strain curve is expressed as

$$\sigma = A\varepsilon_{el} \quad (18)$$

where A is the apparent initial elastic modulus. The elastic and non-linear strains can then be represented as a function of stress:

$$\varepsilon_{el}(\sigma) = \frac{\sigma}{A} \quad (19)$$

$$\varepsilon_{nl}(\sigma) = \varepsilon - \frac{\sigma}{A} \quad (20)$$

The HSR $\sigma - \varepsilon$ curves are transformed to $\sigma - \varepsilon_{nl}$ curves using equation (20) and are plotted as Stress vs. Non-linear Strain to represent the through-thickness response of S-2 glass/vinyl ester composite specimens.

The through-thickness responses of 3Weave1, 3Weave2 and Baseline; all relevant plots, and data tables are on file at 3TEX, and will be provided upon request. Table 13 gives the ASR range for the tests conducted.

Table 13: Material type and average strain rate in Hopkinson bar tests.

Material Type	ASR Range, Sec^{-1}
3Weave1	443 - 1027
3Weave2	535 - 1045
Baseline	519 - 845

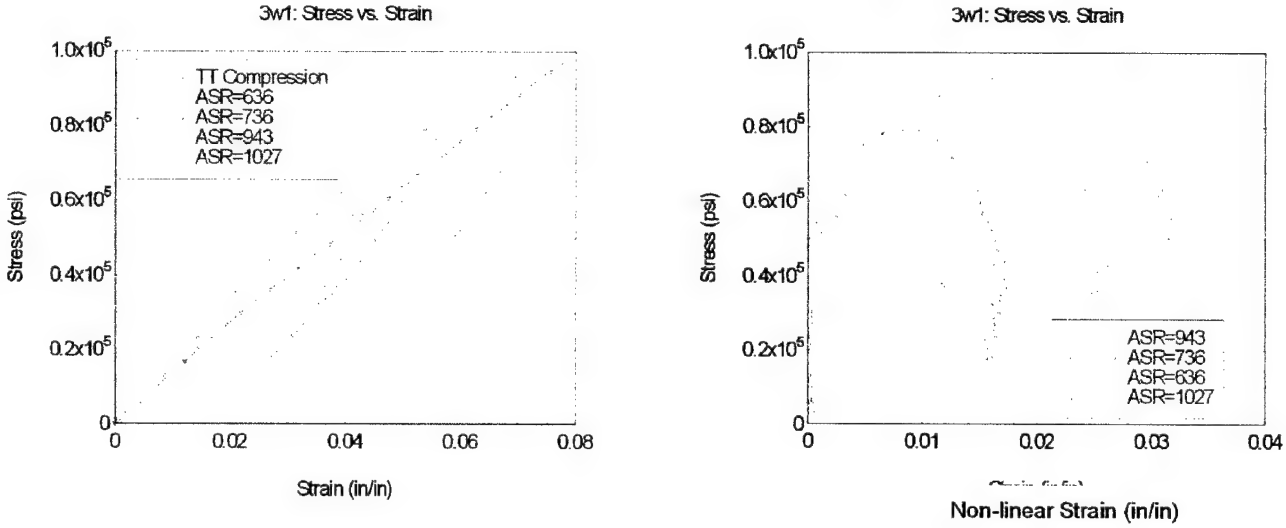

Figure 47: HSR behavior of 3Weave™ #1.

Figure 47 shows the representative engineering stress vs. engineering strain for 3Weave1 specimens. The quasi-static through-thickness (TT) curve is superimposed on the plot. The HSR curves showed non-linear behavior even though the maximum stress attained through these tests never exceeded its corresponding quasi-static strength. However, physical observation of the specimens revealed the presence of small cracks in the resin. The HSR stress vs. non-linear strain

is shown on the right in figure 47, which shows the non-linear behavior under HSR loading condition. Similar plots for 3Weave2 and Baseline are also presented in figures 48-49. The non-linear responses of 3Weave1 and 3Weave2 are similar and so does the baseline showing equivalent behavior.

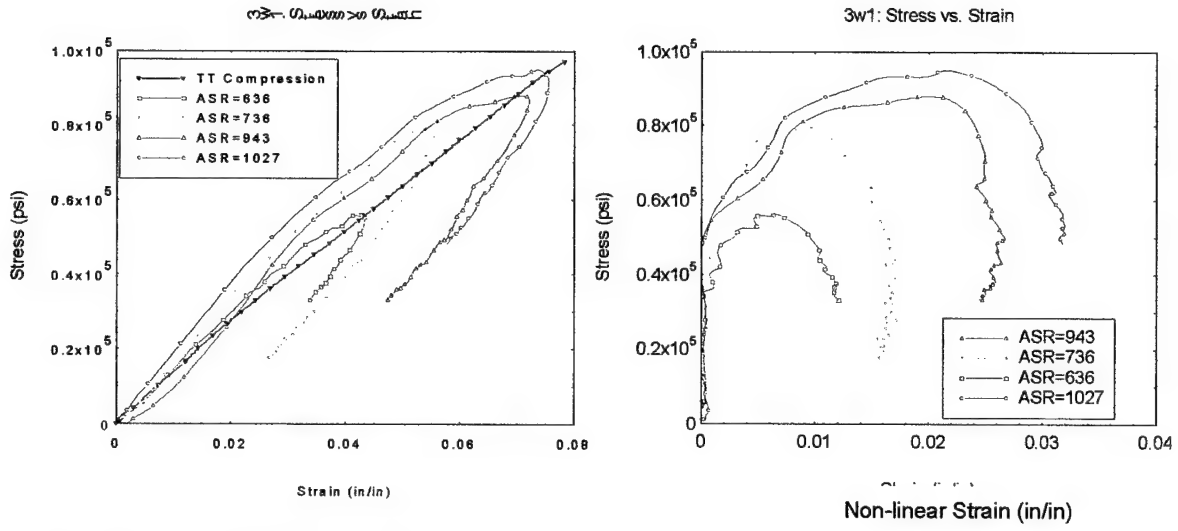

Figure 48: HSR behavior of 3Weave™ #2.

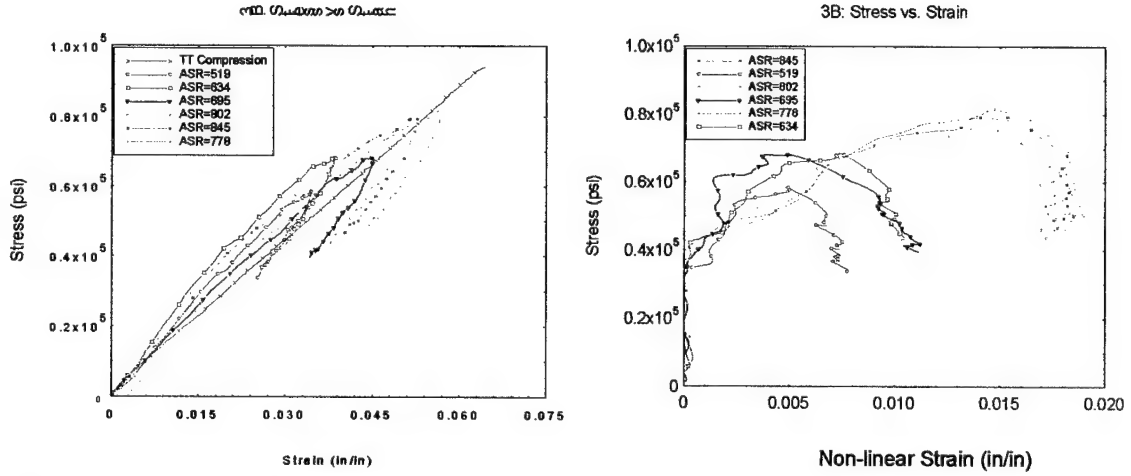

Figure 49: HSR behavior of baseline composite.

5.6 Discussion

The coarse, heterogeneous structure of the 3-D woven glass roving reinforcement obscured ultrasound inspections. This was caused by the resin pockets in each 3-D woven ply, which cause variations in density. Such resin pockets are not necessarily perpendicular to the plate surface, and therefore scatter the transmitted sound, obscuring the boundary of delaminations. Fortunately, the composite panels were translucent, and delaminations can be identified readily by eye. (Visual identification of impact damage extent was used in subsequent, non-perforating ballistic impact tests, described below.)

CAI strengths could not be extrapolated back to zero impact damage, because non-impacted specimens failed at the discontinuity in edge supports near the upper grip of the SACMA fixture. This failure mode is unrelated to the impact damage-induced shearing failures presented here. Therefore, compressive strength retention after impact could not be quantified. The observed failure pattern of laminated 3-D woven plies – failure along an approximately 45 degree inclination to the load, following crowns of z-yarns on each surface – is similar to compressive failure observed in singe ply 3-D woven composites reported in the literature (*e.g.*, [Cox 1995]).

3Weave™ #1 differentiated itself in impact damage area and CAI strength from the baseline and 3Weave™ #2 increasingly as impact energy increased. The poor performance of 3Weave™ #2 may be due to imbalance in composite properties: subsequent static tests of single ply composites of 3Weave™ #2 in Derakane 411-350 vinyl ester showed that the fill direction had about 25% lower modulus and strength in the fill direction than the warp direction. CAI tests were performed in the fill direction.

Through-thickness compression was necessary to determine elastic response, used in subsequent interpretation of SHPB data. As mentioned in section 4.4, [Vaidya *et al.* 1999] performed through-thickness compression tests on 2-D woven S-2 glass / epoxy laminates, stitched with Kevlar® plied cord, and also observed a modest decrease in through-thickness stiffness. They attributed the stiffness decrease to resin pockets through the laminate thickness, surrounding the stitch yarns. Z-yarns in the 3-D orthogonal woven structure are surrounded by similar resin pockets.

SHPB tests were constrained to by the coarseness of the reinforcement unit cell sizes (table 2). Using specimens of sufficient size to integrate across the unit cell constrained the maximum strain achievable. As a result, SHPB specimens could not be loaded to compressive failure, and showed some elastic recovery as the stress weave passed. The stress-strain curves reported represent damage accumulation below the failure point.

6. Ballistic Testing

6.1 Introduction

Two studies of ballistic impact were conducted to compare 3Weave™ and the baseline composites. The first (section 6.2) was non-perforating impact tests, in which plates of 3Weave™ and the baseline fabric were consolidated into backing plates, bonded to aluminum strike faces, and impacted and sub-perforation velocities with 12.7 mm fragment simulating projectiles (FSPs). Damage to both FRP backings were examined. In a second study (section 6.3), not promised in the STTR proposal, the commercial potential of 3Weave™ composites was explored by making prototype body armor inserts, using an alumina core and both 3Weave™ and baseline FRP backings, and subjecting both to NIJ 0101.04 level 3 standalone testing.

6.2 Non-perforation Ballistic Testing

This section describes delamination damage induced by ballistic impact on 3-D orthogonal woven and plain woven S-2 glass / epoxy vinyl ester laminates. Targets composed of aluminum strike faces and S-2 Glass laminate backings were impacted with 12.7 mm FSPs.

6.2.1 Target Construction

Two targets were made. Both targets had 0.375" 6061-T6 aluminum strike faces. Target 1 used 1 ply of 3Weave™ #4, a 270-oz/yd^2 3-D orthogonal fabric woven near the end of phase 1. This

fabric was 15.5-in wide, and was mounted on a 16-in x 15.5-in strike face. Target 2 used 12 plies of the baseline SBA240F 50" 24 oz/yd^2 plain woven rovings. Targets were made via VaRTM infusion with Dow Derakane 8084 rubber-toughened epoxy vinyl ester, and trimmed to size. The 3Weave™ fabric panel could be made between the base mold and a caul plate, without distribution media, leaving two relatively smooth sides. An attempt to infiltrate the stacked plain woven baseline fabric directly between two caul plates failed, apparently because of the lower permeability of the fabric. Therefore, the baseline panel was made with distribution media. This left one smooth and one somewhat rough side.

Fiber volume fractions were estimated from measured preform areal weight and panel thickness (ASTM S2854 method 2), and by assuming no voids and using the nominal specific gravities of S-2 glass (2.49) and Derakane 8084 (1.13). Values are given in table 14. The former method gives lower fiber volume fraction, however, the difference is within one standard deviation of average panel thickness. This may suggest a void content of around 1%, variation in fiber density (which have been noted in picnometric studies by a customer of 3TEX 3-D woven S-2 glass rovings), or variation in resin density. Backing plates were too large to be post cured in an oven at 3TEX. Therefore, they were air cured at room temperature for 24 hours and then at elevated temperature (~140°F) for seven days.

Table 14: construction of backing plates for non-perforating ballistic impact tests.

target	Aluminum face		FRP Backing								
	material	thickness (in)	plies	structure	ply AW (oz/yd^2)	number of plies	total AW (oz/yd^2)	thickness (in)	thickness (std dev)	nominal %V_f by ... thickness	fiber, resin density
1	6061-T6	0.375	1	3-D	270	1	270	0.30	2.7%	47.9%	49.1%
2	6061-T6	0.375	12	2-D	24	12	288	0.30	5.3%	51.5%	53.5%

The aluminum plates were bead-blasted thoroughly on one side, to promote mechanical adhesion. The smoother, tool side of the FRP plates and the bead-blasted side of the aluminum plates were washed with distilled water, then dried with compressed air, then scrubbed with a stiff brush in acetone three times, then dried again with compressed air. An effort was made to either use gloves or to only touch the panels by the edges, to minimize skin oil contaminating the mating surfaces.

The mating surface of the aluminum plates were then smeared with approximately 200 grams each of Sealpak CS3204B2 polysulfide adhesive (mil spec MIL-S8802-FTYCL2). The polysulfide adhesive was smoothed with a squeegee. 0.030-in diameter glass beads were sprinkled across the adhesive, to ensure a minimum bondline thickness. The FRP plates were then slowly lowered onto the adhesive of the aluminum plates, with an effort made to press out any entrapped air. The three adhered aluminum/FRP panels were then stacked on top of each other and pressed under a block of steel weight approximately 2600 lbs, for a nominal pressure of 8-9 psi, for 70 hours at approximately 72F, to develop handling strength. The panels were then unloaded and placed at elevated temperature (approximately 140F) for 24 hours to cure. Figure 50 shows the assembled and cured targets.

6.2.2 Ballistic Testing

The two targets were tested versus unsaboted, 13.4 gram, 12.7 mm FSPs at H.P. White Laboratories. Impact velocity was calculated from the time difference between two in-line light screens, and standard drag tables. The panels were intentionally impacted at velocities below the expected perforation velocity, so that the FRP backing would be damaged from the impact shock wave and subsequent dynamic deflection, but fibers would not be broken by shearing of the

advancing projectile. We estimated the perforation velocity to be around 1500 ft/s. We knew from past experience that, at velocities below about 1000 ft/s, the projectiles' powder charge would not consistently burn uniformly, leading to balloting in the projectile. This would increase the likelihood of impacting the strike face at an oblique angle. Therefore, we tried to limit tests to between 1050-1450 ft/s.

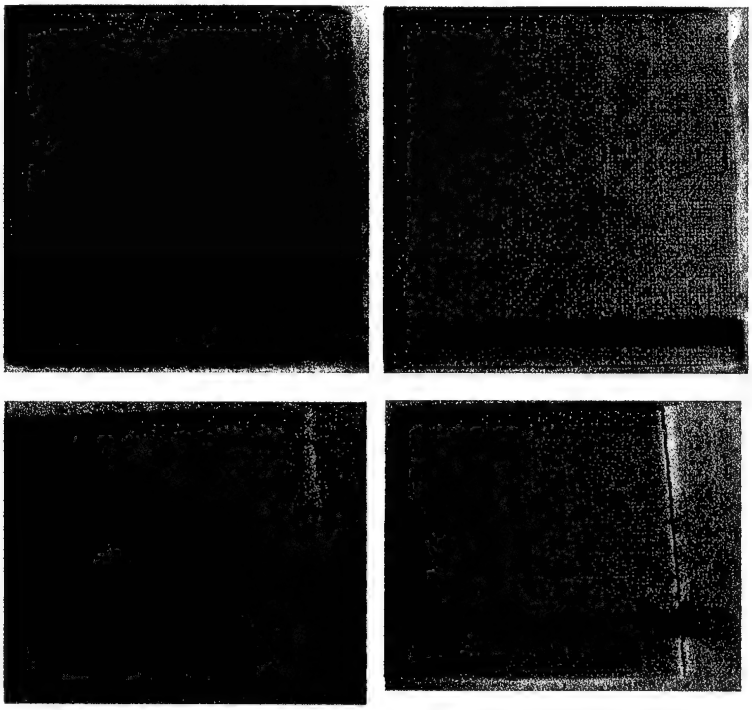

Figure 50: Targets made for non-perforating ballistic impact testing, consisting of 0.375-in 6061-T65 aluminum strike face, bonded to ~0.28-in S-2 glass composite backing plate. Target 2 (12 plies of 24-oz plain weave – the baseline fabric) in backing is shown at top. Target 1 (one ply of 270-oz 3Weave™ – fabric 4) in backing is shown at bottom. An 18-in ruler indicates scale.

Targets were clamped with heavy C-clamps at each corner to two different, welded steel box beam frames. About 0.5-in of the edges of target 1 and about 1-in of the edges of target 2 were supported by the frames. The baseline material (target 2) was shot first. The size of visible damage on the FRP back face required that a maximum of five shots be put into the target, in order to maintain separation between the visible back face damage created by each shot. A five shot pattern was then shot into target 1, over the same range of velocities. Table 15 gives the impact velocities for each target. Note that the smaller size of target 1 (3Weave™ fabric 4) required that the five shots be fired closer together than into target 2 (the baseline).

Table 15: Impact velocities of 12.7 mm FSPs into non-perforating ballistic test targets.

Shot Number	Impact Velocity (ft/s)	
	Target 1	Target 2
	$[270]_1$ 3-D	$[24]_{12}$ 2-D
1	1455	1434
2	1334	1376
3	1411	1336
4	1272	1099
5	1224	1183

6.2.3 Analysis of Tested Panels

After testing, the panels were transported to 3TEX for analysis. The ten FSPs were firmly embedded into the aluminum strike plates, and could not be readily extracted with pliers, indicating that they had deformed within the aluminum plates. A typical FSP is shown in figure 51. No delaminations were visible along the plate peripheries between the aluminum and the FRP. The tested targets are shown in figure 52.

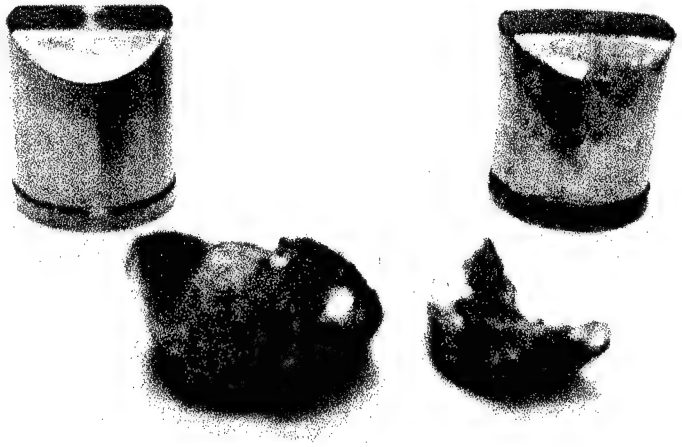

Figure 51: (left) 12.7 mm FSP(unfired), (right) 12.7 mm FSP recovered from shot 5 into target 1, (center foreground) aluminum shear plug from shot 5 into target 1, found almost completely detached from aluminum plate.

The ten impact damage areas on the FRP backings were digitally imaged, each beside a precision ruler for scale. The images were then artificially contrasted, printed onto graph paper, and the visible damage area on the FRP back faces determined by counting the area on the printed images by hand. To assess the uncertainty in damage area induced by this process, it was assumed that the damage areas were circular, and that their diameter could be determined to within one interval on the graph paper. For this case, Kline-McKlintock uncertainty analysis [Kline & McKlintock 1953] gives uncertainties in measured damage area of 4-7%. Impact velocities, damage areas and uncertainties are given table 16. Figure 53 plots the area of visible damage on the target back face versus impact velocity for the two targets, as well as linear fits to the data. The proportionality constant in the two fits, 0.0504- and 0.0244-in^2/(ft/s), differ by a factor of slightly more than 2, suggesting that, for the same impact velocity, the area visibly damaged by the impact is about twice as large for target 2 (the 2-D woven baseline) as target 1 (3Weave™ fabric

4). This is in spite of the fact that target 2 has about 7% higher areal weight in glass, and about 1-in larger spacing between shots to help mitigate damage area coalescence.

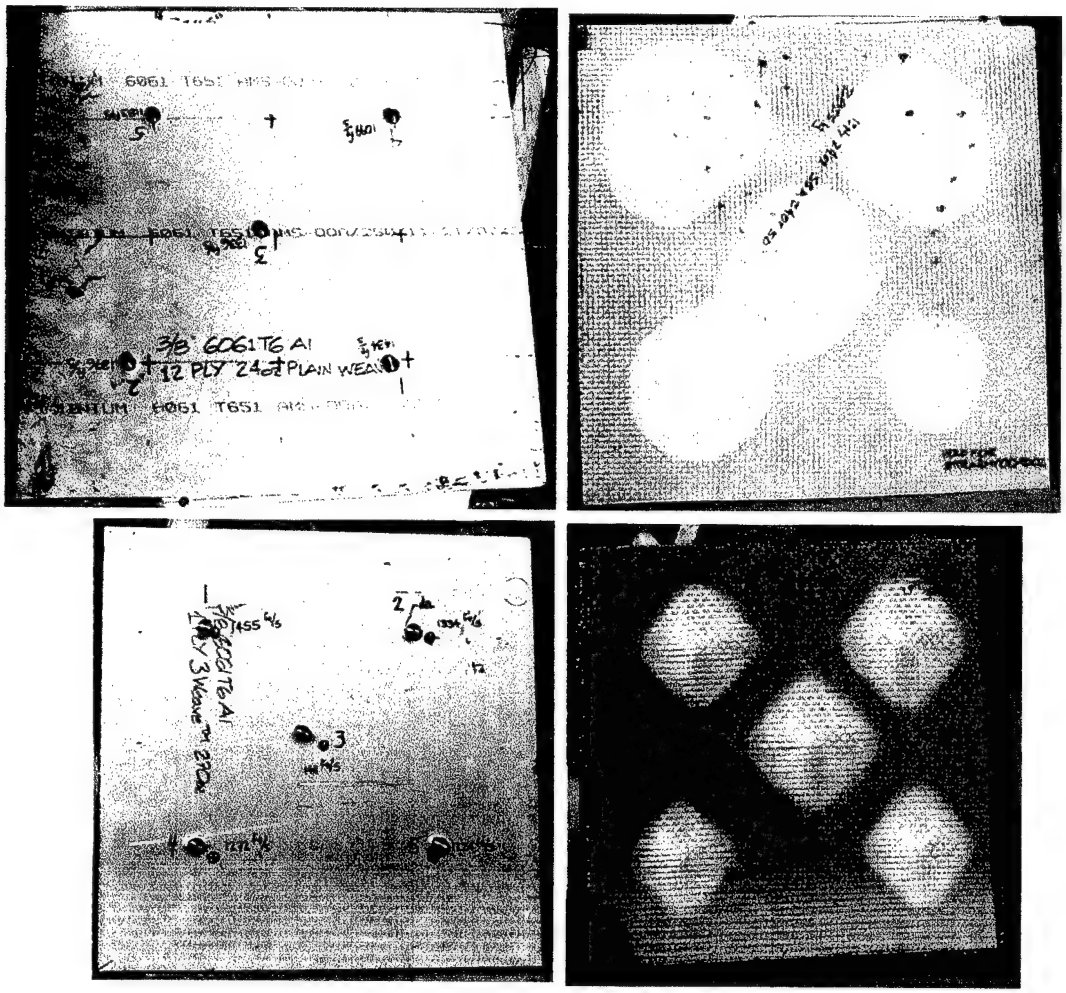

Figure 52: Targets after testing in non-perforating ballistic impact testing, consisting of 0.375-in 6061-T65 aluminum strike face (left), bonded to ~0.28-in S-2 glass composite backing plate (right). 18-in x 18-in target with 12 plies of 24-oz plain weave (the baseline fabric) in backing is shown at top. 16-in x 15.5-in target with one ply of 270-oz 3Weave™ (fabric 4) in backing is shown at bottom. Each target was shot five times with 12.7 mm FSP (shown embedded into the aluminum strike face).

It could be argued that plotting damage area versus impact energy (proportional to the square of velocity) is more physically meaningful than versus impact velocity. Fitting visible back face damage area linearly to the square of impact velocity (*i.e.*, proportional to projectile kinetic energy), gives fit coefficients differing by less than 2% from those in figure 53 ($R^2 = 0.93$ and 0.73 in the former case, and 0.93 and 0.72 in the latter case). It is therefore not clear that examining damage area versus impact energy would be more useful.

Table 16: Impact velocity, visible back face damage area, and estimated uncertainty in measured visible back face damage area for non-perforating ballistic targets.

Target	Shot Number	Impact Velocity (ft/s)	Damage Area (in^2)	Estimated Uncertainty in Area
Target 1	1	1434	31.9	4.2%
$[270]_1$ 3-D	2	1376	29.8	4.3%
	3	1336	27.9	4.1%
	4	1099	13.7	4.8%
	5	1183	22.9	4.4%
Target 2	1	1455	15.6	4.5%
$[24]_{12}$ 2-D	2	1334	14.1	6.6%
	3	1411	18.3	4.3%
	4	1272	13.4	4.8%
	5	1224	11.0	5.3%

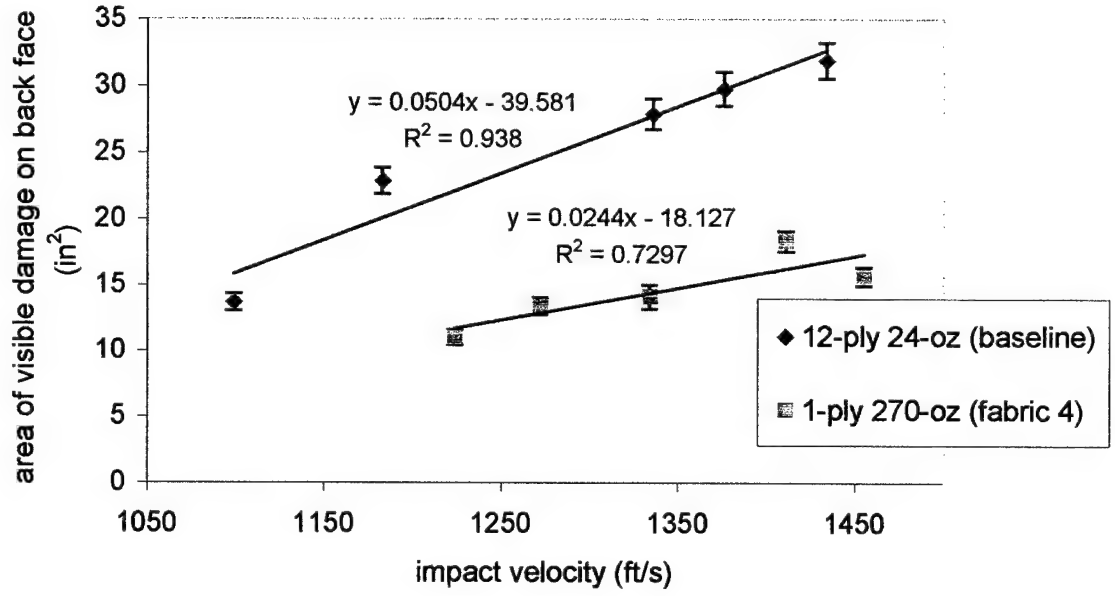

Figure 53: Visible damage area on FRP back face versus impact velocity for non-perforating ballistic strikes, with linear regressions. Error bars are estimated uncertainty in visible back face damage area.

The backing plates were separated from the aluminum strike faces with wooden wedges, to avoid inducing further damage. The polysulfide adhesive appeared to have delaminated at each impact site, to an extent of about one projectile diameter. Outside the immediate vicinity of the impact sites, the adhesive was still bonded to both the aluminum and the FRP, indicating that the adhesive layer was created uniformly and correctly in both panels. The aluminum shear plugs created by the faster projectiles (figure 51) were only connected to the bulk of the aluminum plates by thin ligands, spanning less than 90 degrees of the projectile perimeter. This indicated that the faster impacts were indeed near the ballistic limits of the targets.

Damage in the 3Weave™-reinforced FRP (target 1) consisted of ('front' means toward the aluminum plate strike face):

1. Diamond-shaped areas of visible damage, with the vertices corresponding to the warp- and fill-directions. The vertices were of the same approximate length. The visible damage area on the front and back sides were approximately the same size.
2. Abraded z-yarn crows on the surface of the FRP plate, at the interface with the aluminum plate.
3. Debonding of surface resin pockets between yarns. These resin pockets pulled away with the polysulfide adhesive.
4. Debonding between the frontmost fill layer and the bulk of the FRP.
5. Cracks in the surface resin on both the front and visible at 45 degrees to the warp-and fill-directions. These cracks were oriented at about 45 degrees to the warp- and fill-directions. This location and direction coincides with the highest tensile membrane strains that the orthotropic composite would experience in dynamic deflection.

Damage in the baseline FRP backing plate (target 2) consisted of ('front' means toward the aluminum strike face):

1. Essentially round areas of visible damage. These areas consisted of arcs of varying intensity of whiteness, indicating overlapping delaminations through the panel thickness. Debonding of surface resin pockets between yarns. These resin pockets pulled away with the polysulfide adhesive.
2. Cracks in the surface resin on both the front and visible at 45 degrees to the warp-and fill-directions. These cracks were oriented at about 45 degrees to the warp- and fill-directions. This location and direction coincides with the highest tensile membrane strains that the orthotropic composite would experience in dynamic deflection.
3. Visible impact damage area was smaller on the front face than on the back face.

The damage area behind the fastest impacts (shot 1 in each case) were sectioned with a water-fed tile saw, through the impact center, parallel to the warp direction. The resulting cross sections are shown in figure 54.

Target 1 was cut parallel to the warp direction. The cross-section showed fine cracks, visible across transversely-cut fill yarns. These cracks emanated from the center of impact, and propagated outward and backward (see figure 55), in a direction that would form a classical impact conoid.

Scratching the cut surface of target 2 with a fingernail confirmed that the impact damage seen on the back face corresponded to delaminations, which could be opened by a fingernail. Four delamination planes, all in the back half of the plate, were evident. The first two (front-to-back) were separated by two plies. The last two separated single plies. Delamination area appeared to increased from front to back, as expected.

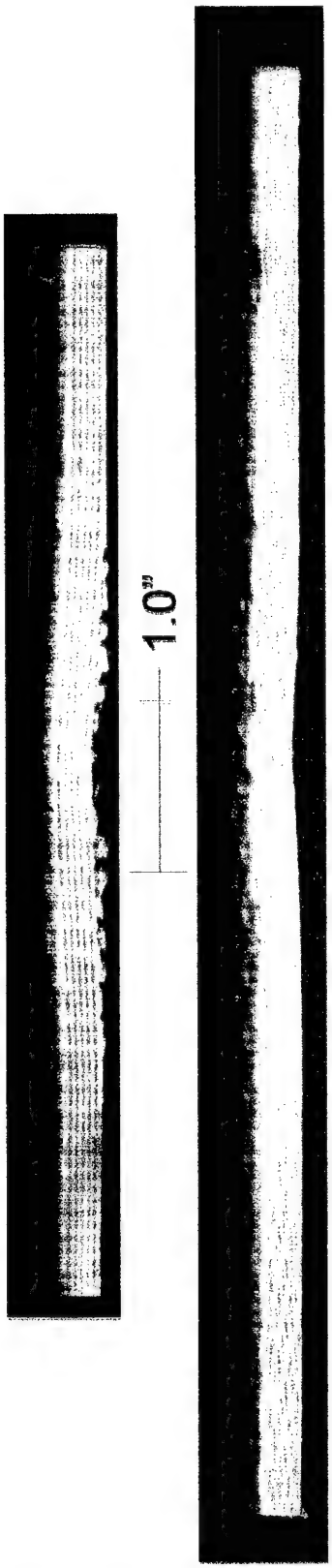

Figure 54: Cross sections parallel to warp direction of FRP backing plates after non-perforating ballistic strike, enclosing visible damage areas. Aluminum strike face was removed. Left: target 1 (1 ply 270-oz 3Weave™), shot 5 (1455 ft/s). Right: target 2 (12 plies 24-oz baseline), shot 5 (1434 ft/s).

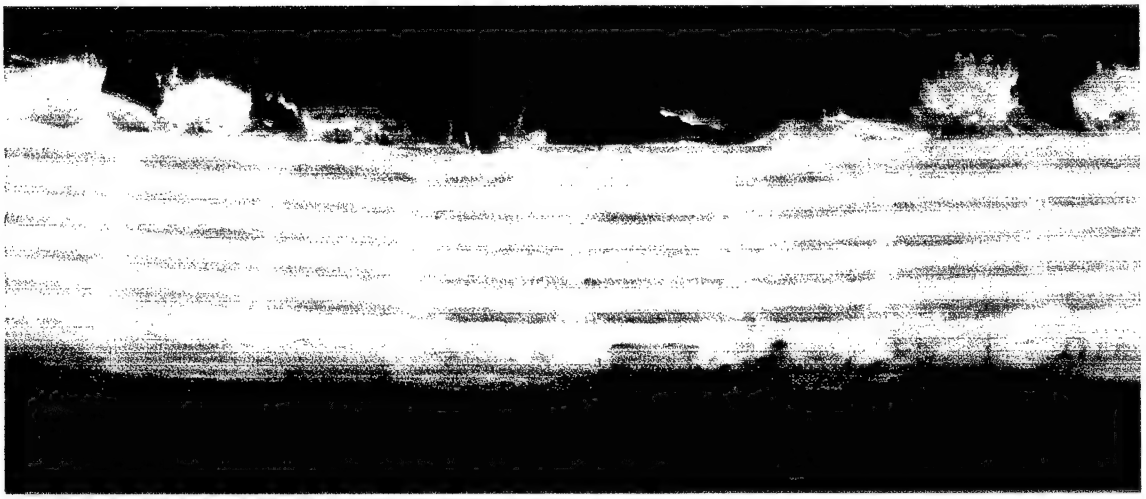

Figure 55: Close-up of cross section in warp-z plane of FRP backing plate in target 1, showing cracking in fill yarns (perpendicular to cut). Aluminum strike face is removed. Impact direction is down. Shot 5, 1455 ft/s. Notethat delamination was suppressed.

6.2.4 Discussion

Non-perforating ballistic impact tests performed, the visible back face damage area in 3Weave™ fabrics was about twice as small as in the baseline fabric, despite the 3Weave™ containing about 7% less fiber reinforcement. Qualitatively, the non-perforating ballistic impact tests performed agreed with conclusions from low-velocity impacts, that:

1. For balanced 3-D weaves (such as fabrics 1 and 4), 3-D woven composites contain impact damage to within significantly smaller areas than the 2-D woven baseline.
2. The difference in the area of damage containment appears to grow as the severity of the impact increases.

These observations suggest the family of 3-D woven composites examined offer advantages in terms of multiple hit integrity. However, they raise the question: *what is the trade-off between damage localization and reduction in ballistic efficiency in 3-D woven-reinforced composites?* We sought to address this question meaningfully in perforating ballistic tests, described in the next section.

6.3 Ballistic Testing of Body Armor Inserts

6.3.1 Introduction

Perforation mechanics are sensitive to penetrator shape and material, penetration velocity, and target boundary conditions (*e.g.*, [Bless & Hartman 1989]). Therefore, an extensive ballistic test protocol might be devised. The time and budget a phase 1 prohibited in-depth exploration. Further, the goal of the STTR program is to develop materials and products of use to the military. From these two constraints, we sought one set of ballistic tests on 2-D- and 3-D-reinforced targets of potential military interest, which could be brought to near-term commercialization by 3TEX.

Further, we sought a test protocol, which could be of military interest. We decided to build prototype body armor inserts (BAIs), comparing the baseline fabric with a 3-D woven FRP backing. We tested the BAIs according to National Institute of Justice (NIJ) standards. These BAIs, the ballistic testing, and the test results are discussed in the next section.

Armor body inserts (BAIs) were built, using 3-D woven S-2 glass, to demonstrate the commercial potential of the materials examined in this study. BAIs of plied 3Weave™ fabric 1 and the baseline were constructed by 3TEX, and tested per National Institute of Justice (NIJ) standard 0101.04 level 3 standalone (*i.e.*, without mounting to a cloth armor vest). This standard is used to certify personnel armor for US law enforcement officers. Level 3 protection requires stopping six 7.62 mm M80 ball rounds, at a velocities in excess of 2750 ft/s. Level 3 was selected because:

1. Current commercial level 3 BAIs use hardened steel or ceramic strike faces, backed by a variety of FRP materials, including more expensive aramids and polyethylene fibers.
2. Because the BAI is struck six times with a high-powered rifle round, level 3 testing places the highest premium on impact damage localization on the FRP backing.

Ceramic strike faces are generally covered with a thin layer of FRP and ballistic nylon on the front of the BAI, to minimize forward-projecting spalls.

6.3.2 Body Armor Insert Construction

Figures 56-59 show the BAIs produced, after ballistic testing. Six BAIs were produced for this study. All used 8.5 mm, single curvature, monolithic, high purity alumina cores, from the same production series, made by CoorsTek, Golden, CO. All used a strike face ply of 24-oz/yd^2 plain-woven fabric S-2 glass rovings, to wrap around the ceramic strike face, and adhere it to the FRP backing plate. The constituents of the FRP backing plates, between the ceramic and the backing ply, differed between the six plates. Three BAIs had backing plates of 2-D weave, and three BAIs had backing plates of 3-D weave. All BAIs used Derakane 8084. To demonstrate that the baseline material used (woven by Knytex), was of normal quality, one of the BAIs with a 2-D fabric backing plate used nominally identical, 24-oz fabric, woven by 3TEX.

All fabrics were cut by hand with shears, after being marked by the same templates. Previous investigations into processing BAIs with 3Weave™ and 2-D fabrics demonstrated that, while 3Weave™-backed BAIs could be molded by VARTM, the lower permeability of the baseline material required that each ply be prewetted before VARTM, in order to ensure that the part was completely wet out, especially at the ceramic/FRP interface. To ensure that all parts were processed identically, and that all parts were completely wetted out, BAIs for this investigation were all made by the combination of wet molding and VARTM necessitated by the lower permeability, baseline fabric. A female mold with an open back was cast around a master of the size of the desired BAIs. Breather and peel plies were laid into the mold. The strike face ply, cut out to allow edges to fold over and around the assembled part, was laid in the mold, then prewetted with a small amount of resin. Then the ceramic element was added, and a small amount of resin was poured onto the body side. Then the plies of the backing plate were added one at a time, with each prewetted and the resin worked in briefly by hand. The higher ply count and manual labor required to prewet each ply made production of the 2-D-reinforced BAIs more labor intensive than the 3-D-reinforced BAIs. Before the last ply was added, the edges of the strike face ply were folded over onto the backing plate. Then the last ply was added, followed by peel and breather ply, the top of the mold sealed and evacuated, and additional resin allowed to flow through the BAI until the resin gelled. The BAIs were allowed to green cure in the mold (approximately one hour), then post cured for four hours at room temperature and 12 hours at 180F.

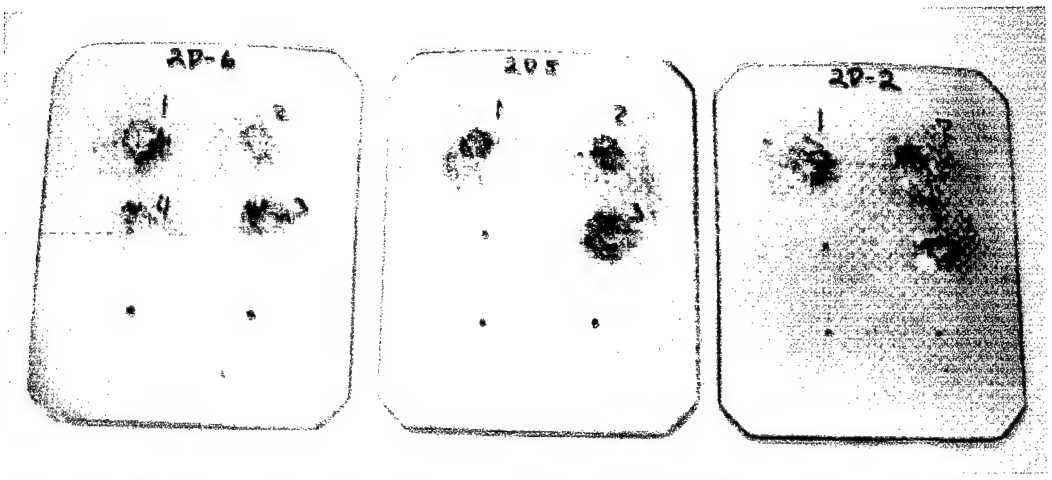

Figure 56: Fronts of armor body inserts made with baseline, 2-D backing, after testing against 7.62 mm M80 ball rounds per NIJ 0101.04. Left to right: inserts 2D-6, 2D-5, 2D-2.

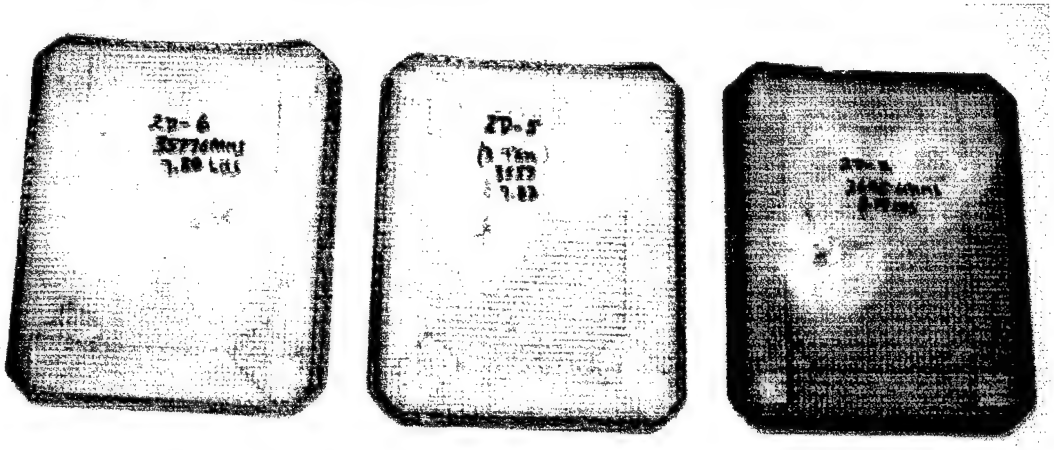

Figure 57: Fronts of armor body inserts made with baseline, 2-D backing, after testing against 7.62 mm M80 ball rounds per NIJ 0101.04. Left to right: inserts 2D-6, 2D-5, 2D-2.

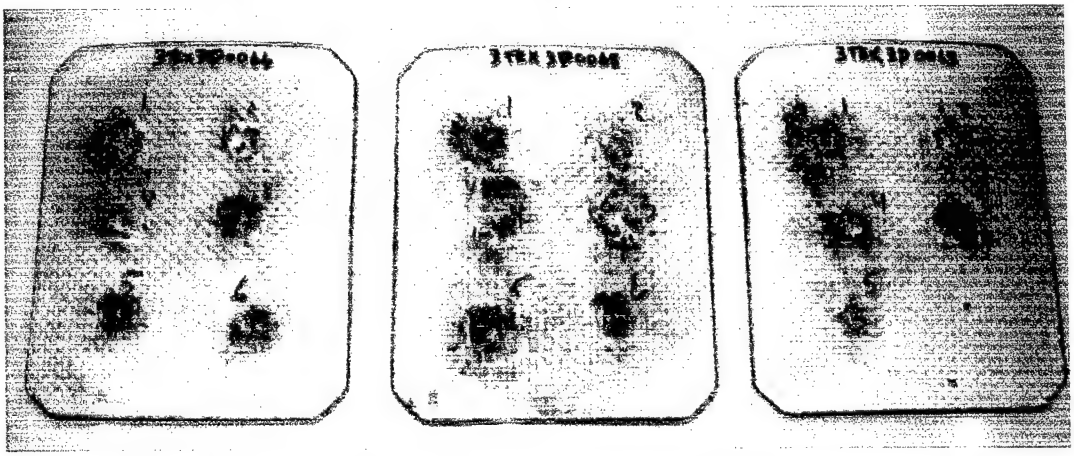

Figure 58: Fronts of armor body inserts made with 3Weave™ 3-D woven backing, after testing against 7.62 mm M80 ball rounds per NIJ 0101.04. Left to right: inserts 0066, 0065, 0063.

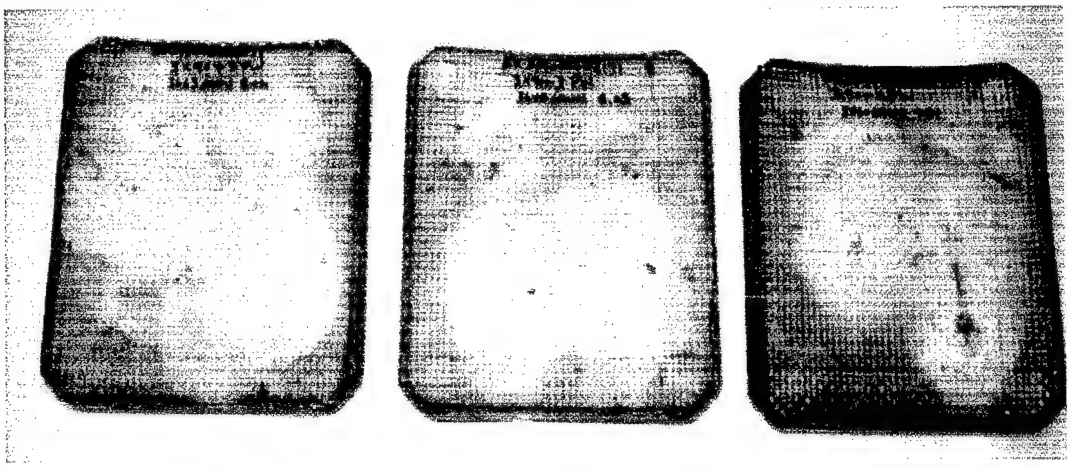

Figure 59: Backs of armor body inserts made with 3Weave™ 3-D woven backing, after testing against 7.62 mm M80 ball rounds per NIJ 0101.04. Left to right: inserts 0066, 0065, 0063.

Creating BAIs from the 2-D and 3-D backings of equal areal weight proved impossible, for two reasons. First, the areal weight of the 3-D woven fabric was not an integer multiple of the areal weight of the baseline. Second, the baseline fabric, lacking through-thickness fiber to constrain its height, tended to absorb more resin than the 3-D woven plies, and swell out of the mold during VARTM infusion. In order to bracket the areal weight of the BAIs with the baseline fabric, varying numbers of 24-oz plies were added to the 3-D-reinforced BAIs, to give comparable total weights of glass.

Table 17: Construction of body armor inserts, using 2-D and 3-D woven S-2 glass backings. FRP stacking sequence denoted by A_i, meaning i plies of A areal weight (in oz/yd^2). FRP contents denonted as 3TEX are 3-D and 2-D woven fabrics made by 3TEX. The default is the baseline, Knytex 24-oz/yd^2 plain woven baseline.

Plate ID #	ceramic mass (g)	FRP cover	FRP backing plate	FRP mass (g)	total plate weight (g)	total plate weight (lb)
2D-2	2338	$[24_1]$	$[24_{13}]$	871	3695	8.15
2D-5	2328	$[24_1]$ - 3TEX	$[24_{13}]$ - 3TEX	868	3553	7.83
2D-6	2340	$[24_1]$	$[24_{13}]$	866	3577	7.89
0063	2342	$[24_1]$ - 3TEX	$[90_3/24_2]$ - 3TEX	845	3560	7.85
0065	2345	$[24_1]$ - 3TEX	$[90_3/24_3]$ - 3TEX	885	3648	8.04
0066	2335	$[24_1]$ - 3TEX	$[90_3/24_3]$ - 3TEX	888	3663	8.08

6.3.3 Body Armor Insert Ballistic Testing Conditions

The six BAIs were tested at H.P. White Laboratories, Street, MD, according to a slight modification of NIJ 0101.04 level 3. Each BAI was mounted on a box of Roma Plastilina clay, conditioned to 85F[4], which was driven into the curvature of the plate. The BAI was then strapped

[4] The 0101.04 standard, which superceded the 0101.03 standard in 2000, increased the temperature of the clay from 75F to 85F or higher to achieve a required decrease in clay stiffness. This seemingly minor change greatly reduces the support that the clay can give to BAIs, making it more difficult to certify level 3 especially. In level 3 testing under NIJ 0101.04, the clay resists the deflecting plate much less, drastically increasing strains experienced by the BAI, and dynamic deflection into the clay. Dynamic deflection imprint into the warmer, less viscous clay, is thus larger than the shot-to-shot spacing. Therefore, subsequent shots fire onto parts of the BAI unsupported by the clay, allowing evenhigher dynamic deflections. 3TEX designs have increased in weight by about 5% in order to accommodate the new, more

to the clay with nylon straps. 7.62 MM M80 ball rounds were fired into the BAI, in a nominally identical shot pattern, until either six shots were fired, or one shot perforated the target, whichever came first. Each round had to be no less than 3-in from any edge, and 3-in from other shots. The velocity of the projectiles was specified at 2750 ft/s, as measured by double sets of digital chronographs connected to two light screens, which measured the time required for the bullet to pass between them. Actual impact velocity varied between 2756-2814 ft/s. After each round was fired, the maximum distance that the BAI deformed the clay was measured, and the (now damaged) BAI was reseated on the (now damaged) clay backing. Testing proceeded until all six rounds were fired, or until the BAI was perforated, whichever came first, then the clay was repaired, and the next BAI mounted and tested. (This was the modification to the test standard: in NIJ certification testing, if one BAI is perforated, the entire lot of BAIs fails certification, and no additional BAIs of the same lot are tested.) In NIJ testing, an insert could also fail if it leaves 44 mm or more dynamic deflection in the clay backing. For the plates tested, no dynamic deflection was greater than 44 mm on partial penetrations.

6.3.4 Body Armor Insert Ballistic Test Results

Perforation results of the test are given in figure 60. Dynamic deflection into clay for each shot is given in figure 61. All 3Weave™-backed BAIs, weighing from 7.85 to 8.08 lbs, outperformed all 2-D weave-backed BAIs, weighing from 7.83 to 8.15 lbs. The two 3Weave™-backed plates between 8.0 and 8.1 lbs met the NIJ 0101.04 criteria. As expected, dynamic deflection tends to increase with each additional round fired into a BAI. This actual dynamic deflection often depends on the size of the ceramic fragment that each bullet encounters, and so has large variation. In all 2-D- and 3-D-reinforced BAIs tested, the dynamic deflection criterion of 44 mm was met if the bullet did not completely perforate the BAI.

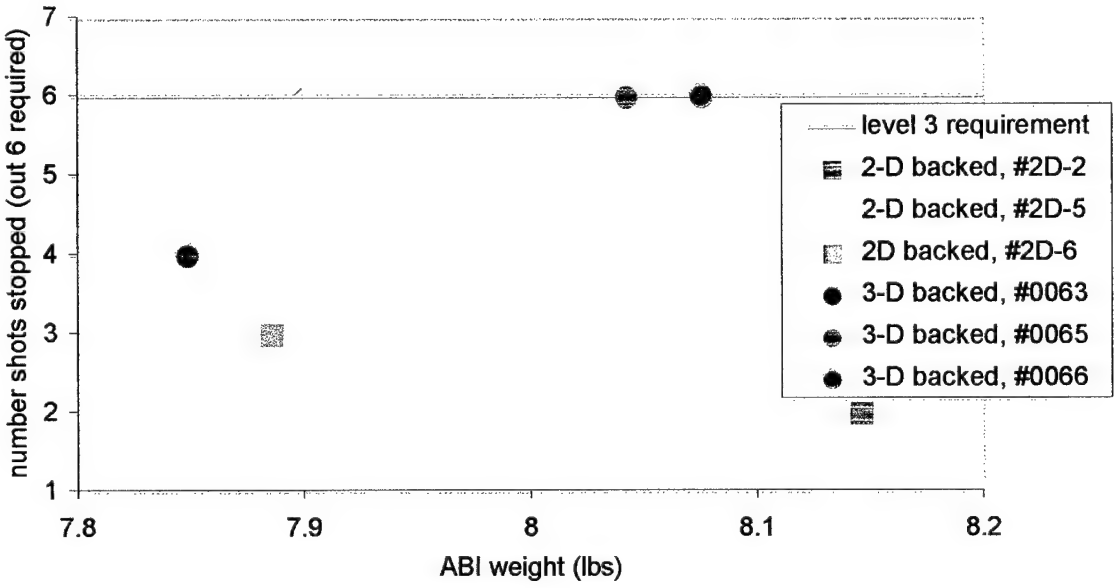

Figure 60: Number of 7.62 mm M80 ball rounds stopped versus BAI weight, for 2-D- and 3-D-reinforced armor body inserts tested per NIJ 0101.04 level 3. Certification requirement is 6 shots.

stringent test. This is why BAI 0063 (the previous design, which met NIJ 0101.03) perforated on the fifth shot, and 0065 and 0066 (the current design) were correspondingly slightly heavier to pass 0101.04.

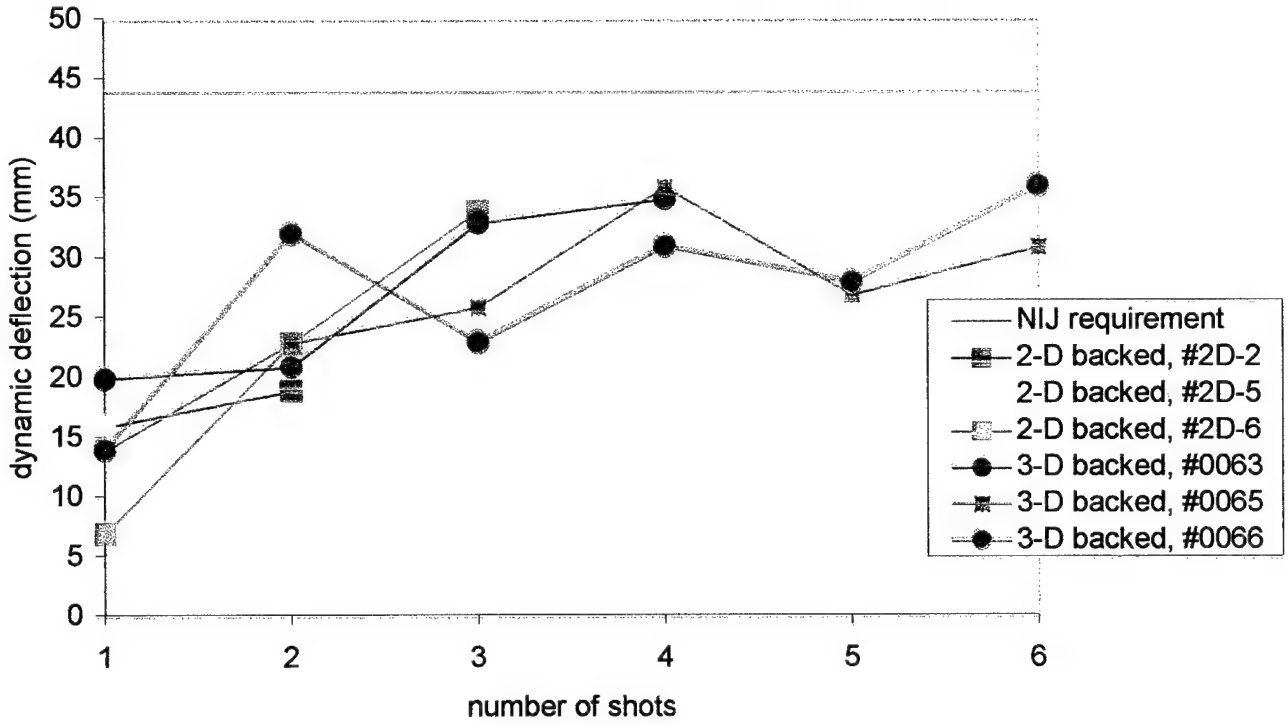

Figure 61: Blunt trauma into clay for each shot not completely perforating armor body insert, for 2-D- and 3-D-reinforced BAIs tested versus 7.62 mm M80 ball round per NIJ 0101.04 level 3. The NIJ requirement is to not exceed 44 mm.

6.3.5 Discussion

Tests on BAIs demonstrated that the improved impact damage tolerance of the 3Weave™ S-2 glass fabrics examined in this study can be used to improve performance of armor systems of practical and immediate interest. Test data reported here is for NIJ level 3 standalone. Additional tests on similar 3Weave™-reinforced plates (reported in the phase 1 proposal) demonstrated they can stop multiple hits from 7.62 mm M2 AP rounds in standalone configuration. To our knowledge, the 3-D woven-reinforced BAIs reported here are lighter than any other, alumina-cored level 3/4 standalone BAIs available to police. Our experience with more expensive, higher mass efficiency ceramics, such as silicon carbide, which are used by the military and are not yet generally available commercially, is that 3Weave™ S-2 glass fabrics used in composite backings allow similar improvements in multiple hit capability.

This improvement in ballistic performance appears to come with the benefit of more economical production. First, the heterogeneity of the 3-D woven structure leads to easier infiltration of composite preforms, simplifying consolidation technique and reducing consumables used in resin transfer. Customers of 3TEX fabrics reported that the improved infiltration allowed them to eliminate ultrasonic testing for dry spots in armor articles, a costly quality control step they found necessary when using the baseline 24-oz fabric. Second, reducing the number of plies used in an article greatly reduces labor costs, and the chance for accidentally using few plies of fabric in the backing reinforcement.

7. Discussion

We examined systems of interest in structural armor applications: S-2 glass rovings in rubber-toughened epoxy vinyl ester and in rubber-toughened epoxy. A family of five related 3-D orthogonal weaves was produced. Composites from those weaves were made along side laminates of 24-oz plain woven S-2 glass, a fabric used commonly in semi-structural and structural armor applications. The composites were tested in for static mechanical properties, low velocity impact and compression strength after impact (CAI), through-thickness strain-rate dependent stress-strain response (via Hopkinson bar), non-perforation ballistic impact (behind an aluminum strike face), and as backing in prototype body armor inserts. This gave broad, but admittedly not deep, evidence about how 3-D woven FRP contrasts 2-D woven FRP in armor systems.

S-2 glass 3-D woven composite materials examined in phase 1 show advantages over the baseline, 2-D woven fabric in:

1. Labor to pattern, cut, and lay up preforms. Labor reductions correspond to number of 2-D plies that can be replaced with 3-D plies. This study looked at 3-D plies equivalent to 4-12 2-D plies.
2. Permeability during resin infusion. We found that the heterogeneous, 3-D woven structure allows faster and more complete resin infusion into thick preforms than the baseline, 2-D fabrics. This observation was not quantified during this study, but could represent a significant advantage over 2-D laminates of S-2 glass rovings, which often prove very difficult to completely wet out through the thickness of a relatively thick laminate during VARTM infusion.
3. Static strength. The static strengths of the 3-D woven composites studied, were around 10-20% higher than for the baseline fabric, or reported in the literature for 2-D S-2 glass laminates being considered for armor applications.
4. Delamination suppression. Quasi-static mode 1 critical strain energy release rate between nested plies of 3-D woven composites was seen to be about 20% higher than the baseline. Mode 1 critical strain energy release rate was seen to be about 500% higher inside 3-D woven plies than in the baseline.
5. Impact damage area containment. In both drop tower and non-perforating ballistic impact, the area of visible impact damage was lower in the 3-D woven composite than the baseline 2-D woven composite. In the former case, the difference in visible damage areas increased with increasing impact energy, to a maximum of 20%. In the latter case, 3-D woven FRP backing reduced visible damage area by about 50%.
6. Impact damage containment. Although admittedly a generalization, it appears from phase 1 testing that reduced area of visible impact damage in FRP correlates with retained structural integrity. This was demonstrated by up to 20% higher CAI strengths after drop tower impact. This was further demonstrated by prototype body armor inserts, in which 3-D woven backings enabled the 10-in x 12-in plates to pass NIJ 0101.04 level 3 stand alone certification at about 8.1 lbs (taking six shots of 7.62 mm M80 ball at ~2750 ft/s), while the same weight 2-D woven backing only stopped two to three rounds before perforation.

It should be remembered that all results were on rubber-toughened resin systems. Since toughened resins tend to increase interlaminar damage tolerance, this comparison would tend to minimize the performance improvements gained by through-thickness reinforcement.

Disadvantages in using 3-D woven fabrics are mostly practical consequences of the differences in weaving between 2-D and 3-D fabrics:

1. 3-D weaving requires a large fiber inventory to start weaving. When set up costs are amortized over full production runs (2000 yards or more for S-2 glass roving fabics), they are competitive with traditional, 2-D weaving costs, because the same length of fabric corresponds to a much higher fabric weight. However, when amortized over small runs, the high set up costs of weaving thick 3-D fabrics can be prohibitive, especially to weave short lengths of broad fabrics.
2. Based on weaving efforts in phase 1, we believe that the thickest fabrics we can currently, practically weave from 250 yd/lb S-2 glass rovings would be 0.3-0.4", corresponding to 270-400-oz/yd^2 areal weight. This is too thin to armor heavy vehicles in a single ply. Note that, as demonstrated by the BAIs tested, using laminates of 3-D woven plies still appears to offer advantages over laminates of 2-D weaves.
3. As fabric thickness increases, fabric drape decreases. Very thick fabrics must therefore be treated as board goods, not rolled goods. This could cause costly changes in weaving practice, transportation, and material handling from current practice of using rolled fabrics. For instance, it may require the weaver to weave fabric to lengths specified by the customer for each desired part, necessitating close cooperation between weaver and composite fabricator.
4. Stress concentrations at ply drop offs will be more difficult to design around in 3-D woven composites. As fabric thickness increases, the resulting ply count decreases. Thick laminates of the baseline, 24-oz weave, used in armor applications may have 60 or more layers. In such thick laminates, stress concentrations around individual ply drops may be neglected when they are well-spaced. However, if thick 3-D woven plies are used, and the ply count drops by an order of magnitude, then the stress concentrations around ply drops may be much more significant. Note that this is not a consideration for preforms with one dimension less than the width of a fabric (currently, 3TEX can weave up to 72-in wide fabrics).

8. Possible Future Development and Commercial Applications

The 3-D woven S-2 glass composites designed, fabricated and characterized in this study show (relative to composites of the baseline, plain woven 2-D fabric) good or superior static strengths and superior mode 1 in-plane critical strain energy release rate. In low-velocity impact testing, they show god or superior damage localization and compression after impact strength, with the improvement over the baseline increasing as the impact energy increases. In ballistic impact, the 3-D woven composites limited impact damage area, and were able to effectively support ceramic cores through more impacts. Additionally, the heterogeneity of the 3-D woven structure was seen to wet out more quickly and more thoroughly than the 2-D structure during resin infiltration, and using heavier, 3-D woven plies reduced the labor required to pattern, cut and assemble preforms.

All these advantages should benefit semi-structural or structural armor applications. 3-D weaves should be especially useful where the following qualities are desired:
1. Labor savings during preforming of thick armor sections.
2. Infiltration quality control and/or part rejection costs of large.
3. Increase integrity of structural armor both before and after impact.
4. Greater multiple hit capability through.

Both personal and vehicle armor systems, in which the FRP component provides structural support to a brittle strike face materials, can benefit from all of these potential improvements. We suggest simultaneously pursuing two avenues in future research:

1. Basic research into the mechanics of ballistic failure of 3-D woven composites (both as single plies, and as laminates), and
2. Processing development to learn how to take advantage of the unique processing opportunities that 3-D woven composites appear to afford.

Both fields of research need to drive development of future 3-D weaving, so that the potential advantages of 3-D woven FRP in armor applications, demonstrated in this research, can be applied to cost-efficient armor production. Phase 1 concluded with up to seven of the nine independent elastic constants of 3-D woven FRP determined experimentally, as well as static strengths, G_{1c} and strain-rate dependent through-thickness stress-strain response. All of this data would be necessary input in numerical simulations, which could support parametric studies of 3-D woven FRP ballistic response.

A fundamental question for further research to resolve is *how much through thickness reinforcement is desirable?* Several previous observations of 2-D woven S-2 glass laminates (*e.g.*, [Bless & Hartman 1987]) concluded those systems can efficiently absorb energy by shearing failure, in addition to the large deformation, membrane loading intuitively associated with FRP armor backings. Increasing through-thickness reinforcement, and reducing or eliminating ply interfaces, will increase FRP rigidity, force more shearing failure, and decrease the size of impact damage. Therefore, it should be possible to increase (single shot) ballistic efficiency above the 2-D woven baseline with the proper amount of ply interfaces and ply through-thickness reinforcement. We have already demonstrated this in a contract with Army Research Laboratory (DAAD17-00-C-0054), concluded during the time of this STTR research. The extent to which through-thickness fiber reinforcement should be increased, and ply interfaces reduced, must depend on the interaction between the FRP and the ceramic strike face it supports. Therefore, without a specific ballistic objective and ceramic system to start from, we did not investigate optimizing through-thickness reinforcement in phase 1. Instead, the amount of through-thickness reinforcement was selected based on the desire to minimize reduction in in-plane stiffnesses and strengths (Section 2).

We did not examine the usefulness of 3-D woven reinforcement in non-structural FRP armor systems. In those systems, where delamination is used to increase the distance through which armor can interact with projectiles, the through-thickness integrity that the 3-D woven structure offers may not be useful[5].

9. Conclusions

3-D and 2-D woven systems were characterized both statically and dynamically to assess the relative advantages of 3-D weaves in armor and impact resistant systems. Five different 3Weave™ 3-D orthogonal fabrics were woven from S-2 glass rovings, including both flat goods and near-net shape preforms. 3Weave™ and a baseline, 2-D fabric were consolidated via VARTM using rubber toughened epoxy vinyl ester and rubber-toughened epoxy. Static mechanical properties, including mode 1 critical strain energy release rate, were determined. Composites were tested in drop tower impact, for visible damage area and compression strength after impact. Composites were tested in through-thickness compression in Hopkinson bar tests at strain rates ranging from 500-1000/s. Composites were used to back aluminum plates, and tested against fragment simulating projectiles in non-perforating ballistic impact, to determine visible damage area. Finally, prototype body armor inserts were developed, using alumina cores, in

[5] Interested readers are referred to [Singletary & Bogdanovich 2000] for the performance of 3-D orthogonal woven aramid cloth armor.

which the 3-D woven backings enabled the design to meet NIJ 0101.04 level 3 standalone requirements at an article weight of 8.1 lbs.

10. References

[Abali *et al.* 2000] F. Abali, A Pora, K. Shivakumar,and S. Ghantae, "Modified Short Beam Shear Test For Measurement Of ILSS Of Carbon-Carbon Composites", AIAA paper 2000-1480, 2000.

[Bless & Hartman 1989] S. J. Bless, D. R. Hartman, "Ballistic Penetration of S-2 Glass® Laminates". 21st International SAMPE Technical Conference, 25-28 September 1989, pp. 852-866.

[Bogdanovich & Pastore 1996] A. E. Bogdanovich and C. M. Pastore, Mechanics of Textile and Laminated Composites, With Applications to Structural Analysis. Chapman and Hall, London, 1996.

[Byun *et al.* 1990] J. H. Byun, J. W. Gillespie Jr. and T.-W. Chou, "Mode 1 delamination of a three-dimensional fabric composite". *Journal of Composite Materials* **24**, pp. 497-519.

[Chou 1992] T.-W. Chou, Microstructural Design of Fiber Composites. Cambridge Solid State Science Series, R. W. Cahn, E. A. Davis and I. M. Ward, Editors. Cambridge University Press, Cambridge, MA, 1992.

[Cox 1995] B. N. Cox, Failure Models for Textile Composites. NASA Contract Report 4686, August, 1995.

[Daniel & Ishai 1994] I. M. Daniel and O. Ishai, Engineering Mechanics of Composite Materials. Oxford University Press, New York, 1994.

[Dickinson *et al.* 1999] L. C. Dickinson, G. L. Farley and M. K. Hinders, *Journal of Composites Science and Technology* **21**, 241 (1999).

[Dow & Ramnath 1987] N. F. Dow and V. Ramnath, "Analysis of Woven Fabrics for Reinforced Composite Materials". NASA Contract Report 178275, April 1987.

[Gama 2001] B. A. Gama, personal communication, March 2001.

[Guenon *et al.* 1989] V. A. Guenon, T.-W. Chou, and J. W. Gillespie Jr., "Toughness properties of a three-dimensional carbon-epoxy composite". *Journal of Materials Science* **24**, pp. 4168-4175.

[Jarmon *et al.* 1998] D. C. Jarmon, C. A. Weeks, R. A. Naik, C. L. Kogstrom, C. P. Logan and P. F. Braun, "Mechanical Property Comparison of 3-D and 2-D Graphite Reinforced Epoxy Composites Fabricated by Resin Transfer Molding". *43rd International SAMPE Symposium and Exhibition*, Anaheim, CA, May 31-June 4, 1998, pp. 2043-2056.

[Kline & McClintock 1953] S. J. Kline and F. A. McClintock, "Describing Uncertainties in Single-Sample Experiments". *Mechanical Engineering*, January 1953, p.3.

[Kregers & Melbardis 1978] A.F. Kregers and Y. G. Melbardis, "Determination of the deformability of three-dimensionally reinforced composites by the stiffness averaging method". *Polymer Mechanics* **14**(1) (English translation) pp. 3-8.

[Mohamed & Zhang 1992] US Patent 5085252 (Feb. 4, 1992) M. Mohamed and Z. Zhang (to North Carolina State University).

[Prosser 1988] R. A. Prosser, "Penetration of Nylon Ballistic Panels by Fragment Simulating Projectiles. Part II: Mechanism of Penetration". *Textile Research Journal*, March 1988, pp. 161-165.

[Singletary & Bogdanovich 2000] J. Singletary and A. Bogdanovich, "3-D Orthogonal Woven Cloth Armor". *Textile Usages á Techniques*, September 2000, pp. 26-31.

[Tarnopol'skii *et al.* 1973] Yu. M. Tarnopol'skii, V. A. Polyakov and I.G. Zhigun, *Polymer Mechanics* **9**(5), 754 (English translation) (1973).

[Tarnopol'skii & Kincis 1985] Yu. M. Tarnopol'skii and T. Kincis, Static Test Methods for Composites. Van Nostrand Reinhold Co., New York, 1985.

[Vaidya *et al.* 1999] U. K. Vaidya, N. C. Jadhav, M. V. Hosur, J. W. Gillespie Jr., and B. K. Fink, "Influence of Through-the-Thickness Stitching on the High Strain Rate Impact Response of Resin Infused S2-Glass/Epoxy Composites". *Proceedings of the 14th American Society for Composites Technical Conference*, J. W. Whitney, Editor. Fairborn, OH, September 27-29, 1999. pp. 141-150.

[Vasudev & Mehlman 1987] A. Vasudev and M. J. Mehlman, "A Comparative Study of the Ballistic Performance of Glass Reinforced Plastic Materials". *SAMPE Quarterly* **18**(4), July 1987, pp. 43-48.

[Yushanov *et al.* 1999] S. P. Yushanov, A. E. Bogdanovich and M. H. Mohamed, *Journal of Thermoplastic Composite Materials* **12**, 70 (1999).

11. Publications and Technical Papers

No publications or technical papers have been planned or made from this research by the date submitted.

12. Participating Scientific Personnel

Dr. James Singletary (principal investigator) – 3TEX
Mr. Robert A. Coffelt – 3TEX
Dr. John W. Gillespie, Jr – CCM (principal investigator – CCM)
Mr. Bazle A. Gama – CCM

No advanced degrees were earned by participating scientific personnel during this investigation.